A NOVEL MAIZE DWARF RESULTING FROM A GAIN-OF-FUNCTION MUTATION IN A GLUTAMATE RECEPTOR GENE

by

Amanpreet Kaur

A Dissertation

Submitted to the Faculty of Purdue University

In Partial Fulfillment of the Requirements for the degree of

Doctor of Philosophy

Department of Botany and Plant Pathology

West Lafayette, Indiana

August 2020

THE PURDUE UNIVERSITY GRADUATE SCHOOL
STATEMENT OF COMMITTEE APPROVAL

Dr. Gurmukh S. Johal, Chair

Department of Botany and Plant Pathology

Dr. Brian Dilkes

Department of Biochemistry

Dr. Damon Lisch

Department of Botany and Plant Pathology

Dr. Yun Zhou

Department of Botany and Plant Pathology

Approved by:

Dr. Christopher J. Staiger

I dedicate this dissertation to my parents (Mrs. Kulvinder Kaur and Mr. Jaswinder Paul Singh) and sister (Amneet Kaur) for their unconditional love, support, and constant faith in me.

ACKNOWLEDGMENTS

TABLE OF CONTENTS

LIST OF TABLES

LIST OF ABBREVIATIONS

BM-NILs	B73/Mo17 Near Isogenic Lines
BR	Brassinosteroid
$[Ca^{2+}]_{cyt}$	Cytosolic Ca^{2+}
CIM	Composite Interval Mapping
CRD	Completely Randomized Design
DEG	Differentially Expressed Gene
DRIL41	Disease Resistance Introgression Line 41
EMS	Ethyl Methanesulfonate
FDR	False Discovery Rate
GAs	Gibberellins
GLR	Glutamate receptor-like
GO	Gene Ontology
GSEA	Gene Set Enrichment Analysis
HPLC/MS	High Performance Liquid Chromatography/Mass Spectrometry
IBM-RIL	Intermated B73-Mo17 Recombinant Inbred Line
iGluR	Ionotropic Glutamate receptor
NJ	Neighbor-Joining
PCA	Principle Component Analysis
PLS-DA	Partial Least Squares Discriminant Analysis
QTL	Quantitative Trait Loci
SAM	Shoot Apical Meristem
SD	Standard deviation
SEA	Singular Enrichment Analysis
SMA	Single Marker Analysis

LIST OF FIGURES

ABSTRACT

Plant height is an important agronomic trait and a major target for crop improvement. Owing to the ease of detection and measurement of plant stature, as well as its high heritability, several height-related mutants have been reported in maize. The genes underlying a few of those mutants have also been identified, with a majority of them related to the biosynthesis or signaling of two key phytohormones - gibberellins (GAs) and brassinosteroids (BRs). However, most other maize dwarfing mutants, and especially those that result from gain-of-function mutations, remain uncharacterized. The present study was undertaken to characterize a novel dominant dwarfing mutant, named *D13*. This mutant appeared in the M1 population of the inbred B73 that was generated by mutagenesis with ethyl methanesulfonate (EMS). Like most other maize dwarfing mutants, the reduction in *D13* height was largely due to the compression of the internodes. However, unlike the GA or BR mutants, *D13* had no defects in the female or male inflorescences. Further, in contrast to the GA and BR mutants, the mesocotyl elongation during etiolation was not impacted in *D13*. *D13* seedlings developed red coloration in two to three lowermost leaves. In addition, *D13* also showed enhanced tillering when the phenotype was very severe. The size of the shoot apical meristem of *D13* was reduced slightly, and significant aberrations in the structure of vascular bundles in the mutant were observed. All anatomical and phenotypic features of *D13* were highly exaggerated in homozygous state, indicating the partially dominant nature of the *D13* mutation. Interestingly, the heterozygous mutants showed remarkable variation in their phenotype, which was maintained across generations. Moreover, the *D13* phenotype was found to be sensitive to the genetic background, being completely suppressed in Mo17, Oh7B, enhanced in CML322, P39 and changed to different degrees in others. To identify the genetic defect responsible for the *D13* mutant phenotype, a map-based cloning approach was used, which identified a single base-pair change from G to A (G2976A) in the coding region of a glutamate receptor gene (Zm00001d015007). The G2976A missense mutation resulted in the replacement of alanine with threonine at the location 670. The replaced alanine is highly conserved in glutamate receptors across all domains of life from cyanobacteria to plants to mammals, suggesting a causal relationship between the G2976A substitution and the *D13* phenotype. To validate this relationship, a targeted EMS-based mutagenesis approach was used to knock-out (inactivate) the *D13* mutant allele. A suppressor mutant was found in which the *D13* mutant phenotype reverted to the normal

tall phenotype. The sequence of the revertant allele, designated *D13**, revealed that the original *D13* mutant allele underwent a second G to A mutation (G1520A) to change glycine into aspartic acid at position 473. This intragenic second-site mutation in the *D13* allele suppressed the function of the *D13* allele, thereby preventing it from interfering with the function of the wild type allele. To further unveil the genes and underlying mechanisms that enable the *D13* mutant to confer a dwarf phenotype, transcriptomic and metabolomic analyses of *D13* mutants were conducted and compared to the wild type sibs. While the omics analysis confirmed that stress responses were upregulated and genes related to shoot system development were downregulated in the mutant, the data did not allow us to pinpoint the underlying mechanisms that connect the *D13* mutation with its dwarfing phenotype. Furthermore, it remains unclear whether these stress and shoot system-related changes result in the manifestation of *D13* phenotype, or the dwarf phenotype due to *D13* mutation activates the stress-related mechanisms. This is the first study that signifies the importance of a glutamate receptor gene in controlling plant height.

CHAPTER 1.   REVIEW OF LITERATURE

1.1   Plant height

Plant height, mainly attributed to elongation of the stem, is a highly heritable agronomic trait that contributes to the yield potential of crop plants. Manipulating the height has a significant impact on the overall yield of the plant. The green revolution during the 1960s and 70s is a great example, where introduction of semi-dwarf wheat and rice varieties in the developing countries, in combination with the increased use of nitrogen fertilizer, resulted in a tremendous increase in the crop yield (Khush 2001). The short height prevented lodging and allowed the plant to utilize energy efficiently to convert the fertilizer inputs into higher yields. Thus, manipulating plant height is an effective strategy to improve crop productivity. However, to achieve this goal, it is fundamental to understand the genetic and molecular mechanisms that regulate plant height.

Plant height, being easily measurable, has been widely studied by breeders and geneticists, and several genes that influence this trait are known. The green revolution genes- *semidwarf1 (sd1)* and *Reduced height (Rht)*, are responsible for the semi-dwarf rice and wheat cultivars, respectively. The *Sd1* gene in rice encodes GA20-oxidase, which is an important enzyme involved in gibberellic acid (GA) biosynthesis (Monna et al. 2002). The wheat *Rht* genes, *Rht-B1* and *Rht-D1,* encode DELLA proteins (Pearce et al. 2011). Mutations in *Sd1* and *Rht* lead to defects in GA biosynthesis and signaling (Peng et al. 1999; Spielmeyer et al. 2002). Utilizing such mutants compromised in plant height is an excellent way to identify the genes related to the trait. Similarly in maize, dwarf mutants have helped to identify several genes responsible for the dwarf phenotype, such as *d1*, *d3*, *d5*, *D8*, *D9*, *na1*, *na2* (Winkler and Helentjaris 1995; Hartwig et al. 2011; Chen et al. 2014; Best et al. 2016). These genes are mainly associated with phytohormones and affect their biosynthesis, transport, or signaling. This chapter provides an overview of the factors that are known or potentially involved in controlling plant height in maize.

1.2   Effect of phytohormones on plant height

Plant hormones are the chemical messengers that control multiple aspects of plant growth and development. All plant processes, starting from the germination of the seed until the production of new seed, involve the activity of these hormones. They are required for cell division,

elongation, response to stimuli, stress response, flowering, maturation, and abscission. The hormones that influence plant height in maize include gibberellins, brassinosteroids, and auxins. Defects in the biosynthesis or signaling of these hormones cause a characteristic phenotype in the mutants, e.g., the appearance of anthers in the ear in GA mutants, and shortening of upper internodes in BR mutants. There are only two known genes *AP2* and *ZmRPH1,* that are not directly related to phytohormones that affect plant height in maize. There is a possibility that these might indirectly influence phytohormone pathway, but the mechanism of action of these is not yet known. Phytohormones are by far the indispensable regulators of plant height in corn.

1.2.1   Gibberellins

The plant hormones gibberellins (GAs) are tetracyclic diterpenoids that regulate seed germination, stem elongation, and induction of flowering (Achard and Genschik 2009). Dwarf maize mutants are grouped into two categories: GA-responsive and GA-nonresponsive mutants, depending on their ability to respond to exogenously applied GA (Fujioka et al. 1988a). Short internodes, short broad leaves, reduced tassel branching, and anther development in the ear are characteristics of typical GA mutants (Bensen et al. 1995; Cassani et al. 2009).

The biosynthesis of GAs takes place in three phases in different cellular compartments catalyzed by three classes of enzymes: terpene synthases (TPPs), cytochrome P450 mono-oxygenases and 2-oxoglutarate-dependent dioxygenases (2ODDs) as described below (Yamaguchi 2008) (Figure 1.1).

Phase I: Conversion of geranylgeranyl phosphate to *ent*-kaurene in the plastid is mediated by two terpene synthases: *ent*-copalyl diphosphate synthase (CPS) and *ent*-kaurene synthase (KS) (Yamaguchi 2008). Mutations that affect these enzymes result in dwarf phenotype in maize. For example, loss of function mutations in the *An1* gene that encodes CPS resulted in GA responsive semi-dwarf phenotype (Bensen et al. 1995). In addition, the *d5* mutants are associated with loss of *ent*-kaurene synthases (KS) due to mutation in the 5'UTR region of the *ZmKSL3* gene (Fu et al. 2016). Exogenous supply of kaurene derivatives (kaurenol and kaurenoic acid) to *an1* and *d5* mutants restores the phenotype in seedlings compared to untreated mutants (Katsumi et al. 1964), thus, revealing the importance of these two genes in controlling plant height.
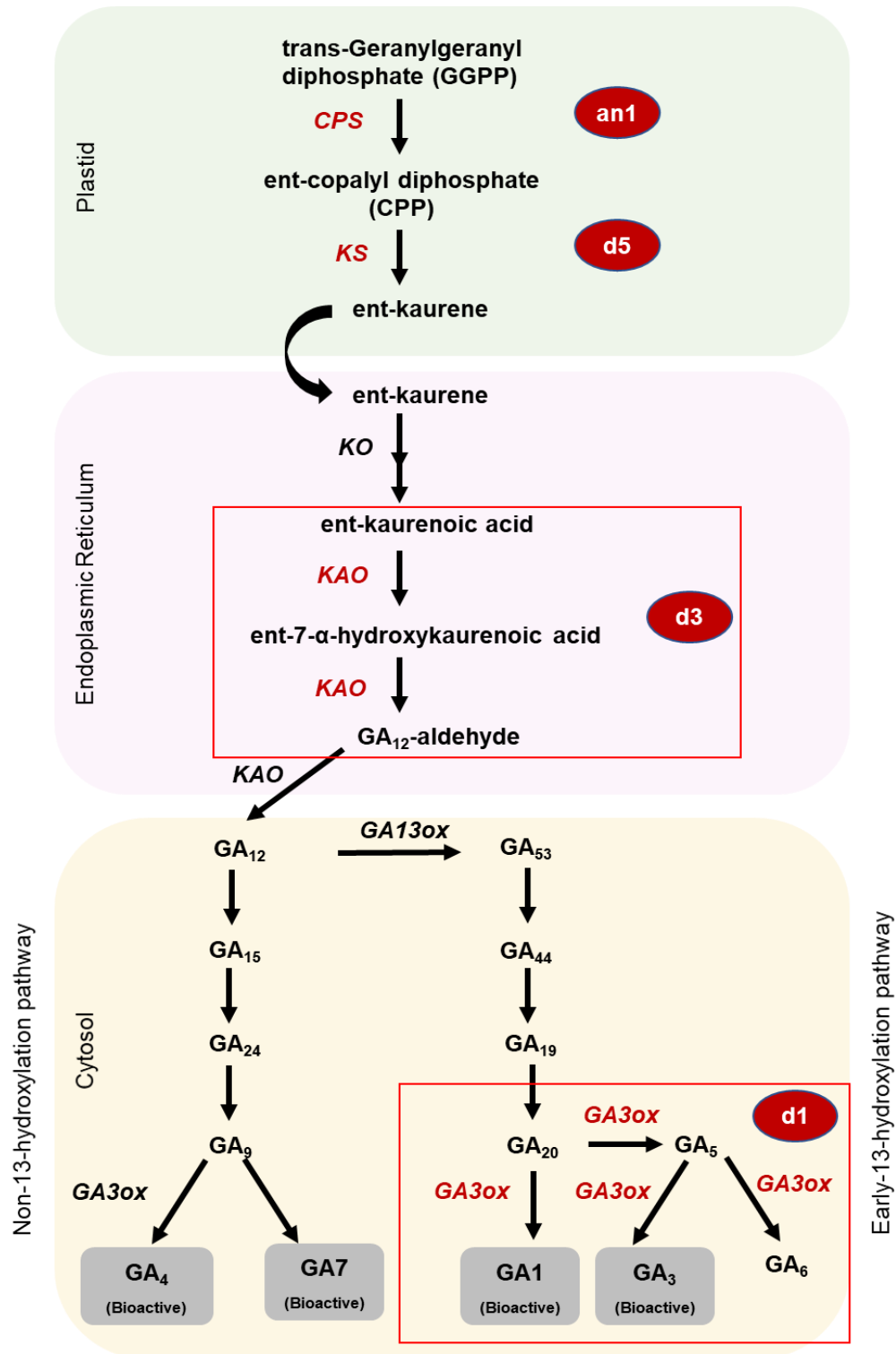
Figure 1.1 Schematic of the GA biosynthesis pathway (modified from Igielski and Kępczyńska 2017). The red circles show the know GA mutants in maize. The enzymes impacted in these mutants are shown in red. The gray boxes represent the active forms of GA.

17

Phase II: Formation of GA12 in the endoplasmic reticulum. GA12 is a common precursor for all GAs in plants (Hedden and Thomas 2012). The conversion of *ent*-kaurene to GA12 is a six-step process carried out by two cytochrome P450 mono-oxygenases: *ent*-kaurene oxidase (KAO) and *ent*-kaurenoic acid oxidase (KAO). Maize gene *Dwarf 3 (D3)* encodes a cytochrome P450 enzyme of subfamily CYP88 (Winkler and Helentjaris 1995). Earlier, it was proposed that mutations in *D3* impact the 13-hydroxylase activity (GA12 → GA53) (Winkler and Helentjaris 1995; Fujioka et al. 1988b), however, later studies suggested that *Dwarf3* likely encodes *KAO* (Helliwell et al. 2001), impacting the biosynthesis of GA12.

Phase III: Production of bioactive GAs in the cytosol. It is the bioactive GAs that regulate various aspects of plant growth and development. Major bioactive GAs in plants include GA1, GA3, GA4, and GA7 (Yamaguchi 2008). The synthesis of these bioactive GAs from GA12, which requires 2ODDs (GA20ox and GA3ox), occurs by hydroxylation of C-13 (13-hydroxylation pathway) and/or C-20 (non-13-hydroxylation pathway). These parallel pathways lead to the production of GA20 and GA9, respectively, by the action of GA20ox. The final steps catalyzed by GA3ox produce bioactive GAs. *Dwarf-1* (*d1*) gene in maize encodes GA3ox that catalyzes four reactions: GA20 to GA3, GA20 to GA1, GA5 to GA3, and GA9 to GA4. Four independent *d1* alleles carrying mutations in GA3ox have been identified. These *d1* mutants are recessive, GA-responsive, and display dwarfism and andromonoecy.

Following the synthesis of GAs, the GA signaling requires a class of plant-specific GRAS family transcription regulators known as DELLA proteins. They are nuclear-localized proteins that act as negative regulators of GA response. DELLA proteins repress the GA response by either physically interacting with other transcription factors like PIF (Phytochrome interacting factors) to inhibit DNA binding or interacting with transcription regulators to inhibit their activity. Some studies also suggest that DELLA proteins function as trans activators (Hirano et al. 2012). DELLA-mediated growth repression is overcome by the proteasomal degradation of DELLA proteins initiated by the availability of GAs. The bioactive GAs bind to the GA binding pocket of a soluble GA receptor, Gibberellin insensitive dwarf 1 (GID1) (Ueguchi-Tanaka et al. 2005) inducing conformational changes in the protein. GID1 then binds to DELLA, forming a GA-GID1-DELLA complex that allows the interaction of DELLA with SLEEPY1/GID2, an F-box protein that recruits DELLA to the SCF[SLY1] E3 ligase complex for ubiquitination and subsequent

degradation via the ubiquitin-26S proteasomal pathway. In maize, two dominant mutants, *Dwarf8* (*D8*) and *D9* (a *D8* paralog) encoding DELLA proteins have been identified. Both are GA-non-responsive mutants and show phenotypes similar to the GA-responsive mutants i.e. dwarfing, delayed flowering, and anthers in ears (Lawit et al. 2010). Transgenic *Arabidopsis* plants that express *D8* and *D9* alleles also exhibit a dwarf phenotype, strongly indicating the relation of these genes to plant height. The *D8-1023* mutant has an insertion in the VHYNP domain (Cassani et al. 2009). This domain, along with another conserved domain DELLA in the N-terminal regions of a DELLA protein, is required for interaction with GID1 and thus, mutations in DELLA and VHYNP domains can impair GA perception and in turn impact plant height.

1.2.2 Brassinosteroids

Brassinosteroids (BRs) are commonly occurring steroid hormones that control many aspects of plant growth and development. More than 70 BRs have been identified in plants (Bajguz 2007; Zhao and Li 2012). The most active form of brassinosteroids is brassinolide (BL). It is synthesized from a phytosterol, campesterol (CR), either via campestanol (CN)-dependent or campestanol-independent pathways (Figure 1.2). In the CN-dependent pathway, CN is converted to castasterone (CS) via early or late C-6 oxidation pathways, which is then finally converted to BL. Plants defective in brassinosteroid signaling or biosynthesis result in a typical dwarf phenotype, delayed flowering time, and de-etiolated phenotype in dark-grown plants (Clouse and Sasse 1998). In addition, BR deficiency in maize results in a tassel seed phenotype (Hartwig et al. 2011; Best et al. 2016). Several BR mutants have been identified in *Arabidopsis*, tomato, and rice (Bishop 2003). However, only three brassinosteroid biosynthesis mutants have been characterized in maize.

The maize dwarf mutant *nana1* (*na1*) carries a loss of function mutation in the *DET2* (*DE-ETIOLATED2*) homolog in the BR biosynthetic pathway (Hartwig et al. 2011). *DET2* encodes a steroid 5α-reductase involved in BR biosynthesis in *Arabidopsis*. This enzyme catalyzes the conversion of 4-en-3-one to 3-one (Noguchi et al. 1999; Fujioka et al. 1997). Defects in the *DET2* enzyme lead to accumulation of the substrate 4-en-3-one resulting in BR deficiency. The *na1* mutant is one-third of the height of wild type plants and shows a decrease in internode length and a tassel seed phenotype.
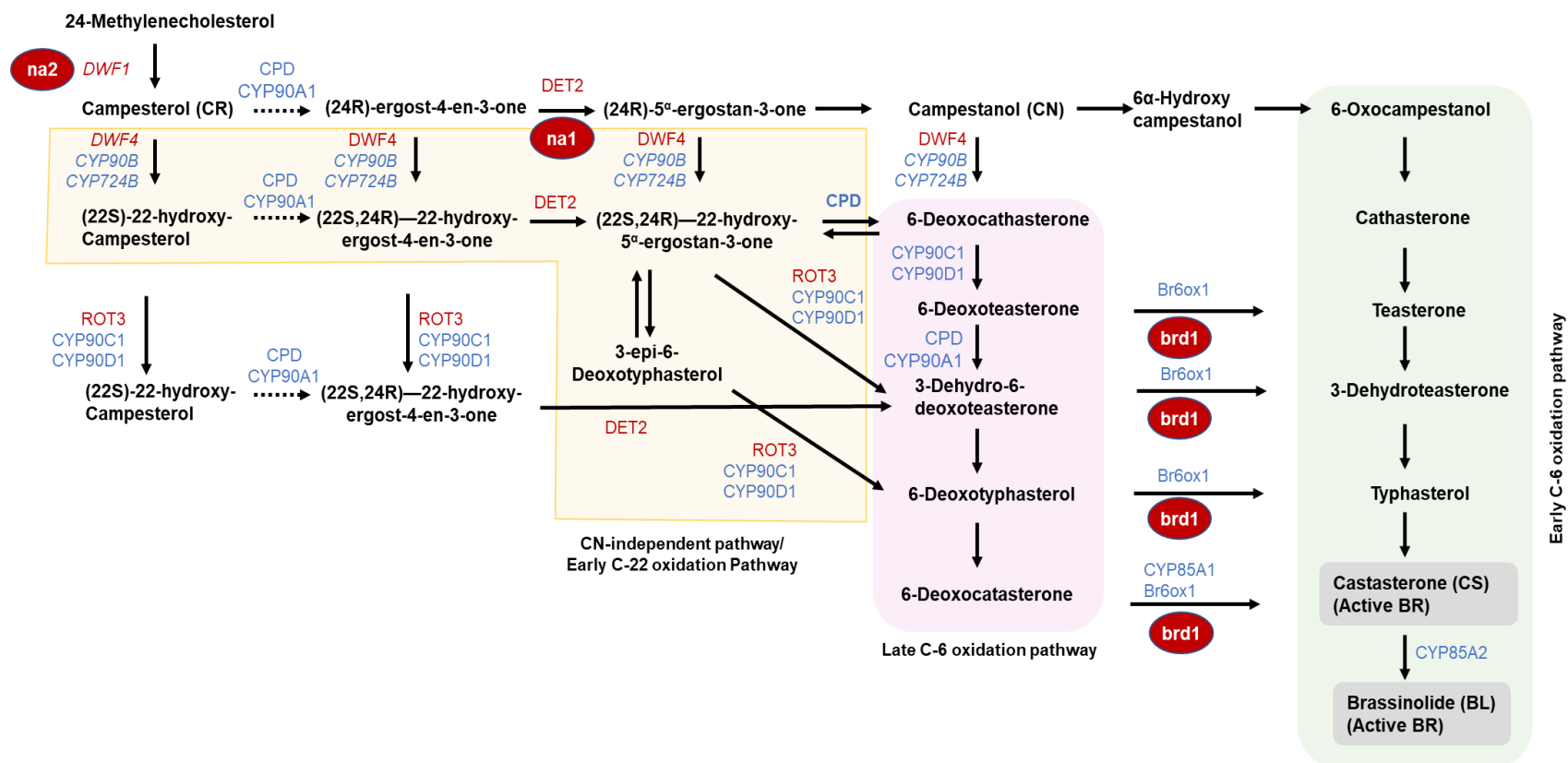
Figure 1.2 Schematic of Brassinosteroid biosynthesis pathway modified from Chung & Choe, 2013. Yellow color marks the CN-independent pathway, and the rest is CN-dependent pathway. The CN-dependent pathway is further divided into the early C-6 oxidation pathway (Green) and the late C-6 oxidation pathway (Pink). Active BRs are highlighted in gray. The known maize mutants are shown in red circles alongside the reactions that are disrupted in those mutants.

Similar to *na1* mutants, *nana2 (na2)* mutants show severe dwarf and tassel seed phenotypes (Best et al. 2016). The *na2* mutants accumulate 24-methylenecholesterol and have reduced levels of downstream intermediate campesterol. These findings suggest that the *na2* phenotype is due to a defect in Δ^{24}-sterol reductase. The maize *na2* gene is an ortholog of the *Arabidopsis DWF1* gene involved in the conversion of 24-methylenecholesterol to campesterol. Sequencing of *na2-1* mutant plants revealed a C to T change that generated a premature stop codon resulting in a loss of 110 amino acids from the protein. Three additional alleles *na2-2*, *na2-3,* and *na2-4* identified from the dwarf plants carry novel G to A mutations in the same gene, further strengthening the link between *na2* and plant height.

Another mutant, *brd1*, is also defective in BR biosynthesis (Makarevitch et al. 2012). The mutant exhibits a very severe dwarf phenotype with no internode elongation. The mutation is mapped to chromosome 1 in a region containing four genes. Among the four genes, only *brassinosteroids-deficient dwarf 1* (*brd1)* has a mutation in the exonic region. The *brd1* gene in maize encodes brassinosteroid C-6 oxidase (Br-6-ox), which is involved in the final steps of BR biosynthesis. A single base change leading to a premature stop codon results in the loss of cyp450 domain, thus rendering the protein non-functional. The mutant phenotype can be partially rescued by the exogenous supply of BRs in the growth media. The mutants possess an increased quantity of *brd1* transcripts, which are reduced by exogenous brassinolide treatment, suggesting negative feedback regulation of *brd1* by brassinolide.

The formation of the active BRs in plants initiates BR signaling cascades. Most of our understanding of BR signaling is derived from studies in *Arabidopsis*, whereas it is not well understood in maize. The active BRs, e.g., BL bind directly to a leucine-rich repeat (LRR) containing receptor-like kinase (RLK) known as Brassinosteroid insensitive 1 (BRI1) localized in the plasma membrane. The binding of BL to BRI1 allows the formation of BRI1-BAK1 (Brassinosteroid insensitive-1-associated receptor kinase) complex. This heterodimer formation activates a phosphorylation cascade in the plant. BRI1 gets activated by auto- and transphosphorylation events between BRI1 and BAK1. The activation of BRI1 leads to the activation of BR signaling kinases (BSK1, BSK2, and BSK3). These kinases then bind to and activate BRI1 suppressor1 (BSU1), which dephosphorylates BIN2 (Brassinosteroid insensitive 2). In the absence of BR, BIN2 inactivates BZR and BES1 protein through phosphorylation. Inactive

BZR/BES1 proteins are retained in the cytoplasm by binding to 14-3-3 proteins. Dephosphorylation of BIN2 renders it inactive and allows its degradation by 26S proteasome, eliminating its inhibitory effect on BZR/BES1 proteins. The active forms of BZR and BES1 bind to the promoter of target genes and regulate the transcription of many BR- responsive genes, thus regulating BR-mediated plant development.

Arabidopsis and rice contain one BRI1 and three functionally redundant BRI1-like receptor kinases (BRL1, BRL2, and BRL3) (Cano-Delgado 2004; Nakamura et al. 2006). Maize contains two BRI1 homologs and three BRLs (Kir et al. 2015). Transgenic plants developed by knockdown of the five BRI1/BRLs in maize exhibit reduced height. The reduction in height was due to shortening of internodes, especially above the ear (Kir et al. 2015). This is the only report in maize that shows the effect of BR signaling on the height of plants

1.2.3 Other genes

All the genes influencing plant height in maize discussed so far are related to hormone biosynthesis, signaling, or transport. Besides these, some additional height-related genes like *Dil1* and *ZmRPH1* have been identified, but their mode of action is not well understood.

Dil1 (dwarf and irregular leaf 1) affects the leaf and stalk development in maize (Jiang et al. 2012). Two semi-dwarf mutants, *dil474* and *dil338* identified through EMS mutagenesis have shorter internodes and small size of stalk parenchyma cells. *Dil1* encodes an *AP2* transcription factor-like gene. Sequence comparison of this gene in both the mutants and wild type plants shows independent point mutations. The mechanism of action of *dil1* is not yet known but it is believed that it might influence the expression of genes related to hormonal pathways. Another gene *ZmRPH1 (Reducing Plant Height1)* encodes a microtubule-associated protein (MAP) (Li et al. 2019). Overexpression of this gene in maize inbred line B73 leads to a reduction in the mesocotyl length as well as the size of parenchyma cells. The seedlings also exhibit reduced root length. At later stages, the plants show reduced internode length. Overexpression of *ZmRPH1* in *Arabidopsis* also results in shorter hypocotyls in the transgenic lines.

1.2.4   Auxins

In addition to GAs and BRs, auxins have emerged as another important class of hormones influencing plant height in corn. The *brachytic 2* (*br2*) mutant in maize shows defects in polar auxin transport in a light-dependent manner (Multani et al. 2003). The reduced height of this mutant is caused by shortening of lower stalk internodes. The dwarf plants also display an increase in the diameter of affected internodes. This increase in girth is a result of an increase in the number of stalk cells and not an increase in the size of cells. The *br2* mutation in maize leads to loss of function of a transporter of the multidrug-resistant (MDR) class of P glycoproteins (PGPs). Mutations in PGPs in *Arabidopsis* also impact the auxin transport, strongly suggesting the role of PGPs in polar movement of auxins. Multani *et al.* further extended their study to *dw3* mutants in sorghum. The interest in these mutants arose because of their strikingly similar dwarfing phenotype to *br2*. The sequence of *dw3* gene shows high similarity to the *br2* gene further suggesting the role of auxin in regulating plant height.

1.2.5   Hormone crosstalk to regulate plant height

BR and GA mutants exhibit severe dwarfing phenotype and defects in floral development. These hormones have been shown to interact with each other in rice and *Arabidopsis*. Best et al. (2016) studied the interaction between these hormones in maize. They developed BR and GA biosynthetic double mutants using the BR mutants *na2-1*, *na1-1,* and GA mutants, *d1* and *d5*. BR and GA have an additive effect on plant height. The double mutants have much shorter internodes than the individual mutants. The treatment of *na2-1* mutants with GA results in a similar increase in length of the internodes as the wild type counterparts, therefore, indicating that these hormones independently influence plant height and show no interaction in maize. However, Best et al. reported that tiller number and reproductive organ development are influenced by interactions between these hormones (Best et al. 2016).

There are other studies that show direct cross talk between GA and BR. Hu et al. utilized GA and BR inhibitors, Ucz (Uniconazole) and Pcz (Propiconazole), respectively, to mimic the effect of GA and BR biosynthetic mutants in maize (Hu et al. 2017). Both inhibitors independently affect plant height in backcross families of a stiff stalk crossed to a tropical line. However, they

also discovered that lines more tolerant to one of the inhibitors also show similar response to the second inhibitor. In addition, GWAS analysis identified one SNP marker, that was linked to a BR signaling pathway gene *ZmBSU1*, that is associated with both BR and GA indicating that BSU1 may be involved in interaction between GA and BR. Recent studies in *Arabidopsis* have also demonstrated that direct interactions between BZR/BES1 and DELLA mediate BR/GA crosstalk to control cell elongation (Li and He 2013). DELLA proteins act as negative regulators of the BR pathway, whereas BZR1 positively regulates the GA pathway.

The interaction between BR and GA in maize is complex and there is no defined mode of communication. More studies are needed to better understand the influence of crosstalk between the two hormones on plant growth and development.

1.3 Plant glutamate receptor genes

The glutamate receptor gene family is well known for its role in mammalian excitatory neurotransmission (Ozawa 1998). Mammalian glutamate receptors act as non-selective cation channels and transport cations, including Na^+, K^+, and Ca^{2+} across the cell membrane (Mayer and Armstrong 2004; Ozawa 1998). They are broadly divided into two categories: ionotropic and metabotropic receptors (Nakanishi 1992). Ionotropic glutamate receptors (iGluRs) themselves act as ion channels and allow passage of cations across the membrane, whereas metabotropic receptors (mGluRs) are G-protein coupled receptors that work indirectly by activating other ion channels. The iGluRs further group into different classes based on the selective agonist: NMDA, AMPA, kainate, and delta receptors.

Plant glutamate receptors (GLRs) are homologs of ionotropic class of mammalian glutamate receptors (iGluRs) (Lam et al. 1998; Davenport 2002). This gene family was first identified in *Arabidopsis* and is comprised of 20 members (Lam et al. 1998; Chiu et al. 2002). GLRs have been identified in other plant species, including mosses, rice and tomato (Li et al. 2006; Aouini et al. 2012; Lu et al. 2014; Ortiz-Ramírez et al. 2017). In contrast to mammalian GluRs, plant GLRs play a role in plethora of processes, including light signaling, carbon-nitrogen metabolism, defense response, stomatal closure, pollen tube growth, root growth and development, and drought tolerance. Since the discovery of this gene family in plants, scientists have been interested in determining its roles and mechanism of action. However, progress has been slow due to high gene

redundancy. Fully characterizing this receptor family has been a challenge due to a lack of mutants with an apparent phenotype. Most of our knowledge about plant GLRs relies heavily on their similarity with their mammalian counterparts.

1.4 Evolution of plant glutamate receptor genes

Before the discovery of glutamate receptors in plants in 1998, these receptors were predominantly associated with neurotransmission. The occurrence of this receptor family in plants was surprising initially because plants lack nervous system. The initial studies focused on placing the newly discovered plant GLRs in the evolutionary tree. Plant GLRs share common ancestry with iGluRs but diverged very early from animal iGluRs, before the divergence of different classes of iGluRs (Chiu et al. 1999; 2002). Primitive GluR signaling mechanisms existed even before the separation of plants and animals, as is indicated by the presence of GluRs in the prokaryotes, cyanobacteria *Synechocystis (GluR0) and Anabaena* (Chen et al.1999; Chiu et al. 2002). Thus, this receptor family is not unique to animals and evolved in both plants and animals. High similarity of functional domains in glutamate receptors with other proteins suggests that glutamate receptors originated by the fusion of a periplasmic binding protein (PBP) with a potassium ion channel (Galen Wo and Oswald 1995).

Arabidopsis possesses 20 glutamate receptor-like genes (AtGLRs), which are grouped into three clades based on sequence similarity, with clade I and II being sister clades (Chiu et al. 2002). Tomato contains 13 GLRs, which are also grouped into three clades. Comparison of tomato and *Arabidopsis* GLRs shows homology between two of the three clades (clade II and III), whereas clade I of tomato is distinct from *Arabidopsis* clade I (Aouini et al. 2012). The rice GLRs also divide into three clades, but one of the rice GLR clades does not group with any of the three clades in *Arabidopsis* (Ni et al. 2016). These studies indicated the presence of a distinct clade in plants apart from the three clades in *Arabidopsis*, which was later identified by Bortoli et al. (2016). The fourth clade contains sequences from tomato and rice that did not group with the three *Arabidopsis* clades. Besides these, clade IV also contains sequences from *Phoenix dactylifera*, *E. guineensis*, *M. acuminate*, and *C. melo* (Bortoli et al. 2016). The GLRs in mosses (*Physcomitrella patens*) and gymnosperms (*Ginkgo biloba*) group with the clade III in *Arabidopsis* indicating that clade III is the most ancient among all the clades (Bortoli et al. 2016).

The clade classification of mammalian glutamate receptors into NMDA, AMPA/KA, delta receptors conforms to their division based on ligand binding and electrophysiological properties. However, no such distinctions have been established for plant GLRs. The differentiation of clades in plants is independent of specific function or expression patterns (Chiu et al. 2002). While clade I and III genes in *Arabidopsis* are ubiquitously expressed (leaves, siliques, roots, and flowers) with high expression in the roots, clade II genes are mostly root specific.

1.5   Structure of glutamate receptors

Although the plant and animal iGluRs diverged very early on during evolution, they do share a similar structure consisting of an N terminal domain (NTD), two ligand-binding domains, three transmembrane domains (M1, M3, M4), a pore domain (M2) and a C terminal domain (Madden 2002; Lam et al. 1998). The structural domains share sequence identity ranging from 16 to 63%, with the M3 region showing the highest identity (Lam et al. 1998; Chiu et al. 1999). The N-terminal domain and the two ligand-binding domains are on the extracellular side of the membrane, and the C-terminal domain is intracellular. Between these lie the transmembrane domains that form the channel for the cations to pass through.

Mammalian iGluRs assemble as homo- or hetero-tetramers to form a functional ion channel (Madden 2002; Traynelis et al. 2010). Dimerization is facilitated by a strong interaction between the NTDs of two subunits. A subsequent dimerization takes place through interactions of the ligand-binding domains and transmembrane domains. Functional channels are formed by interactions between the subunits within the same iGluR class (Nath et al. 1988). Studies suggest that glutamate receptors form multimeric complexes in plants but the subunits that make up plant GLRs are not well known. Roy *et al.* (2008) proposed the possibility of heteromer formation when they observed co-expression of an average of five to six AtGLRs in single epidermal and mesophyll cells obtained from leaves. AtGLRs 3.2 and 3.4 physically interact with each other when expressed in mammalian HEK293 cells as well as *Nicotiana benthamiana* (Vincill et al. 2012; 2013). Homomer formation for AtGLRs 1.1 and 3.4 has also been reported (Price et al. 2013). A modified yeast-2-hybrid system approach known as "yeast mating-based split ubiquitin system (mbSUS)" identified interactions between various subunits (1.1, 2.1, 2.9, 3.2, and 3.4). These studies highlight that the interactions between plant iGluRs are not clade-specific (Price et

al. 2013). Members from any of the three clades can come together to form multimeric complexes, that contrasts with mammalian iGluRs, which only interact within their clade.

The four subunits of a functional ion channel cross each other at a conserved "SYTANLAA" motif in the M3 domains (Wollmuth 2004). This motif, also referred to as the "gating motif," lines the opening of the channel on the extracellular side of the membrane. This motif is highly conserved in all the iGluRs and mutations in this region significantly alter the channel activity. The lurcher mutant (Lc) in mice is a result of the spontaneous conversion of alanine at position 8 to threonine in the δ2 glutamate receptor (Zuo et al. 1997). It is a semi-dominant neurological mutation that constitutively activates the ion channel and subsequently causes the death of all the cerebellar Purkinje cells. The T648A (T3A) mutation in NMDA GluRs produced large holding currents, suggesting that channel is constitutively open in these mutants (Kashiwagi et al. 2002). Similarly, an increase in leak currents is observed with the A4C mutation (Sobolevsky et al. 2007). A slightly modified form of the "SYTANLAA" motif is present in plant GLRs. Most of the plant GLRs contain "SYTASLTS" motif (Aouini et al. 2012; Price et al. 2012; Wudick et al. 2018a). The Alanine at position 4 is the most conserved residue and is present in all the mammalian, plant, and bacterial glutamate receptors. This particular Alanine (A4 in SYT$\underline{A}$NLAA motif) acts as the "hinge" and pulls the M3 helices away from each other, thus opening the channel gate on the extracellular side (Twomey and Sobolevsky 2018).

Activation of the channel requires the binding of a specific ligand(s) to the ligand-binding domains, which leads to conformational changes causing the channel to open. L-glutamate is the primary ligand that binds to the GluR channels in mammals. Some of the other amino acids, like glycine, aspartate, and D-serine, have also been reported to bind to these channels. The similarity of the GLR structure in animals and plants led to the belief that plants GLRs might be gated by the same amino acids as their mammalian counterparts. However, studies indicate that plant GLRs have a broader ligand specificity than animal iGluRs (Forde and Roberts 2014; Vincill et al. 2012; Tapken et al. 2013). Glutamate is still the most common ligand that activates the channel. However, membrane depolarizations and Ca^{2+} influxes have also been observed with glycine, asparagine, serine, alanine, cysteine, methionine and even glutathione (Dubos et al. 2003; Michard et al. 2011; Vincill et al. 2012; Li et al. 2013; Tapken et al. 2013; Forde and Roberts 2014).

1.6   Sub-cellular localization of GLRs

Determining the subcellular localization of GLRs can be a step towards better understanding their specific role in a cell. The analysis of the N terminal domain (NTD) sequence indicates their involvement in the secretory pathway. Thus, they are most likely located in the plasma membrane (Meyerhoff et al. 2005; Vincill et al. 2012). However, they are also predicted to be targeted to other cellular compartments (http://aramemnon.botanik.uni-koeln.de/). AtGLR3.4 is localized in both the plastid and the plasma membranes (Teardo et al. 2011). Dual targeting to mitochondria and chloroplast was observed for AtGLR3.5 guided by alternative splicing (Teardo et al. 2015). Kong et al. (2016) reported AtGLR3.5 localization in the plasma membrane as well as chloroplast. AtGLR2.1 and AtGLR3.3 are the two GLRs highly expressed in the pollen. Subcellular localization studies with these two GLRs demonstrated AtGLR2.1-GFP localized to the tonoplast, whereas AtGLR3.3-GFP is found in the sperm plasma membrane as well as the endomembranes (Wudick et al. 2018b).

1.7   Role of glutamate receptors in plants

GLRs in plants are implicated in a wide array of processes, including carbon-nitrogen metabolism, defense response, stomatal closure, pollen tube growth, root growth and development, and drought tolerance.

1.7.1   Light signal transduction

Lam et al. (1998) demonstrated the role of AtGLRs in transmitting light signals in *Arabidopsis*. Hypocotyl length is an important indicator of light-driven development in plants. *Arabidopsis* seedlings grown in normal light conditions exhibit short hypocotyls, whereas limiting light leads to hypocotyl elongation. *Arabidopsis* seedlings treated with DNQX, an antagonist of animal iGluRs, show an increase in hypocotyl length and reduction in light-induced chlorophyll accumulation when grown in light. Dark grown plants do not show any effect on either of these traits. The treatment of light-grown *Arabidopsis* plants with BMAA, an agonist of animal iGluRs, also promotes hypocotyl elongation and inhibits cotyledon opening (Brenner et al. 2000).

1.7.2 Defense response

Glutamate receptors play both direct and indirect roles in plant defense response. Over-expression of a GLR from small radish, *Raphanus sativus* (RsGLR) in *Arabidopsis* improves resistance to necrotic fungal pathogen *Botrytis cinerea* (Kang et al. 2006). AtGLR3.3 is involved in mediating resistance to downy mildew, caused by the oomycete, *Hyaloperonospora arabidopsidis* (Manzoor et al. 2013). In addition, AtGLR3.3 plays a role in glutathione (GSH) mediated defense response against the bacterial pathogen, *Pseudomonas syringae* (Li et al. 2013) as well as in defense response to mechanical wounding (Mousavi et al. 2013).

Plants recognize MAMPs (Microbe Associated Molecular Patterns) and DAMPs (Damage Associated Molecular Patterns) as foreign molecules and elicit a defense response. Bacterial and fungal MAMPs (elf18, flg22, and chitin) trigger a rapid influx of calcium ions from the apoplast (Kwaaitaal et al. 2011). This MAMP-triggered Ca^{2+} flow is disrupted by inhibition of the GLRs using iGluR antagonists (AP-5, AP-7, kynurenic acid). The treatment with kynurenic acid also causes a decrease in transcripts of some of the MAMP-triggered defense genes. Damage to the plant cell wall elicits the production of oligogalacturonides (OGs), which in turn induce a defense response. Manzoor et al. (2013) demonstrated the involvement of AtGLR3.3 in OGs-triggered immune response. Antagonists of iGluRs, including DNQX, CNQX, and MK-801 cause a 55–60% reduction in OGs-triggered cytosolic calcium ($[Ca^{2+}]_{cyt}$) variations.

Induced plant defense response generally involves the production of reactive oxygen species (ROS), variation in cytosolic calcium concentrations, production of reactive nitrogen species like NO, membrane depolarizations, production of antimicrobial compounds such as phytoalexins and accumulation of defense gene transcripts (War et al. 2012). Vatsa *et al.* (2011) demonstrated the role of GLRs in cryptogein-induced Ca^{2+} influx and NO production. Cryptogein triggers the influx of Ca^{2+} and is a well-known elicitor of hypersensitive response in tobacco. Treatment of tobacco cells with iGluR antagonists shows a reduction in cryptogein-induced Ca^{2+} influx as well as a decrease in NO.

Jasmonate dependent defense response was observed in plants upon mechanical wounding. Mousavi et al. (2013) showed that electrical signals generated upon wounding travel to the distal leaves in *Arabidopsis* and are followed by the accumulation of jasmonates and expression of jasmonate responsive genes. These wound-activated surface potential (WASP) changes travel at

an average speed of 5.86 ± 1.1 cm/min from the wounded leaf to the distal unwounded leaves. AtGLR3.3 and AtGLR3.6 are involved in propagating these wound-induced signals rather than generating them (Hedrich et al. 2016). These findings are consistent with another study by Salvador-Recatalà (2016), which reported that GLR3.3 and GLR3.6 mediate the propagation of signal from the wounded leaf to the neighboring unwounded leaves, whereas GLR3.5 acts as off switch and prevents the transmission of the wound signal. Toyota et al. (2018) demonstrated a rapid increase in the $[Ca^{2+}]_{cyt}$ at the site of wounding induced by feeding caterpillar or mechanical damage. The velocity and pattern of $[Ca^{2+}]_{cyt}$ changes are similar to that of WASPs observed by Mousavi et al. (2013). The increase in cytosolic Ca^{2+} is accompanied by an increase in the expression of defense responsive genes and accumulation of JA and JA-Ile. The double mutant *glr3.3glr3.6* completely inhibits the propagation of $[Ca^{2+}]_{cyt}$ signal.

1.7.3   Stomatal movement

AtGLR3.1 and AtGLR3.5 are two GLRs highly expressed in the guard cells suggesting their role in guard cell signaling (Yoshida et al. 2016; Cho et al. 2009). Transgenic plants overexpressing AtGLR3.1 show an impaired stomatal closure in response to external Ca^{2+} (Cho et al. 2009). Cytosolic calcium concentration regulates the stomatal closure by two mechanisms: short-term calcium reactive closure and long-term closure (Allen et al. 2001). Short-term closure occurs rapidly upon an increase in $[Ca^{2+}]_{cyt,}$ whereas the $[Ca^{2+}]_{cyt}$ oscillations program long term closure. Yoshida *et al.* (2016) showed the involvement of GLR3.5 in Glu-induced stomatal closure in both *Arabidopsis* and fava bean. Ca^{2+}-reactive stomatal closure is significantly impaired in the *glr3.1/3.5* double mutants (Kong et al. 2016) with no impact on the maintenance of stomatal closure.

1.7.4   Stress response

Sivaguru et al. (2003) suggested that GLRs are involved in mediating a response to aluminum (Al). Both Al and glutamate inhibit root elongation in *Arabidopsis* and cause depolymerization of the membrane. Treatment with an iGluR antagonist AP-5 inhibits the responses produced by both Al and glutamate, suggesting their involvement in a single pathway. GLRs are also involved in response to cold stress. Two-week-old *Arabidopsis* plants exposed to

touch or cold show a three to six-fold increase in the expression of *AtGLR3.4* (Meyerhoff et al. 2005). Cold stress also induces an increase in cytosolic calcium levels. Lu *et al.* (2014) showed enhanced drought tolerance in rice and *Arabidopsis* plants overexpressing either of the two rice GLRs, *OsGLR1* and *OsGLR2*.

1.7.5   Root architecture

GLR3.4 and GLR3.2 are involved in lateral root initiation in *Arabidopsis* (Vincill et al. 2013). Knockout mutants *glr3.4* and *glr3.2* produce an increased number of lateral root primordia as compared to wild type. However, the number of emerged lateral roots is not affected. The mutant phenotype is reversed by expressing GLR3.4 in the mutant plants. Both GLR3.2 and 3.4 are localized in the phloem sieve plates and interact with each other. Li *et al.* (2006) demonstrated the role of GLR3.1 in regulating cell division in root apical meristem. Loss of function mutation in GLR3.1 due to T-DNA insertion inhibits root elongation giving rise to a short root phenotype.

1.7.6   Pollen tube growth

Michard et al. (2011) reported the role of GLRs in pollen tube growth. GLR antagonists significantly inhibit the pollen tube growth rate in tobacco. The knockout mutant in *Arabidopsis*, *Atglr2.1,* displays abnormal pollen tube phenotype with deformed tips. Another mutant *Atglr3.7* shows a decrease in the pollen tube growth rate. The GLRs at the tip of the pollen tube are activated by D-Serine ligand, which induces a Ca^{2+} influx.

1.7.7   Carbon and nitrogen metabolism

Carbon and nitrogen are imperative for optimal growth and development in plants. These are involved in various cellular functions, so plants need to maintain carbon/nitrogen balance. Kang and Turano (2003) reported that *AtGLR1.1* is involved in regulating carbon/nitrogen metabolism and controls the germination of seedlings through its effect on ABA biosynthesis. Disrupting the function of *AtGLR* by using DNQX or antisense lines increases ABA levels, which in turn inhibit seed germination.

This chapter summarizes the genes and mechanisms that are known to influence plant height in maize. In addition, we described the glutamate gene family in plants and its role in plant growth and development. Although glutamate receptor gene family influences a plethora of processes in plants but have never been associated with control of plant height. Moreover, this gene family has not been studied in maize. The present study will give insights into role of a glutamate receptor gene in controlling plant height in maize.

CHAPTER 2.   A NOVEL SEMI-DOMINANT DWARF MUTANT IN MAIZE EXHIBITING SENSITIVITY TO GENETIC BACKGROUND

2.1   Introduction

Plant height is a complex agronomic trait that is an important component of plant architecture. Mainly attributed to the total length of the internodes of a plant, plant height is highly heritable and a major contributor to the overall productivity of crops. As explained in chapter 1, it was the introduction of semi-dwarf varieties of wheat and rice during the 1960s and 70s along with the widespread use of fertilizers that led to the green revolution (Khush 2001). Dwarf plants not only responded better to agricultural inputs but were also resistant to lodging. Studies on the green revolution genes *Sd1* in rice and *Rht* in wheat revealed their association with phytohormone gibberellin function (Peng et al. 1999; Monna et al. 2002) and allowed identification of primary targets for crop improvement. In other words, the knowledge of the genes and mechanisms that control plant height helps facilitate breeding programs aimed at manipulating this trait to achieve higher yields.

While dwarfism has not been exploited to improve crop productivity in maize but studies on dwarf mutants such as *an1*, *d1*, *d3*, *d5*, *D8*, *D9, na1, na2, brd1 and br2* have led to the cloning of several genes influencing plant height (Bensen et al. 1995; Winkler and Helentjaris 1995; Multani et al. 2003; Cassani et al. 2009; Lawit et al. 2010; Hartwig et al. 2011; Makarevitch et al. 2012; Chen et al. 2014; Best et al. 2016; Fu et al. 2016). These genes are associated with two key phytohormones gibberellins (GA) and brassinosteroids (BR), which are described in greater detail in chapter 1CHAPTER 1. The *an1, d3* (*dwarf3*), and *d5* are associated with gibberellin biosynthesis; *Dwarf8* and *Dwarf9* encode DELLA proteins and impact gibberellin signaling; *nana1* encoding *DET2* homolog*,* and *nana2* encoding a sterol reductase, disrupt BR biosynthesis; *brd1* encodes a brassinosteroid C6 oxidase involved in final steps of brassinosteroid biosynthesis; and *br2* shows defects in polar auxin transport. The knowledge of various regions in the genome associated with a particular trait is very important to the breeders to achieve higher crop yields. The lack of information, such as unidentified genome regions specific to a particular trait, may hinder the desired outcome. An excellent example of this is a highly complex trait such as plant height, which is not just impacted by hormone biosynthesis or signaling, but is also controlled by

genes like the *AP2* transcription factor-like gene and *ZmRPH1* in maize. (Jiang et al. 2012; Li et al. 2019). However, the functions of these genes are not well understood, which highlights the need to characterize new dwarf maize mutants that will not only allow us to pinpoint the functions of known genes but also make it possible to identify new genes and pathways that regulate the height of a plant.

The results of a breeding program are likely to be influenced by the genetic background of the line into which a trait is introduced. Two lines of maize can be as genetically distinct from each other as are humans and chimpanzees (Buckler et al. 2006). The comparison of whole-genomes of B73 and Mo17 revealed several thousand presence/absence variation sequences that are present in B73 but completely missing in Mo17 and vice versa (Springer et al. 2009). There are several hundred regions that exist in both genomes but exhibit a high rate of copy number variation (Springer et al. 2009). This natural genetic variation is useful in identifying main-effect QTLs that have a significant impact on the phenotypes (Kaeppler et al. 2000; Mickelson et al. 2002; Eichten et al. 2011; Sorgini et al. 2019; Szalma et al. 2007). However, introgression of a main-effect QTL into a different background does not always result in the desired phenotype due to interactions with other loci in the new background (Bocianowski 2013). In hybrid backgrounds like Mo17/B73, where the two parents are highly diverse, the interactions of single-locus QTLs with the other regions can either enhance or suppress the effect of the original QTL. Several studies with maize mutants have shown the impact of genetic background on different traits like plant architecture (Lukens and Doebley 1999; Anderson et al. 2019) and lesion mimics (Hoisington et al. 1982; Penning et al. 2004). The mutants in one genetic background might show a severe phenotype, whereas in another background the phenotype can be partially or even completely suppressed.

In this dissertation, we report a semi-dominant dwarf mutant, *D13* with a unique phenotype that is unlike any of the known dwarf mutants. The plants have short stature and accumulate red pigmentation in the tips of juvenile leaves. We describe the effect of genetic background on the *D13* phenotype. The mutant phenotype is clearly visible in B73, whereas it completely disappears when introduced into some other backgrounds such as Mo17 and Oh7B. To map the *D13* modifiers, disease resistance introgression lines (DRIL41) (Lopez Zuniga et al. 2016) were crossed to *D13*/+:B73 heterozygotes and mutant plant height was recorded in the F_1 progeny of each cross. Single marker analysis and composite interval mapping revealed three chromosomal regions associated with the suppressed plant height.

2.2   Material and Methods

2.2.1   Plant material

The *D13* mutant was identified previously in our lab in an M1 population of EMS mutagenized B73. The mutant plant was used as a pollen parent and crossed to inbred B73 to generate progeny segregating 1:1 for wild-type (WT) and *D13*/+:B73 heterozygotes. The mutant has been maintained in heterozygous condition by repeated backcrossing to B73. The heterozygotes show instability in phenotype at maturity so only the severe *D13* plants were used for backcrossing to B73. Homozygous *D13* mutants were obtained by selfing an intermediate *D13*/+:B73 plant. *D13* homozygotes are sterile, so they cannot be used for crossing.

Two F_2 populations generated previously by crossing *D13* heterozygotes with Mo17 and Mo20W were used for mapping *D13* locus. The Mo17 background profoundly suppressed the phenotype of the mutants, whereas mutants were intermediate height in Mo20W. The three backgrounds B73, Mo17, and Mo20W, showed considerable differences in plant height of *D13* mutants, indicating a high impact of genetic background on the mutant phenotype. To further test this in other backgrounds, the mutants from progeny of B73 x *D13*/+:B73, segregating 1:1 for mutant and WT sibling, were crossed to inbreds (A632, Mo20W, and W22) and 25 NAM lines in summer of 2017. As the *D13* heterozygotes in B73 show variable severity in the plant height, so to ensure uniformity, only severe *D13* plants were used for crossing. *D13* heterozygotes were also crossed with 70 DRIL41 lines (Lopez Zuniga et al. 2016) in the summer of 2019 for mapping the modifiers. Seed for 70 DRIL41 lines was provided by Peter Balint-Kurti at NC State University, Raleigh, North Carolina.

2.2.2   Experimental design

The greenhouse experiments were conducted at Lilly greenhouses, Purdue University, West Lafayette, Indiana. The *D13* mutants, both heterozygous and homozygous, were screened under greenhouse as well as field conditions.

The field experiments were conducted at Purdue agronomy center for research and education (ACRE) in West Lafayette, Indiana. Seeds from B73 x *D13*/+:B73, segregating 1:1 for wild type and *D13* heterozygotes were planted in two replications for the phenotypic characterization experiments. The F_1s derived from crossing NAMs and inbreds with *D13*

heterozygotes were evaluated in single replications in 2018 and two replications in a completely randomized design (CRD) during 2019. The 70 F_1 families derived by crossing $D13$/+:B73 with DRIL41 population were evaluated in 2019 with two replications in CRD. Each plot was 3.84 m in length and contained 15-16 kernels. The row-to-row spacing for all experiments was 0.79 meters. The inbred lines B73 and Mo17, B73 x $D13$/+:B73, and Mo17 x $D13$:B73 were included as controls. The F_1 progenies were expected to segregate 1:1 for the mutant and wild type plants.

2.2.3   Phenotyping

The mutants were phenotyped for appearance of anthocyanin pigmentation in the leaves at the seedling stage and for plant height at maturity. Seeds from B73 x $D13$/+:B73 were planted in the greenhouse and the presence/absence of red color on leaves was recorded three weeks after planting.

To study the variation in mutant and wild type at seedling stage, the seeds were germinated in paper towel rolls. Thirty seeds from the cross B73 x $D13$/+:B73 were placed on the unrolled paper towel about 1 inch apart. The paper was then rolled and placed vertically in a beaker containing 100 ml of water. The setup was placed in dark at room temperature and seeds were allowed to germinate for ten days. The root, mesocotyl, and shoot length of the seedlings were measured manually. The root length was measured from the root-mesocotyl transition zone to the tip of the main root. The mesocotyl length was measured from the root-mesocotyl transition zone to the first node. The shoot length included the length of the coleoptile and the first leaf (does not include mesocotyl).

Adult plant height was measured in centimeters from the base of the plant to the topmost leaf collar at maturity. Three mutants and three wild type plants were randomly selected in each F_1 family of inbreds and NAMs crossed to $D13/$+:B73. For the DRIL41 derived F_1s, height was measured for all the plants in each F_1 family. However, only the data of severe mutants were used for QTL mapping. The internode measurements were done for 8-10 plants from all five height groups of $D13$ heterozygotes as well as wild type plants selected from the field. The leaves were removed to expose the stem, and number of internodes was counted from top to bottom, the internode below the tassel being the first. The length of individual internodes was then manually measured on all the plants.

2.2.4 Genotyping

D13 region was mapped to chromosome 5 by map-based cloning in collaboration with Pioneer/Dupont (now Corteva Agriscience). An InDel marker (polymorphic between B73 and Mo17) in the *D13* region was designed to distinguish *D13* heterozygotes and homozygotes in Mo17 background. PCR to detect the InDel marker was performed using forward primer 5'-ATATATCGCATGCAGCGGGG -3' and reverse primer 5'- GCTAGCTGCTTCTTCCGGTT -3'. PCR products were resolved on 3% agarose gel.

The genotypic data for the DRIL41 population was obtained from Peter Balint-Kurti at NC State University, Raleigh, North Carolina. The data was comprised of a total of 337 markers. The genetic map and the map positions of each marker were also obtained from NC State University. The genotypic data was converted into A, B, and H format using "A" for B73, "B" for Mo17, "H" for the heterozygous individuals and "-" for the missing data. A chi-square analysis was performed to determine the segregation ratios of individual markers.

2.2.5 Statistical analysis

The phenotypic data were tested for normality by the Shapiro-Wilk test (Shapiro and Wilk 1965) using SigmaPlot version 14.0 (https://systatsoftware.com/). Paired t-test was also performed using the same software.

2.2.6 Histological analysis

The tissue for histostaining was collected from four-week-old mutant and wildtype plants obtained from B73 x *D13*/+:B73. The leaves were removed from the plants to collect the stems. This experiment was done in collaboration with Yun Zhou and Han Han at Purdue University, West Lafayette, IN. The stem tissues were fixed in FAA solution and embedded in wax. The wax-embedded samples were sectioned with a microtome to observe the shoot apical meristems. The sections were de-waxed, hydrated and stained with toluidine blue as described previously (Zhou et al. 2018).

2.2.7   QTL mapping

QTL mapping was performed using the data for 70 DRIL41 lines. Single marker analysis (SMA) and composite interval mapping (CIM) were executed using WinQTL cartographer version 2.5 (http://statgen.ncsu.edu/qtlcart/WQTLCart.htm). Threshold values were calculated using a 1000 permutation test (Churchill & Doerge, 1994).

2.3   Results

2.3.1   A novel mutant '*D13*' exhibits a semi-dominant dwarfing phenotype

D13 is a novel dwarf mutant that was identified in an EMS mutagenized population of the inbred line B73. Homozygous *D13* plants show a severe reduction in plant height, with the mutants being only 4-10 cm tall while the wild type plants are 160-180 cm tall (Figure 2.1A, B). The phenotype starts to show very early during growth (one week after planting) with the plants appearing very tiny and bearing red pigmentation on the leaves. Figure 2.1C depicts three-week-old *D13* homozygotes showing extensive anthocyanin accumulation in the leaves when grown in the greenhouse. These plants die 3-4 weeks after planting in the greenhouse when all the leaves turn red. On the contrary, *D13* homozygotes in the field show relatively less red pigmentation in the leaves and survive until maturity; however, these do not produce any ears or tassel, and cannot be used for crossing. Also, homozygous *D13* plants tiller profusely in the field (Figure 2.1B).

The *D13* phenotype is semi-dominant, with homozygous plants showing more severity in phenotype than the heterozygotes. *D13* heterozygotes start to show the phenotype much later than the homozygotes. We measured the mesocotyl length, root length, and shoot length in 10-day old-seedlings obtained from B73 x *D13*/+:B73. At this stage of development, the heterozygous *D13* mutants were indistinguishable from their wild type siblings (Figure 2.1D, Figure 2.2). The phenotypic variation began to appear two to three weeks after sowing when the leaf tips in the mutant start accumulating anthocyanin (Figure 2.1E). The red pigment in the leaf tips starts to emerge in the first collar leaf and is also observed at the tips of the second and third leaves but is rarely visible on the fourth leaf or beyond. The reduction in height is noticeable at the V5-V6 stage, approximately four weeks after sowing. At the V6 stage, mutants are shorter in height, and the adjacent leaves are closer to each other, indicating a reduced length of the internodes (Figure 2.1F).

38
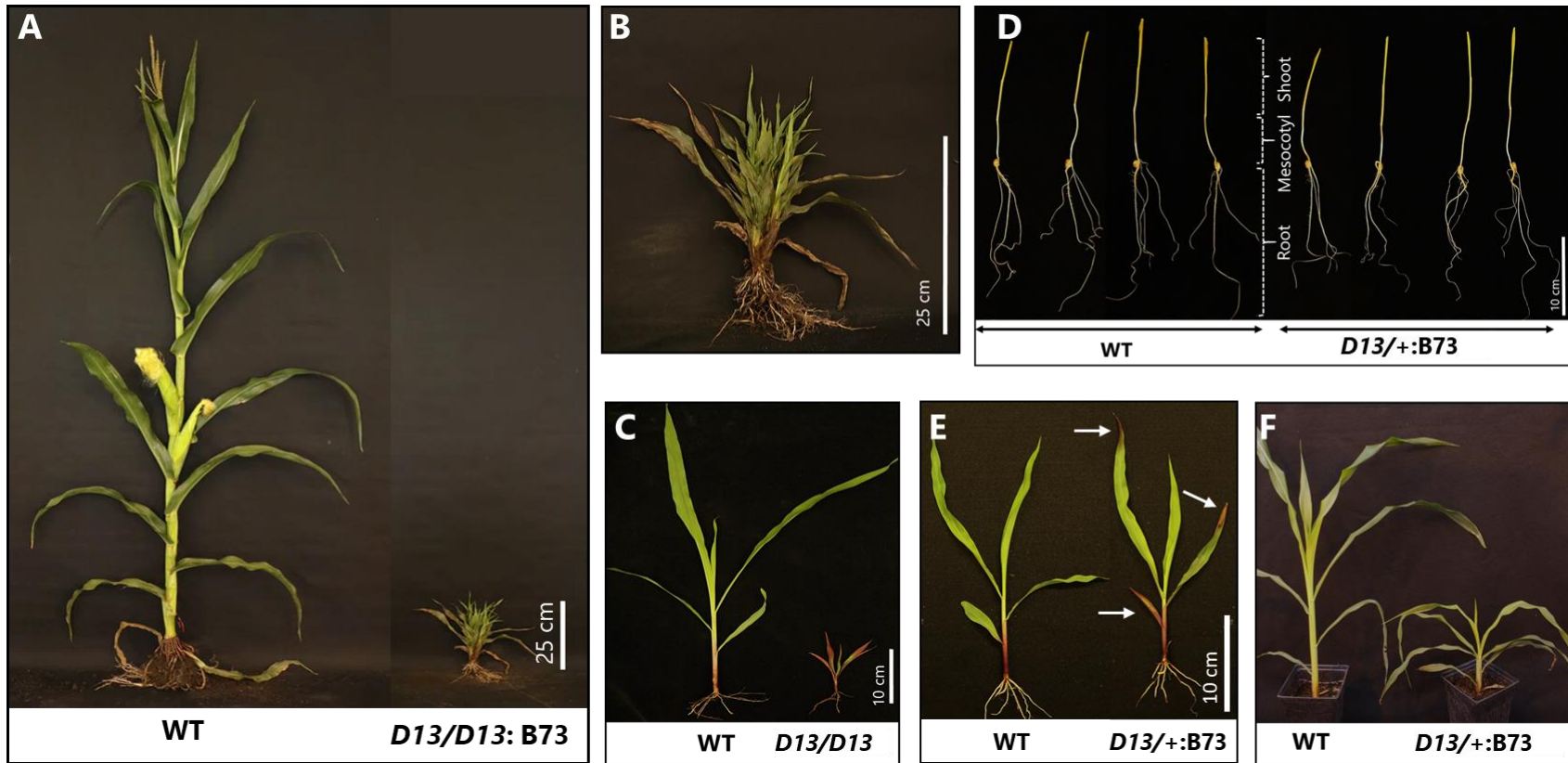
Figure 2.1 Morphology of the *D13* mutant. (A) Variation in the height of wild type (WT) and the homozygous *D13* mutant. (B) Close up view of homozygous *D13* plant showing stunted growth and profuse tillering. (C) Three-week-old WT and *D13* homozygote. The leaves of the mutants turn red. (D) Dark-grown ten-day-old WT and mutant seedlings obtained from B73 x *D13*/+:B73. (E) Three -week -old WT and *D13* heterozygous plants obtained from B73 x *D13*/+:B73. The arrows indicate the red coloration of tips in the mutant. (F) Four-week-old WT and *D13*/+:B73 showing variation in plant height.
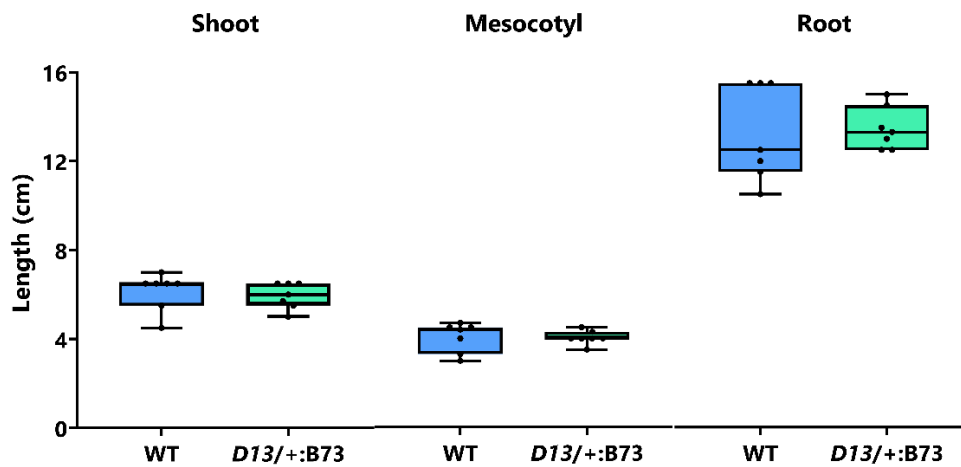
Figure 2.2 The distribution of shoot, mesocotyl, and root length in dark-grown ten-day-old wild type (WT) and mutant (*D13*/+:B73) seedlings obtained from B73 x *D13*/+:B73.
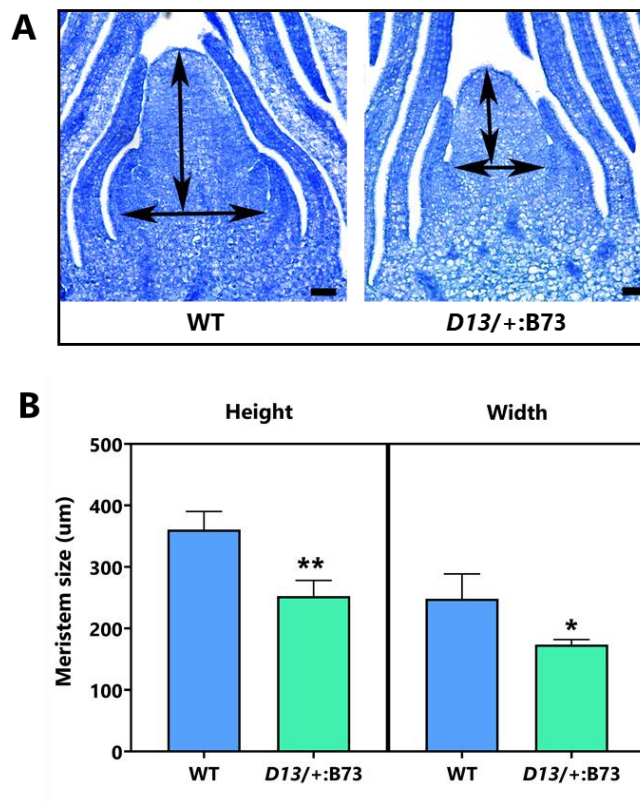
Figure 2.3 The *D13* mutants have a reduced meristem size. (A) The meristem of the wild type (WT) and *D13* heterozygotes obtained from four-week-old B73 x *D13*/+:B73. Scale bar = 250 µm. (B) The distribution of meristem height and width in WT and *D13* heterozygotes.

The *D13*/+ mutants also have smaller shoot apical meristems (SAM), both horizontally and vertically, relative to the wild type siblings (Figure 2.3).

2.3.2   *D13* phenotype is unstable in heterozygous condition

We observed instability in height within the *D13* heterozygotes at maturity (Figure 2.4A). The height of mutants ranged from 13 cm to 140 cm. The mutants could be grouped into five height categories: very severe (v. severe), severe, intermediate (int), intermediate plus (int+) and intermediate ++ (int++). The height of plants in each of the groups, along with the standard deviation (SD) is presented in Table 2.1. A paired student's t-test shows a significant difference in the height of each class compared to the wild type plants as well as other classes. The variability is observed in both greenhouse and field conditions as well as over the years and thus does not appear to be influenced by environmental conditions. The ratio of mutant height to the wild type plant height in B73 ranges from 0.07-0.82.

Table 2.1 Plant height of wild type (WT) and *D13* mutants

Phenotype	n	Average Plant height ± SD	Mutant/WT plant height
WT (B73)	8	170.63 ± 7.5	
Int++	10	140.05 ± 11.37	0.820
Int+	8	101.16 ± 10.53	0.593
Int	10	60.6± 12.97	0.356
Severe	8	35.95 ± 6.48	0.210
V. severe	10	12.96 ± 3.62	0.076
D13/*D13*:B73	5	6.0 ± 2	0.035

The severe and very severe *D13* mutants exhibit high tillering, whereas the taller mutants do not produce any tillers (Figure 2.4A). *D13* heterozygotes flower at the same time as the wild type plants, but variations in the floral organ development exist among the different groups. The very severe and severe mutants mostly bear a tassel and no ear. Ears are sometimes formed in both these groups but are tiny and do not produce any seed. All three intermediate types produce functi-
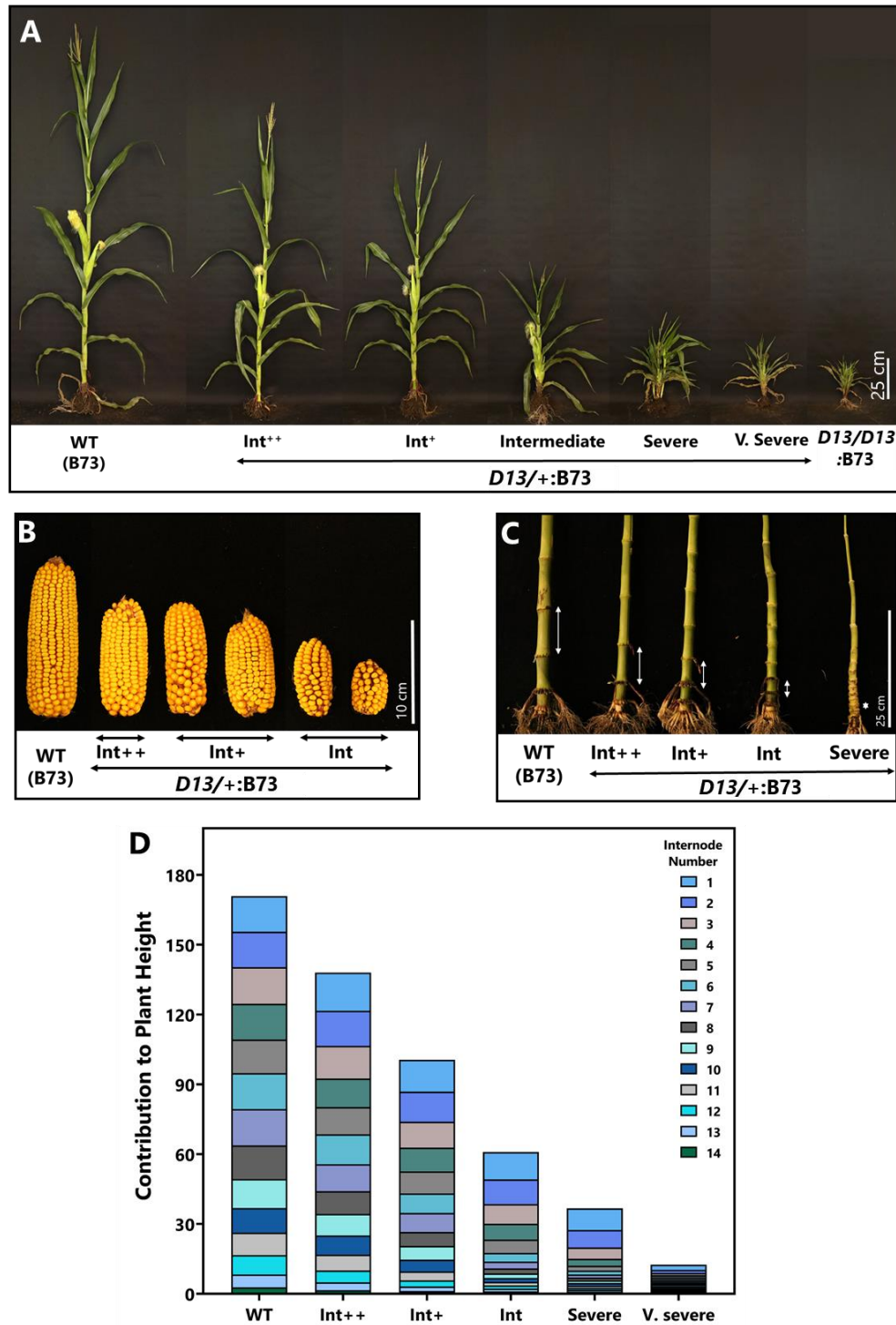
Figure 2.4 The phenotype of *D13* heterozygotes is unstable at maturity. (A) The phenotype of WT and *D13* heterozygotes obtained from B73 x *D13*/+:B73 and *D13* homozygote (extreme right). (B) Size of ear obtained from selfed WT and *D13* heterozygotes. (C and D) Differences in internode length of WT and *D13* heterozygotes obtained from B73 x *D13*/+:B73.

-onal tassels and ears; the sizes of which vary depending on the height of the plant (Figure 2.4B). The reduction in the height of the *D13* plants is due to reduced internode length (Figure 2.4C, D). The decrease is evident in all the *D13* heterozygotes but is relative to the height of the mutant. The very severe mutants have much shorter internodes than the relatively larger intermediate classes. The number of internodes is same in both the mutants and their wild type siblings. Thus, the overall height of the plant is due to the contribution of each internode and not the number of internodes.

2.3.3 *D13* phenotype is sensitive to genetic background

D13/+:B73 heterozygotes, when crossed to Mo17, show complete suppression of the mutant phenotype. The mutant height is similar to the wild type (WT) siblings and is not clearly distinguishable (Figure 2.5A, B). The ratio of mutant/WT height in Mo17/B73 hybrid is 0.9. To further study the effect of genetic background, *D13*/+:B73 heterozygotes were crossed to 25 NAM lines and three inbred lines (A632, Mo20W, and W22). The plant height of the resulting F_1 progenies from all the crosses was measured in one replication in 2018 and two replications during 2019. *D13* was found to be extremely sensitive to the genetic background. As observed in the B73 background, the *D13* phenotype was enhanced (E) in F_1 hybrids obtained from A632, CML228, CML322, and P39. On the other hand, F_1 hybrids from NC350, Oh7B, and Tx303 showed complete suppression similar to that observed in Mo17. In all the other lines, the mutant plants showed an intermediate phenotype. To eliminate environmental effects over the years and between the replications, all plant height data is presented as the ratio of mutant and wild type plants. Mutant to wild type height ratios were consistent for both years in all F_1 families. The average data for both the years is presented in Figure 2.5C.

2.3.4 Mapping of the *D13* locus

An F_2 mapping population was created earlier in the lab using heterozygous *D13* (*D13*/+:B73) as a donor to introgress the *D13* region into Mo17. *D13* was first mapped to the long arm of chromosome 5 (Ch 5) flanked by markers umc1935 and umc1591. A set of 276 plants was selected from the F_2 population for fine scale mapping . In collaboration with Pioneer/Dupont (now Corteva Agriscience), the region was mapped to a ~1.3 Mb interval. To obtain higher mapping
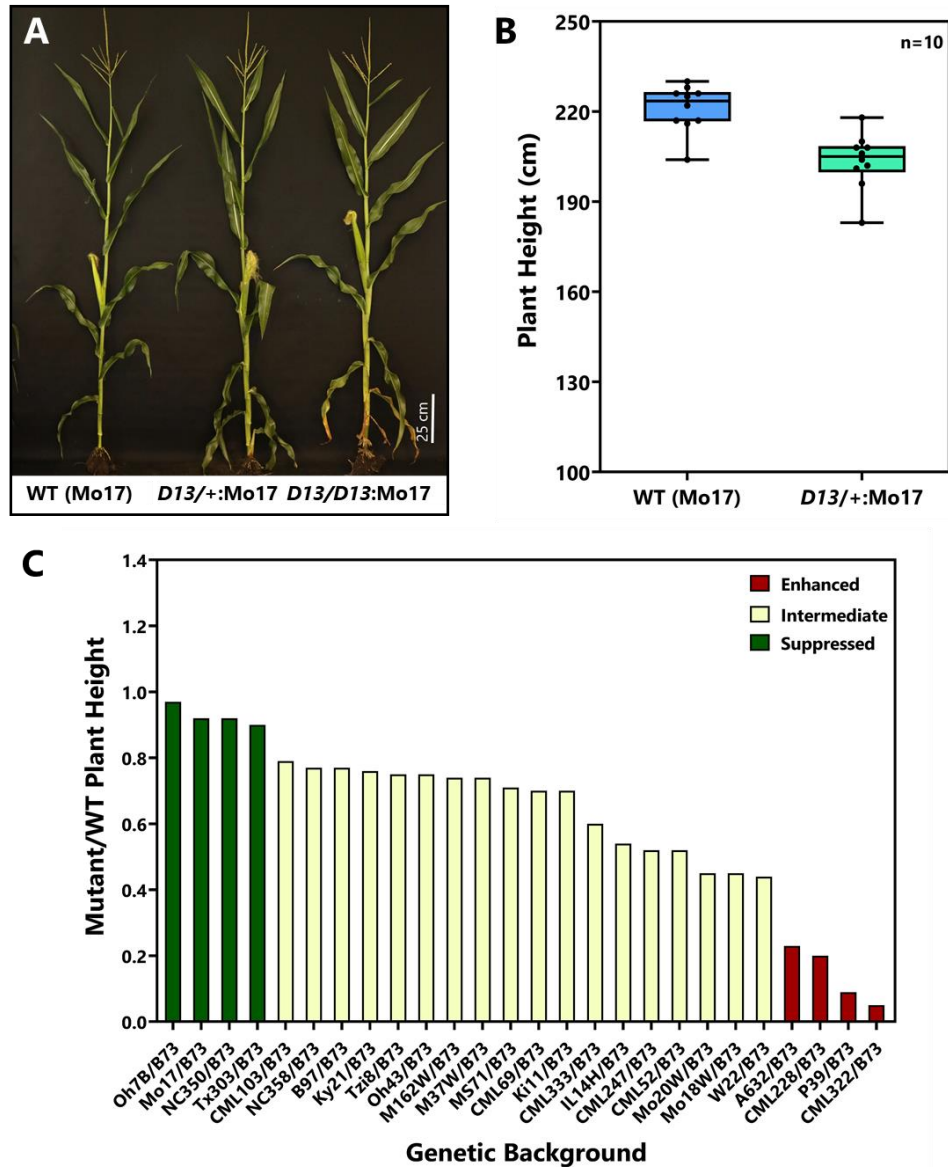
Figure 2.5 Effect of genetic background on *D13* mutants. (A) The phenotype of WT (Mo17), *D13* heterozygote and *D13* homozygote in the Mo17 background. (B) Distribution of plant height in WT (Mo17) and *D13* heterozygotes (*D13*/+:Mo17). (C) The ratio of Mutant/WT plant height in F$_1$s generated by crossing inbreds and NAM lines to *D13*/+:B73.

resolution, 1026 F_2 plants from Mo17 x $D13$/+: B73 were planted. Among these, six recombinants were identified for progeny testing, and the $D13$ region was narrowed down to 630 kb (Figure S1). Mo20W enhances the $D13$ phenotype, so it is easier to screen for the mutant phenotype. This population allowed the mapping of $D13$ to a ~530 kb region, which overlapped with the previously identified $D13$ region. The $D13$ interval contained a total of 15 genes.

2.3.5 DRIL41 population used for mapping the modifier loci

As mentioned above, the $D13$ phenotype shows variable severity in different genetic backgrounds. We hypothesized that the variation in mutant height in different maize lines could be due to the presence of modifier loci. To map these potential modifiers, a mapping population was generated by crossing 70 disease resistance introgression lines (DRIL41) (Lopez Zuniga et al. 2016) to severe $D13$/+:B73 heterozygotes. A single $D13$ heterozygote produces a small amount of pollen, so multiple mutant plants were used as male parents, but pollen from each male parent was kept separate. Only the male parents showing similar severity of the $D13$ phenotype were selected for crossing. The resulting F_1 families from each of these crosses segregated 1:1 for the mutant and wild type phenotypes. The heights of all plants in each F_1 family were measured. Although approximately half of the plants in a F_1 family were mutant, they did not have the same height. Mutants with severe as well as intermediate heights were seen in the same F_1 family. As mentioned earlier, $D13$ mutants in B73 also exhibit such variation, so to eliminate the noise in QTL mapping that could arise by inclusion of suppressed mutants, we only selected the three shortest mutants from each F_1 family for further analysis. Only the F_1 families that did not show any enhanced phenotype in both replications were considered highly suppressed. The mutant/wild type plant height ratio in the 70 DRIL41 F_1s ranged from 0.034 to 0.869, with a mean of 0.454 (Figure 2.6A). The data presented here is the average of two replications. The frequency curve followed a normal distribution with a low skewness value of -0.12 (Figure 2.6B). We identified 12 suppressed F_1 progenies out of 70, with a mutant/wild type ratio of > 0.7.

DRIL 41 is a set of chromosome segment substitution lines ($BC_3F_{4:5}$) generated by crossing Mo17 as the donor to recurrent parent B73. Since we are using a BC_3F_4 population, the background is mostly uniform with variations due to the Mo17 introgression. The considerable variation in mutant height could be due to two reasons: first, it could be due to the differences that we see in the B73 background. Second, it could be due to Mo17 introgression in the regions that suppress
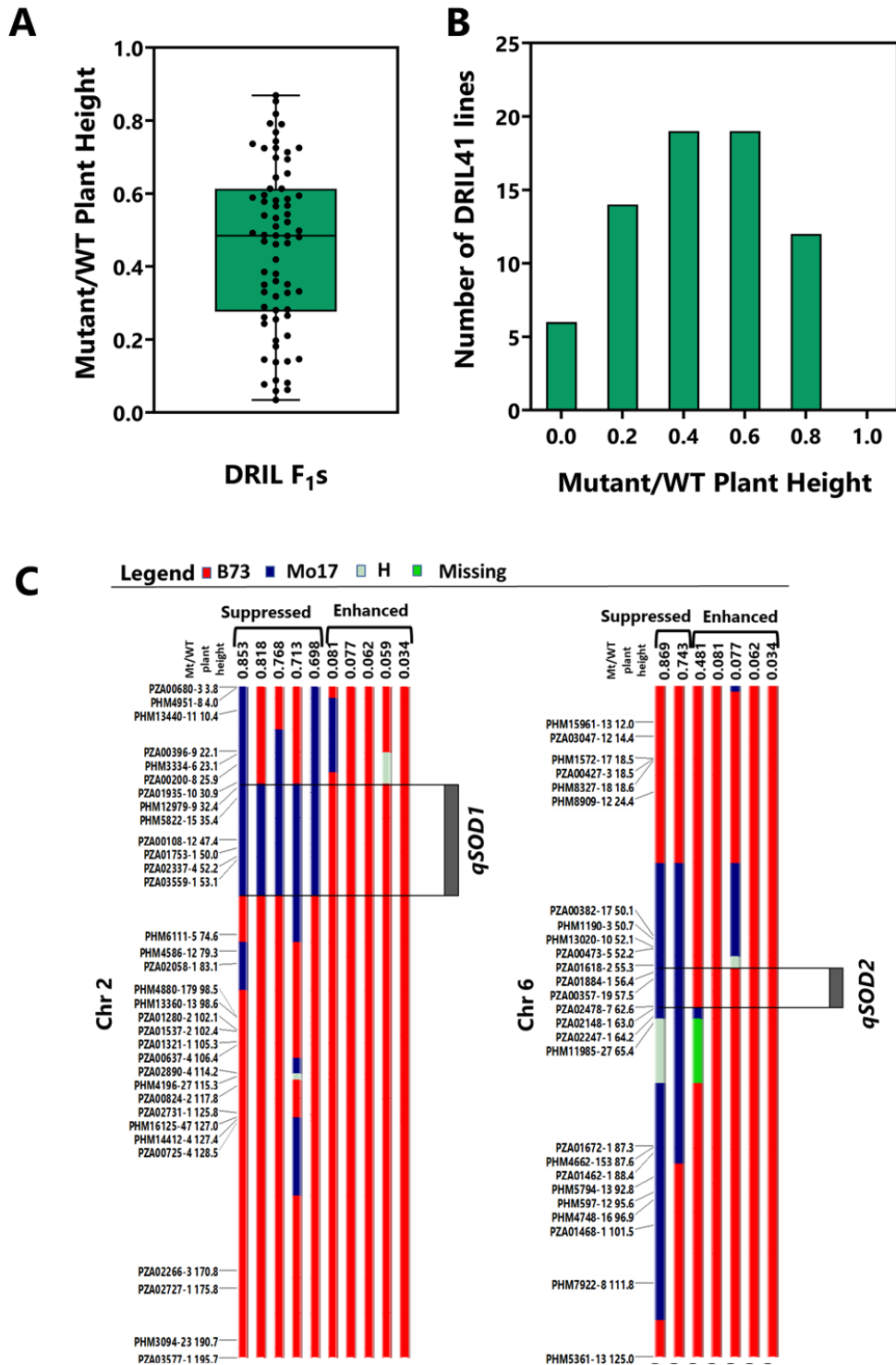
Figure 2.6 Identifying the modifiers of *D13*. (A) Ratio of mutant (Mt) to wildtype (WT) plant height in 70 DRIL41 derived F$_1$s. (B) Frequency distribution of Mt/WT plant height in DRIL41 derived F$_1$ families. (C) The location of QTLs controlling suppression of *D13* on chromosomes 2 and 6. Red bars depict chromosomal regions from B73 background and blue bars represent regions introgressed from Mo17. The grey bars represent the QTLs.

46

the effect of *D13*. To rule out the variation of phenotype that we already see in B73, we only picked the severe mutants in each line.

2.3.6   Identification of *D13* modifying regions

Single marker analysis (SMA) revealed markers associated with the suppression of plant height. The details of the SMA are presented in Table 2.2. A p-value of < 0.5 was selected as the cutoff to select the markers linked to the phenotype. Genotypic data of each selected marker was manually checked to verify that suppressed lines had the Mo17 chromosomal region at these sites (Figure 2.6C) in each DRIL. The selected markers that showed similar Mo17 introgression in enhanced and suppressed lines were not considered as significantly associated with the phenotype. We identified three putative regions on chromosomes 2, 3, and 6 as the potential modifiers. Some of the suppressed lines had Mo17 introgression in these regions, while none of the enhanced lines had any shared introgression of Mo17 genetic material. The introgressed regions that did exhibit a suppressive effect on the mutant were designated as *qSOD1* (Suppressor of *D13*), *qSOD2*, and *qSOD3* (Table 2.2).

Table 2.2 Single marker analysis (SMA)

QTL	Chromosome	Marker	
qSOD1	2	PHM12979-9	<0.01 ***
		PHM58222-15	<0.01 ***
		PZA00108-12	<0.001 ****
		PZA01753-1	<0.001 ****
		PZA02337-4	<0.001 ****
		PZA03559-1	<0.001 ****
qSOD2	6	PZA01884-1	<0.05 **
		PZA00357-19	<0.05 **
		PZA02478-7	<0.05 **
		PZA02148-1	<0.05 **
		PZA02247-1	<0.05 **
		PHM11985-27	<0.05 **
qSOD3	3	PZA00892-5	<0.05 **
		PHM3688-14	<0.05 **

A composite interval mapping approach was then used to identify the QTL associated with plant height in the DRIL41 F_1 population. We detected two QTLs on chromosomes 2 and 6 (Figure 2.6 C). The QTL *qSOD1* explained 17 percent of phenotypic variance, had a LOD score of 3.58 and was localized in a 39.1 cM region, which is ~12 Mb in size. The QTL on chromosome 6, *qSOD2,* explained 11.75 percent of phenotypic variance with an additive effect of 0.2 and LOD score of 3.38. It was located in a 7.29 cM region (~11 Mb). The QTL analysis was also conducted on the wild type data, which confirmed that these QTLs were unique and not an artifact of the DRIL41 population.

2.4   Discussion

The maize dwarfing mutant described in this chapter appeared in an M1 population of B73 that was generated by pollen mutagenesis with EMS. Since recessive mutations do not have a phenotype in the M1 generation, this mutation was expected to inherit in dominant or partially dominant manner. Its re-appearance in an outcross progeny of the mutant with B73 supported this hypothesis. The mutant dwarfing phenotype segregated in a 1:1 ratio with the wild type siblings in this population, indicating that the mutation was dominant and conferred by a single gene. Further characterization of the mutant indicated the mutation to be partially dominant, as the phenotype of the plants homozygous for the mutation is more severe than heterozygous phenotype. This dwarfing-mutation mapped to a region on chromosome 5 where no other dwarfing locus has been previously reported, strongly indicating that the mutation belongs to a new dwarfing locus, which we designated as *d13*, and the mutant allele is designated as *D13*. This new dwarfing locus has been given the number 13 because dwarf loci up to *d12* have already been described (https://www.maizegdb.org/).

In addition to the dwarf stature, *D13* has two other phenotypic aberrations including the reddening of seedling leaves, and enhanced tillering. While both these additional phenotypes are prominent in *D13* homozygotes, they also show up in severe *D13* heterozygotes. The reddening of the leaves is restricted to the tips of the first 3 to 4 leaves on *D13* heterozygotes, whereas it covers almost the entire leaf blade in homozygotes. This red color is likely due to the accumulation of anthocyanins, which form in maize either because the plants are experiencing stress (biotic or abiotic), or the leaves are compromised in their ability to export sugars (Efeoğlu et al. 2009; Christie et al. 1994; Braun et al. 2006; Janda et al. 1996). We were able to rule out the latter

possibility (unpublished data), implying that the red coloration of the leaves is likely due to some physiological stress that the *D13* mutation imposes on maize seedlings. Enhanced tillering in *D13* suggests that the mutants either suffer from auxin deficiency, which would release the lateral shoots from apical inhibition, or aberration in the function of strigolactones, a class of phytohormones that control branching in plants (McSteen 2009).

The dwarf stature of *D13* mutants results from the shortening of the internodes, with no change in the total number of internodes. Internode elongation is mediated by cell division, cell elongation, or a combination of these two processes and is mainly regulated by phytohormones including gibberellins (GAs), brassinosteroids (BRs), auxins and strigolactones (Wang et al. 2018). GAs influences both cell elongation and cell division, whereas auxins and BRs mainly control cell elongation. Stem elongation can also be controlled by interactions between various phytohormones. However, the mechanisms by which these hormones promote cell elongation or division are not fully understood. The dwarf mutants characterized in maize show variable patterns of internode elongation, which suggests that the underlying mechanisms in these mutants might be variable. In maize, most of the GA and BR mutants usually have uniformly short internodes (Bensen et al. 1995; Cassani et al. 2009; Wang et al. 2013; Best et al. 2016). However, there are other mutants like BR-deficient *na1* in which internodes are not equally reduced in length. Moreover, internode lengths are also variable among *na1* mutants. In *brevis plant1* mutants, which are proposed to be involved in auxin mediated signaling, all internodes are shorter than wild type, but the reduction is more prominent in the upper internodes. In contrast, *br2* mutants (associated with polar auxin transport) are characterized by reduction in length of lower stalk internodes (Multani et al. 2003). The internodes of the *D13* heterozygotes are not equally reduced in height. The very severe and severe mutants show higher reduction in the length of each internode than all the intermediate *D13* mutants. The decrease in length is observed in all the internodes and is not restricted to top or bottom internodes.

One question that arises here is whether the *D13* dwarfing phenotype results from the functional impairment of some of the major pathways known to mediate cell elongation in maize, such as the GA or the BR pathway. Mutants of these two pathways are not only dwarf but also impacted in the development of male and female inflorescences (Bortiri and Hake 2007). For instance, GAs prevent the development of male floral primordia in the ear (the female inflorescence), thereby causing it to have only ovules (Bortiri and Hake 2007). But when GAs are

49

not produced or perceived, the male primordia are not arrested, allowing the ears to develop functional anthers (called the anther-ear or andromonoecious phenotype) (Harberd and Freeling 1989; Bensen et al. 1995; Cassani et al. 2009; Chen et al. 2014). In contrast, the BRs terminate the development of female primordia in the tassel (male inflorescence). When BR production or perception is hindered, the ovules continue to develop in the tassel, giving it a tassel-seed (gynomonoecious) phenotype (Hartwig et al. 2011; Makarevitch et al. 2012; Best et al. 2016). The *D13* mutants do not exhibit either of these sexually aberrant phenotypes, indicating that their dwarfing phenotype may not result from impairments in either the GA or the BR pathway. Another indication that the *D13* phenotype is unrelated to those pathways comes from the elongation phenotype of the mesocotyl, which is an embryonic stem whose function is to push the coleoptile (shoot/modified leaf) out of the soil. In both the GA and BR mutants, the mesocotyl fails to elongate in etiolated seedlings (Landoni et al. 2007; Cassani et al. 2009; Hartwig et al. 2011; Makarevitch et al. 2012; Best et al. 2016), while this elongation remains largely unaltered in *D13* seedlings. Furthermore, none of the 15 genes, that lie in the genomic region delimiting *d13* locus, have ever been shown to have a role in the function of GAs or BRs, or any other phytohormone. Therefore, it is very likely that the *D13* phenotype results from a novel mechanism not found to be associated with dwarfing in plants thus far.

An intriguing feature of *D13*/+ heterozygous mutants is their phenotypic instability. Even in the completely uniform background of B73, the *D13* heterozygotes can range in height from being less than a foot to more than 4 feet tall. This kind of variability in plant height has not been reported for any of the known dwarf mutants in maize or any other plant species. What causes *D13*/+ to have this height variability remains unclear. One possibility is that it is the result of epigenetic changes in the mutant gene or the genes that it interacts with. It has been previously shown that plants can undergo epigenetic regulation in response to stresses to ensure survival and adapt to environmental fluctuations (Thiebaut et al. 2019; Chinnusamy and Zhu 2009). In fact , there are indications of increased stress response in *D13* that are discussed in detail in chapter 3.

Another interesting feature of *D13* is the dramatic sensitivity of its phenotype to the genetic background. While some genetic backgrounds such as CML322 enhance its phenotype, others suppress it to varying degrees, indicating the involvement of genetic modifiers in shaping the trait underlying *D13*. This dependence of *D13* on genetic background was first observed with Mo17, which suppressed the mutant almost completely. As a result, it was possible to generate *D13*

homozygotes, which looked identical to wild type Mo17. To dissect the genetic basis of this suppression by Mo17, we used a NIL population in which the Mo17 genome had been introgressed as fragments into the B73 genome. Three QTL regions on chromosomes 2, 3, and 6 were identified that modified the height of *D13* plants. These QTL regions are still fairly large and need to be narrowed down further to identify the modifier genes.

CHAPTER 3.   A GAIN-OF FUNCTION MUTATION IN A GLUTAMATE RECEPTOR GENE IMPACTS PLANT ARCHITECTURE AND TRIGGERS STRESS RESPONSE IN CORN

3.1   Introduction

Glutamate receptors are tetrameric non-selective cation channels well-known for their role in neurotransmission in the mammalian central nervous system. While mammals have two types of glutamate receptors: ionotropic (iGluRs) and metabotropic (mGluRs), only ionotropic glutamate receptor-like (GLR) genes have been found in plants, which were first discovered in *Arabidopsis* in 1998 (Lam et al. 1998). A*rabidopsis* has 20 GLRs (AtGLRs) grouped into three clades based on their sequence similarity (Chiu et al. 2002). GLR gene families have also been identified in other plants like mosses, tomato and rice with each comprising 2, 13 and 24 genes respectively (Ortiz-Ramírez et al. 2017; Aouini et al. 2012; Lu et al. 2014; J. Li et al. 2006; Singh et al. 2014). In addition to the three clades initially identified in *Arabidopsis*, a fourth clade of GLRs also exists among the land plants (Bortoli et al. 2016). The glutamate receptors in plants share common ancestry with iGluRs but diverged very early from animal iGluRs, even before the divergence of different classes of iGluRs (Chiu et al., 1999; 2002).

Despite their early divergence, plant GLRs are structurally similar to animal iGluRs consisting of an N terminal domain (NTD), two ligand-binding domains, three transmembrane domains (M1, M3, M4), a pore domain (M2) and a C terminal domain (Madden 2002; Lam et al. 1998). The structural domains share 16 to 63% sequence identity with the highest identity in the M3 region (Lam et al. 1998; Chiu et al. 1999). GLRs in *Arabidopsis* have been shown to mainly localize at the plasma membrane (Meyerhoff et al. 2005; Vincill et al. 2012), however, they can also be targeted to other cellular compartments like chloroplasts, mitochondria, and vacuoles (Teardo et al. 2011; Kong et al. 2016; Wudick et al. 2018b).

Since their discovery, plant GLRs have paved the way for understanding signaling and communication in plants. They have been shown to influence a plethora of processes, including pollen tube growth, stomatal closure, root growth and development, light signal transduction, drought tolerance, and defense response. It is not possible to generalize the functions of this

receptor family, but their roles can be divided into two major categories: (i) plant growth and development, and (ii) plant response to environmental stress.

The effects of GLRs on plant growth and development have been reported from the very first stage of plant growth i.e. seed germination. *AtGLR3.5* promotes germination by increasing cytosolic Ca^{2+} concentration that, in turn, mitigates the inhibitory effect of ABA (Kong et al. 2015). GLRs also influence shoot architecture in plants. The first report of glutamate receptors in *Arabidopsis* revealed that blocking the GLRs by treatment with DNQX (an antagonist of iGluRs) led to an increase in hypocotyl length in light-grown seedlings. The treatment of light-grown *Arabidopsis* plants with BMAA (an agonist of animal iGluRs) also promotes hypocotyl elongation (Brenner et al. 2000). *AtGLR3.4* and *AtGLR3.2* are involved in lateral root initiation in *Arabidopsis* (Vincill et al. 2013). *AtGLR3.6* plays a role in regulating root architecture in *Arabidopsis* (Singh et al. 2016). A T-DNA insertion mutant (*atglr3.6-1*) displays a reduction in primary and lateral root density as well as the size of root apical meristem, whereas *AtGLR3.6* overexpression enhances the root growth. A loss of function mutation in rice *GLR3.1* leads to a short-root phenotype in the early seedling stage (Li et al. 2006). The mutant phenotype comprising a reduced length of primary and lateral roots and smaller diameter of primary root apex can be restored to wild type by genetic complementation with the *GLR3.1* gene, thus, confirming the role of this gene in root development. Michard et al. (2011) reported a role for GLRs in pollen tube growth in tobacco and *Arabidopsis*. Glutamate receptors also play a role in the stomatal movement in plants (Cho et al. 2009; Yoshida et al. 2016; Kong et al. 2016). However, there are no reports of glutamate receptors directly or indirectly influencing plant height.

Besides their role in growth and development, glutamate receptors are also involved in response to environmental stimuli like pathogens, wounding, or abiotic stresses. *AtGLR3.3* mediates resistance to downy mildew caused by *Hyaloperonospora arabidopsidis* (Manzoor et al. 2013). Besides, *AtGLR3.3* is required for GSH (reduced glutathione) mediated Ca^{2+} signaling in *Arabidopsis*. The loss of function *atglr3.3* mutant shows a reduction in expression of pathogen-induced defense genes and an increased susceptibility to the bacterial pathogen *Pseudomonas syringae* pv *tomato* DC3000 (Li et al. 2013). Overexpression of small radish GLR (*RsGLR)* in *Arabidopsis* improves resistance to *Botrytis cinerea* by upregulating jasmonic acid (JA) responsive and biosynthetic genes (Kang et al. 2006). Similarly, the resistance of tomato fruits to *Botrytis cinerea* can be achieved by pre-treatment with L-glutamate that leads to an upregulation of GLRs

and pathogenesis-related (PR) proteins (Sun et al. 2019). Tomato fruits treated with DNQX, do not show resistance to pathogen despite the presence of L-glutamate, thus suggesting that enhanced resistance due to L-glutamate treatment is mediated through GLRs.

Plants respond to mechanical wounding (caused by herbivore feeding or insect damage) by inducing a jasmonate dependent defense response in the unwounded regions, which is made possible by long-distance electrical signaling from the wounded tissue to the unwounded parts of the plant. GLRs (*AtGLR3.3* and *AtGLR3.6*) are involved in the propagation of these wound-induced signals in leaves (Hedrich et al. 2016; Mousavi et al. 2013; Salvador-Recatalà 2016). The electrical activity is greatly reduced in the wounded leaves of the *glr3.3 glr3.6* double mutant. Toyota et al. (2018) demonstrated that GLRs trigger a rapid increase in $[Ca^{2+}]_{cyt}$ in response to wounding caused by a feeding caterpillar or mechanical damage.

Glutamate receptors are also involved in response to abiotic stimuli like salt, cold, and drought. In *Arabidopsis*, *AtGLR1.2* and *AtGLR1.3*, confer cold tolerance by increasing endogenous jasmonate levels and promoting the CBF/DREB1 cold response pathway (Zheng et al. 2018). Meyerhoff et al. (2005) reported a three to six-fold increase in the expression of *AtGLR3.4* in two-week-old *Arabidopsis* plants when exposed to touch, cold, or osmotic stress in a calcium-dependent manner. In tomato, *SlGLR3.3* and *SlGLR3.5* are involved in cold acclimation-induced chilling tolerance (Li et al. 2019). The exposure of *Arabidopsis* wild type seeds to NaCl has an inhibitory effect on seed germination, that is alleviated by exogenous supply of amino acids (Cheng et al. 2016). The mutants *atglr3.4* and *atglr3.7* have even lower germination rates than the wild type when exposed to NaCl and the exogenous amino acids are less effective in mitigating NaCl-induced inhibition in mutants. Also, the germination rates of mutants were less sensitive to DNQX under salt stress than the wild type plants. These results indicate that GLRs are involved in seed germination under salt stress (Cheng et al. 2016). Another study reported that mutant line *glr3.7-2* shows a much lower increase in $[Ca^{2+}]_{cyt}$ concentration than the wild type when exposed to salt stress (Wang et al. 2019) and the GLR3.7-S860A overexpression line is less sensitive to salt stress than wild type.

Significant progress has been made in determining the function of glutamate receptors in *Arabidopsis* in the last few years, yet we know very little about their function in other plant species. Considering that this gene family was identified 22 years ago, the progress in *Arabidopsis* has been

slow as it is a challenge to fully characterize this receptor family due to lack of mutants with clear phenotypes. This is likely a result of high gene redundancy and functional overlap between the 20 members of this gene family in *Arabidopsis*. Therefore, it is important to develop mutants with clear phenotypes to fully understand the functions of the plant GLR gene family. Only four of the knockout mutants developed so far in *Arabidopsis* (*glr3.2*, *glr3.4*, *glr2.1,* and *glr3.7*) have a clear phenotype. The mutants *glr3.2* and *glr3.4* show an overproduction of lateral root primordia (Meyerhoff et al. 2005; Vincill et al. 2013). The other two mutants, *glr2.1* and *glr3.7,* are defective in pollen tube growth (Michard et al. 2011). None of these mutants show any defects in shoot architecture and moreover, there are no mutants for this gene family available in maize.

In chapter 2, we described a novel semi-dominant dwarf mutant (*D13*) in maize identified from an EMS mutagenized population of B73. The *D13* homozygotes show a severe reduction in height with an accumulation of red pigmentation at leaf tips in young seedlings. Compared to *D13* homozygotes, the phenotype is relatively less severe in the heterozygous condition. *D13* mutants are also characterized by shorter internodes and a smaller shoot apical meristem (SAM) as compared to wild type. The phenotype of *D13* mutants is unlike any of the know dwarf mutants in maize. In addition, genetic background has a significant impact on the mutant phenotype with some backgrounds highly enhancing the phenotype while others completely suppressing it.

In this study, we report that a single base change in one of the glutamate receptor genes is responsible for the *D13* dwarfing phenotype. This change occurs in a highly conserved motif. We generated a second mutation in the gene using EMS mutagenesis to validate the causal effect of this gene on the *D13* phenotype. Transcriptomic and metabolomic profiling was performed to shed light on the biological processes impacted in the mutants. In addition, we identified seventeen glutamate receptor genes in maize and studied their phylogenetic relationship with other known GLRs.

3.2   Material and Methods

3.2.1   Plant material

We have maintained *D13* mutant (*D13*/+:B73) in our lab in heterozygous condition by repeated backcrossing to inbred line B73. The progenies of crosses B73 x *D13*/+:B73, segregating 1:1 for wild type:mutant phenotypes were used for co-segregation analysis, stem cross-sections,

RNA-sequencing, and metabolite profiling. The *D13* region was introgressed into inbred Mo17 by crossing with *D13*/+:B73 and repeated backcrossing with Mo17 for six generations. BC_6 progenies were planted in the greenhouse and heterozygous plants were sib mated to generate homozygotes. Pollen from three randomly selected *D13* homozygotes (*D13*/*D13*:Mo17) was treated with EMS and individually crossed to CML322 during the summer of 2017 and the M1 families were screened for loss of *D13* phenotype in summer 2018. Tall M1 plants were identified and crossed to B73 and the resulting progenies were screened in summer 2019.

3.2.2   Experimental design

The field experiments were conducted at Purdue agronomy center for research and education (ACRE) in West Lafayette, Indiana. Each plot was 3.84 m in length and contained 15-16 kernels. The row-to-row spacing for all experiments was 0.79 meters.

A total of 296 seeds from *D13*/+:Mo17 sib-mated progeny were planted in the field along with the inbreds B73 and Mo17, and B73 x *D13*/+:B73 progeny included as controls. Two rows of inbred line CML322 were planted immediately adjacent to this material. Three homozygous plants (*D13*/*D13*:Mo17) were selected from the above 296 plants and pollen mutagenized with EMS. The mutagenized pollen was then put on the ears of CML322. The ears produced from crosses with the three pollen parents were harvested separately. A total of 16230 M1 seeds (216 ears) from three M1 families were planted in summer 2018. Unlike Mo17/B73, CML322/Mo17 hybrid background does not mask the *D13* phenotype. The M1 plants in CML322/Mo17 background were expected to be shorter than the parents, and only the plants with the knockout of the *D13* allele were expected to be tall like the wild type. Tall M1 plants were selected and crossed to inbred B73 for progeny testing. The resulting F_1 families were planted in two replications in completely randomized design (CRD) in summer 2019. The inbred lines B73, Mo17, CML322, and progeny of B73 x *D13*/+:B73, CML322 x *D13*/+:Mo17 were included as controls. The tall plants, being CML322/Mo17/B73 hybrids, were expected to be taller than all the inbreds. Only F_1 families in which all the plants were tall in both the replications were considered as true positives and used for further analysis. The selected families were genotyped with an Indel linked to *D13* locus to confirm the presence of *D13* allele and rule out any contaminants. The crossing scheme for this experiment is represented in Figure 3.1.
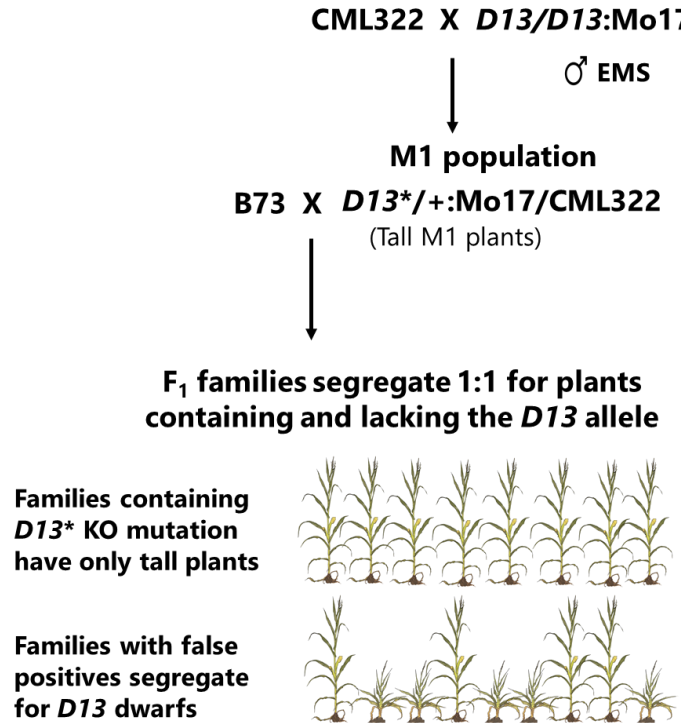
CML322 X *D13/D13*:Mo17

♂ EMS

M1 population

B73 X *D13*/+:Mo17/CML322

(Tall M1 plants)

F₁ families segregate 1:1 for plants containing and lacking the *D13* allele

Families containing *D13** KO mutation have only tall plants

Families with false positives segregate for *D13* dwarfs

Figure 3.1 Schematics of the experimental design to knockout (KO) *D13* allele by EMS mutagenesis.

Co-segregation analysis: Exome sequencing identified a G to A change in coding region of gene Zm00001d015007 in the *D13* mutants. To test the co-segregation of plant height with the G to A SNP in Zm00001d015007 gene, we selected 192 individuals (96 wild type and 96 mutant) displaying the wild type or dwarfing phenotypes from the progeny of B73 x *D13*/+:B73 in the field. The data for the presence or absence of red leaf tip phenotype was collected in the greenhouse. Sets of 54 plants with no red pigmentation and 60 plants displaying red pigmentation on leaf tips were selected from the cross B73 x *D13*/+:B73.

Stem and root cross-section: Heterozygous *D13* plants (*D13*/+:B73) were selfed to generate *D13* homozygotes. The selfed seed was planted in soil beds in the greenhouse. The stems were collected from three homozygous, heterozygotes and wild type plants each, three weeks after planting. For the four-week old stem samples, the progeny of B73 x *D13*/:B73 was planted in the greenhouse in 6-inch pots to obtain *D13* heterozygotes and wild type. The mesocotyl and root samples from ten-day old seedlings were obtained by germinating the seeds from B73 x *D13*/+:B73 in paper towel rolls. The paper towel rolls were placed vertically in a beaker containing 100 ml of water and the setup was placed in dark at room temperature.

RNA-sequencing and metabolite profiling: The seeds from two crosses, B73 x *D13*/:B73 and Mo17 x *D13*/:Mo17, were planted in 99 six-inch square pots in the greenhouse with two seeds per pot. All plants were genotyped to identify the wild type and *D13* heterozygotes. The mutant and wild type plants were divided into three groups/biological replicates each, with ten plants per replication. The samples, comprising one-inch stem sections from base of the plant, were collected four-weeks after planting (around V5 developmental stage). Samples were placed immediately in liquid nitrogen and stored at -80°C. The one-inch sections included the stem, the shoot apical meristem (SAM), and the surrounding leaf sheaths. Metabolite profiling was performed using same mutant and wild type samples but only in B73 background.

3.2.3   EMS mutagenesis

Targeted EMS mutagenesis to knockout the *D13* allele was performed as described by Neuffer (Neuffer 1994). EMS stock solution was prepared by dissolving 1 mL of EMS (Sigma-Aldrich) in 99 mL of paraffin oil overnight. Fresh working solution was then made by mixing 1ml of stock solution with 14ml paraffin oil. Pollen was collected from three *D13* homozygotes (*D13*/*D13*:Mo17) and placed in individual small Nalgene bottles. Freshly prepared EMS working solution was added to the bottle in a ratio of 10 parts solution to 1-part pollen. The bottles were placed on ice for 45 minutes and gently inverted every 5 minutes. The treated pollen was then spread onto the silks of inbred line CML322. The ears from crosses with the three pollen parents were harvested separately.

3.2.4   Genotyping

A dCAPS marker designed using the G to A change in Zm00001d015007 gene was used to distinguish the mutant and wild type plants in the progeny of crosses: B73 x *D13*/+:B73. DNA was extracted using the standard CTAB method (Doyle 1991). PCR amplification was performed in a 12 µl reaction (Saiki 1990) using the forward primer 5'- GCCTTTCCTGTTCAGTCCTTC -3' and reverse primer 5'- TGCACGGTTAGGATGGAAGTAAGACCTG -3'. The PCR products were digested with *PstI* enzyme (New England Biolabs, MA, USA) for 3 hours at 37°C. An InDel marker flanking the *D13* region was designed to genotype the progeny of Mo17 x *D13*/:Mo17 and B73 x *D13*/+:CML322/Mo17 crosses. PCR to detect the InDel marker was performed using

forward primer 5'- ATATATCGCATGCAGCGGGG -3' and reverse primer 5'-GCTAGCTGCTTCTTCCGGTT -3'. PCR products were resolved on 3% agarose gel.

3.2.5 Histological analysis

Histostaining was performed in collaboration with Yun Zhou and Han Han at Purdue University, West Lafayette, IN. The tissues collected from *D13* (both homozygous and heterozygous) as well as wild type plants were fixed in FAA solution and embedded in wax. The wax-embedded samples were sectioned with a microtome. The cross-sections of the stem were obtained from second internode, counted from the bottom. The mesocotyl and root cross-sections of ten-day old seedlings were obtained at approximately 1 cm from the root-shoot interface. The sections were de-waxed, hydrated and stained with a combination of Alcian blue and Safranin O, as described previously (Zhou et al. 2015). In addition, the mesocotyl and root cross-sections were also stained with toluidine blue as described previously (Zhou et al. 2018).

3.2.6 Sequencing

The nucleotide sequence of the glutamate receptor gene (Zm00001d015007) was obtained from MaizeGDB. Four overlapping primers were designed spanning the whole gene. Each primer amplified approximately a 1.4-2.0 kbp region, and there was an overlap of 300 bp between the amplicons. The primers were searched against the maize genome using Primer-BLAST to avoid any untargeted binding. PCR amplification of *D13* locus from genomic DNA was performed using the following four primer pairs:

   a) forward primer AK-*D13*-G1-F 5'- GTCTCTTGGCATCAACCTCCT -3' and reverse primer AK-*D13*-G1-R 5'- AATCCATACATAGCCATTGCCCA -3'

   b) forward primer AK-*D13*-G2-F 5'- GGACTATGCCCAGCGATCTC -3' and reverse primer AK-*D13*-G2-R 5'- TGTTAGATGTTCCATTGCGAAAGG -3'

   c) forward primer AK-*D13*-G3-F 5'- GCAACATGTTTCACTTGATTGG -3' and reverse primer AK-*D13*-G3-R 5'- ATTGGCCCATAGATGATGTATTCC -3'

   d) forward primer AK-*D13*-G4-F 5'- CGCCAGTACCTGAGACATGAG -3' and reverse primer AK-*D13*-G4-R 5'- CACTCCAGTTCTGCTTATTGTCC -3'

PCR products from all the four reactions were run on 1% TAE gel. The bands were eluted and purified using ZymoClean gel DNA recovery Kit. The purified products were quantified using Nanodrop 2000c spectrophotometer (Thermo Scientific). The four reactions of each sample were then pooled in equal concentrations and sent for sequencing. Wide-seq and SNP calling was performed by Purdue genomics core facility at Purdue University, West Lafayette, IN. The SNPs were called by aligning the reads to the Zm00001d015007sequence in reference B73. Multiple sequence alignment was carried out using ClustalX 2.1 (Larkin et al. 2007).

3.2.7   Transcriptome analysis

The tissues collected from 10 plants within each replication were crushed individually to a fine powder in liquid nitrogen, and equal amounts from each were pooled. The pooled tissue samples were sent to Pioneer/Dupont, Johnston, IA for RNA sequencing. They constructed libraries using Illumina TruSeq stranded mRNA kits. Single end reads of 50 bp were aligned to maize reference genome (Zm-B73-REFERENCE-GRAMENE-4.0) using Tophat 2.1.0 (Trapnell et al. 2009). Aligned sequences were analyzed separately by cufflinks 2.2.1 (Trapnell et al. 2012). Cufflinks assembles the aligned reads into set of transcripts and estimates their relative abundance. The transcriptome assemblies from cufflinks for all conditions were merged and compared to reference annotation using cuffmerge. The BAM files generated by Tophat and merged annotation from cuffmerge were input in htseq-count to generate counts files containing number of aligned reads corresponding to each gene (Anders et al. 2015). Differentially expressed genes (DEGs) were identified using DESeq2 (Love et al. 2014). DEGs were defined as genes having padj < 0.05 and |log2 fold change| ≥ 1. Heatmaps were generated using pheatmap package in R.

3.2.8   GO Enrichment and pathway analysis

Gene Ontology (GO) annotation of DEGs was performed using singular enrichment analysis (SEA) in a web-based ontology tool AgriGO v2.0 (Tian et al. 2017). SEA was carried out separately for the upregulated and downregulated genes by comparing them to the background gene set comprising 39324 genes. Significant GO terms (FDR < 0.05) were determined using Fisher's exact test and Yekutieli (FDR) correction method (Yekutieli and Benjamini 2001). KEGG

pathway analysis (FDR < 0.2) was performed using ShinyGO v0.61. MapMan software (Usadel et al. 2005) was utilized for visualizing the DEG data.

3.2.9 Metabolite profiling and pathway analysis

The metabolites were extracted from the ground stem tissue (100 mg) of four-week old wild type and *D13* heterozygotes using Bligh-Dyer method (Sündermann et al. 2016). Untargeted metabolite profiling was performed using high performance liquid chromatography/mass spectrometry (HPLC/MS) platform at Metabolite profiling facility, Bindley Bioscience Center, Purdue University. The data was converted to mzXML format using msConvert (Adusumilli and Mallick 2017).

Univariate and multivariate statistical analyses were performed using the web-based tool suite MetaboAnalyst 4.0 (Chong et al. 2019). Data was filtered based on relative standard variation (RSD) and normalized using autoscaling. Univariate analysis included two-paired t-test and fold change analysis to identify significantly differential mass features between wild type and mutant samples. FDR was used to adjust for multiple tests. Differential mass features were defined as those with FDR adjusted p-value < 0.05 and |log2 fold change| > 1. Multivariate analysis was performed using PCA and partial least squares discriminant analysis (PLS-DA). Variable importance in projection (VIP) score > 1 was used to identify the most important features discriminating the two groups. Pathway analysis for differential mass features was conducted with MS peaks to pathways module of MetaboAnalyst 4.0 using the *Arabidopsis thaliana* KEGG pathway library. Both mummichog and gene set enrichment analysis (GSEA) algorithms were used for pathway analysis. However, the mummichog algorithm yielded few significant pathways. Therefore, the pathways with GSEA p-value < 0.05 were considered significant. The combined p-value for these pathways from both the algorithms was < 0.2.

3.2.10 Identification of ZmGLRs

The protein sequences of the 20 AtGLRs were downloaded from the NCBI database. These AtGLR protein sequences were used as queries in a BLAST search against the maize genome (Altschul et al. 1990). All the hits were downloaded, and duplicate entries were removed. The remaining entries were then individually searched on NCBI using the accession numbers to remove

any redundant entries. A set of seventeen independent maize GLRs (ZmGLRs) was identified. The gene IDs for all the ZmGLRs were obtained from NCBI and the chromosomal locations were identified from MaizeGDB (Portwood et al. 2019). The chromosomal positions correspond to the B73 v4 assembly (Zm-B73-Reference-Gramene-4.0). The protein sequences of newly discovered ZmGLRs were analyzed using InterProScan and HMMER to check the presence of characteristic glutamate receptor domains. Transmembrane domains were predicted using Polyphobius (http://phobius.sbc.su.se/poly.html). The localization of ZmGLRs was predicted by using aramemnon (http://aramemnon.uni-koeln.de/), a plant membrane protein database (Schwacke and Flügge 2018). This database uses several targeting prediction algorithms like Chloro P, TargetP, PCLR, SignalP to predict the localization of proteins and gives a consensus from all the different tools.

3.2.11 Phylogenetic analysis

The protein sequences of known iGluRs in Humans, mice, and *Drosophila* were retrieved from GenBank. The sequences of gymnosperm *Ginkgo biloba* were obtained from Medicinal plant genomics resource (http://medicinalplantgenomics.msu.edu/). The predicted protein sequences from crops, including *Oryza sativa*, *Sorghum bicolor*, *Triticum aestivum*, were retrieved from NCBI BLAST search using AtGLRs as queries. The complete list of plant GLRs used in this analysis is provided in supplemental file 1. The full-length amino acid sequences of glutamate receptors in maize, cyanobacteria *Synechocystis* and all the above organisms were aligned with MEGA X Clustal W using the following alignment parameters: gap opening penalty: 10; gap extension cost: 1.0; amino acid substitution matrix: Blosum 30. A phylogenetic tree was constructed by the neighbor-joining (NJ) method (Saitou and Nei 1987) using p-distance substitution model. Bootstrap values were generated using 1000 bootstraps. The sequence of a prokaryotic glutamate receptor from cyanobacteria *Synechocystis* (GluR0) was used as an outgroup. The protein sequences used in this analysis are available in supplemental file 2.

3.3 Results

3.3.1 A glutamate receptor gene is responsible for *D13* phenotype

The *D13* mutant initially identified in B73 exhibits reduced plant height due to reduction in the length of the internodes, behaves in a semi-dominant fashion and is highly sensitive to the genetic background (see chapter 2). *D13* was mapped to a 530kbp region on chromosome 5 comprising 15 genes. Exome sequencing of these fifteen genes in *D13* mutants, in collaboration with Pioneer/Dupont (now Corteva Agriscience), revealed a G to A change in exon 5 of the gene Zm00001d015007, encoding a glutamate receptor (Figure 3.2A). This G2976A change in the gene was selected as a putative candidate responsible for the *D13* phenotype. The other fourteen genes did not show any variation in protein-coding regions in the mutant as compared to the wild type. We sequenced the full-length gene Zm00001d015007 in the wild type and *D13* heterozygotes to confirm the SNP. All the mutants had the G2976A change. The rest of the gene sequence was completely identical in wild types and mutants.

The glutamate receptor gene, Zm00001d015007, contains the signature three plus one transmembrane domains of an ionotropic glutamate receptor, which includes three transmembrane domains (M1,M3, and M4) and a pore loop (M2) (Figure S2). The G2976A mutation did not impact the transmembrane domain structure.

The G to A change in the *D13* mutants was determined to be a missense mutation that led to the replacement of non-polar alanine (A) with polar threonine (T) at position 4 (A4T) in a highly conserved nine-amino acid motif in the third transmembrane domain (M3) of the glutamate receptor (Figure 3.2D). The amino acid sequence of the M3 domain of mutant Zm00001d015007 (*D13*) was compared to the glutamate receptor homologs in maize, sorghum, rice, and *Arabidopsis,* as well as other organisms – humans, mice, *Drosophila*, and cyanobacteria. The A4 residue of SYTA̲NLAA motif was found to be conserved in ionotropic glutamate receptors in all the organisms (Figure 3.2B), which strongly indicates that the *D13* phenotype is the result of the A4T mutation in a highly conserved region of the glutamate receptor gene.

A dCAPs marker associated with the G to A SNP in the Zm00001d015007 gene was tested for linkage with the *D13* phenotype. We selected 96 wild type and 96 mutants (*D13*/+:B73) from B73 x *D13*/+B73 progeny with reduced height. The marker clearly differentiated the wild type and mutant plants, showing a complete co-segregation of the phenotype and genotype (Figure 3.2C).
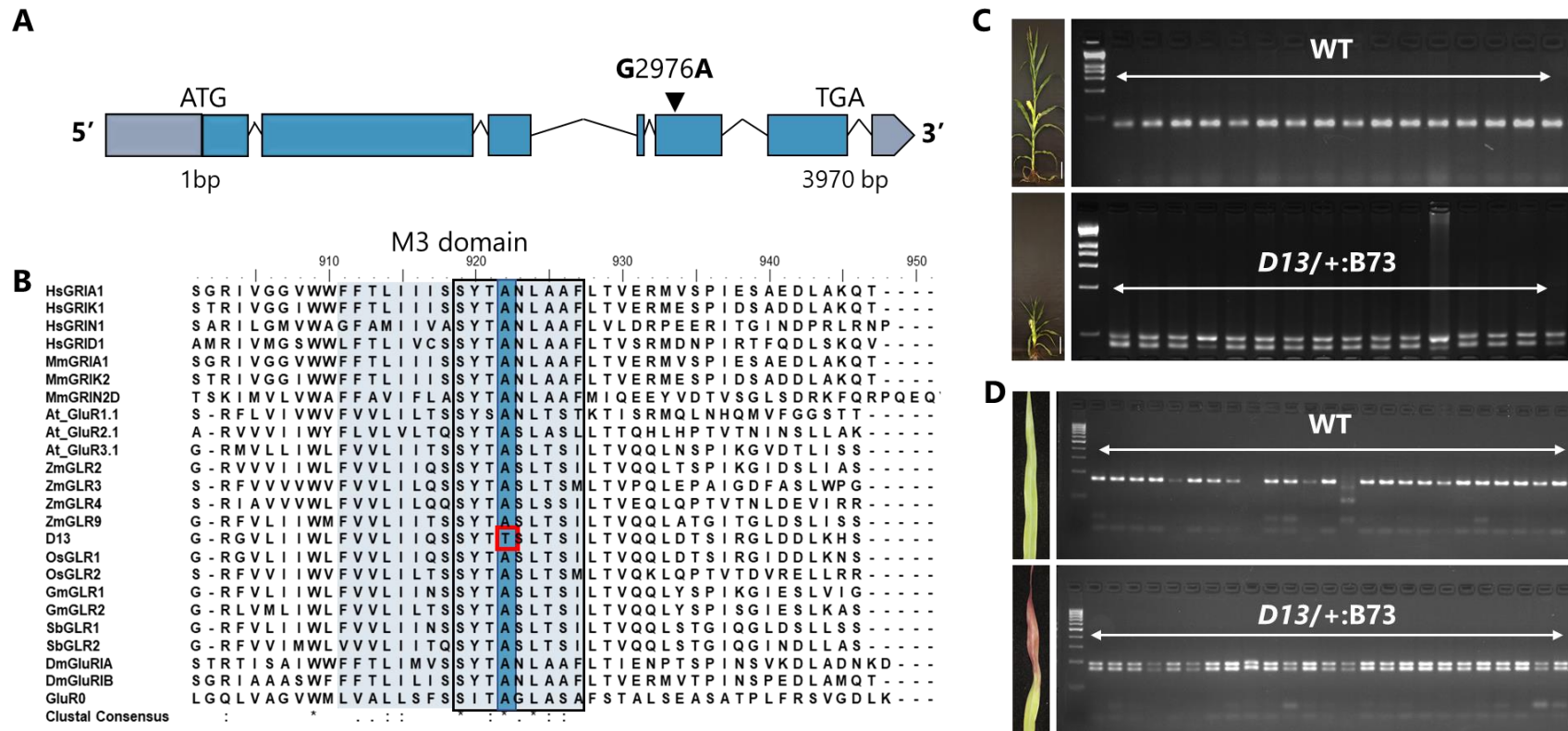
Figure 3.2 Mutation in a glutamate receptor gene is responsible for *D13* phenotype. (A) Structure of glutamate receptor gene (Zm00001d015007). Exons and introns are drawn in proportion to their lengths. The black arrow indicates the position of the G to A mutation in exon 5. (B) Amino acid sequence comparison of M3 domain of Zm00001d015007 gene in *D13* mutants with glutamate receptors in other species (Hs: *Homo sapiens*, Mm: *Mus musculus*, At: *Arabidopsis thaliana*, Zm: *Zea mays*, Os: *Oryza sativa*, Gm: *Glycine max*, Sb: *Sorghum bicolor*, Dm: *Drosophila melanogaster*). The grey rectangle highlights the M3 transmembrane domain, black rectangle indicates conserved SYTANLAA motif and the blue box highlights the conserved alanine. The alanine residue that is changed to threonine in *D13* mutants is highlighted with a red box. (C) Co-segregation analysis of plant height with *D13* mutation. The left panel shows the height of the selected plants and the right panel depicts their genotype. (D) Co-segregation analysis of red leaf phenotype with *D13* mutation.

Another striking phenotype of *D13* mutants was the accumulation of red pigmentation, specifically at the leaf tips of juvenile seedlings. While we did occasionally observe red pigmentation in wild type plants, it had a scattered pattern and was not restricted to the tips of the leaves. Our evaluation showed that all plants with red leaf tips were heterozygous for the *D13* mutation, whereas the ones without the red leaf tips were wild types (Figure 3.2D). In conclusion, our data confirmed complete linkage of the G2976A SNP in the glutamate receptor gene (Zm00001d015007) with the *D13* phenotype.

3.3.2 *D13* mutants display defects in the plant vasculature

Visualization of transverse sections of the second internode of three-week-old *D13*/*D13*:B73 indicated severe defects in the morphology of vascular bundles (Figure 3.3 A-D). Typically, a vascular bundle in a monocot stem follows a collateral arrangement where xylem is located on the inner side and phloem is on the outer side of the bundle. However, in the stem cross-section of homozygous *D13*, phloem was localized to the center of the vascular bundle and the xylem tissue was not fully developed (Figure 3.3D). Unlike that of *D13* homozygotes, the arrangement of vascular tissue within the bundles in *D13* heterozygotes was similar to that of wild type plants, however, the vessel elements were smaller and fewer than in wild type (Figure 3.3E-H). While the vascular bundles were randomly distributed throughout the stem in *D13* mutants (both homozygotes and heterozygotes), as is expected in a monocot, they were densely packed in the mutants as compared to the wild type (Figure 3.4). This was probably because of the reduced diameter of the stem in the mutants in comparison to the wild type. We also looked at the cross-section of the mesocotyl and root in ten-day-old *D13*/+:B73 and wild type seedlings. The mutant sections looked identical to the wild type (Figure 3.5), which was consistent with our phenotypic observations that *D13* heterozygotes were indistinguishable from wild type at this stage of development.

3.3.3 A second-site mutation in *D13* gene reverts the mutant phenotype to wild type

The *D13* phenotype exhibits marked sensitivity to the genetic background. We exploited this background variation to generate a second site mutation in the *D13* gene, taking advantage of the CML322/Mo17 background. The suppressed *D13* phenotype in Mo17 allowed us to obtain *D13* homozygous pollen to make enough crosses required for screening and the mutant phenotype was
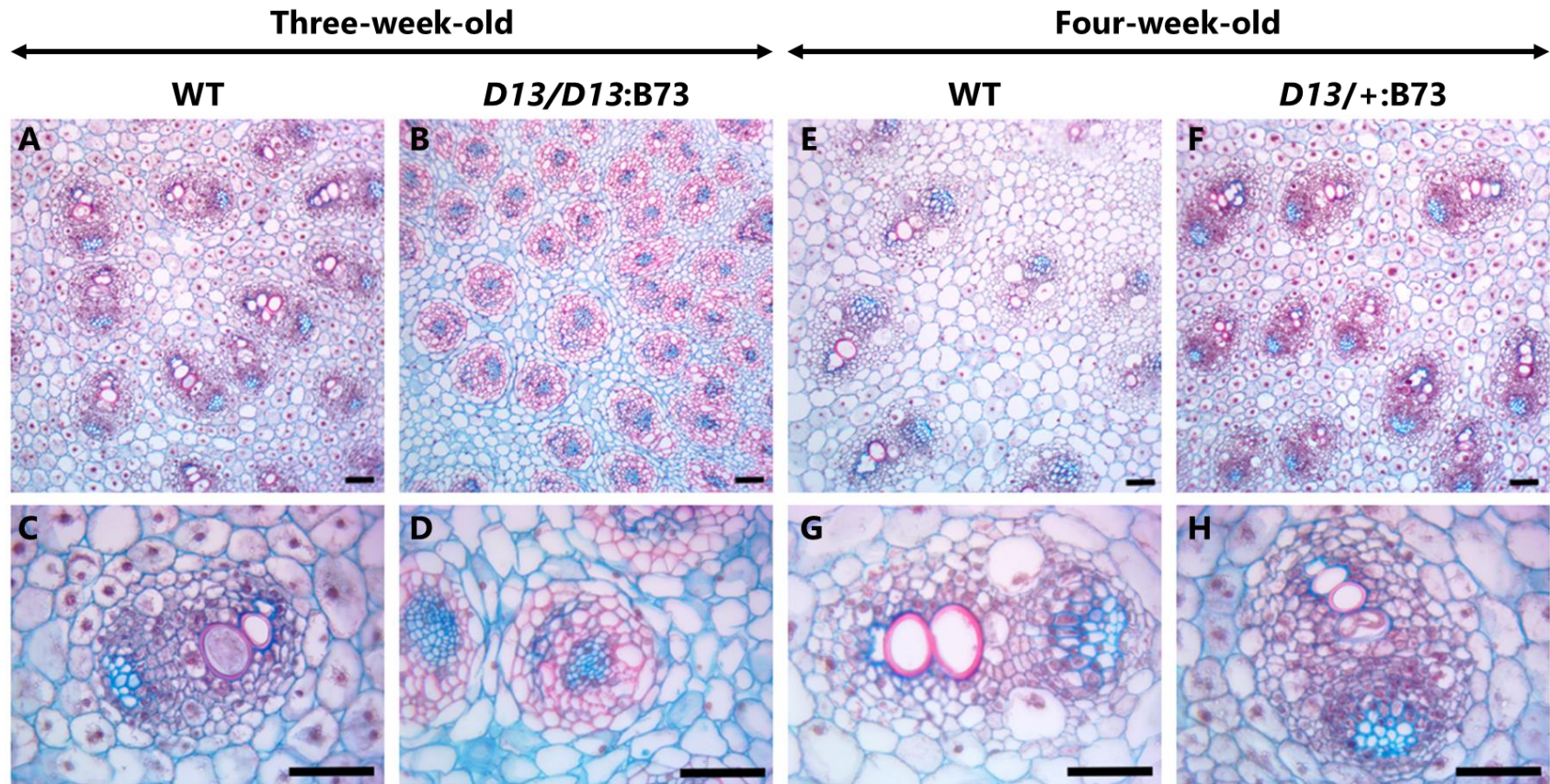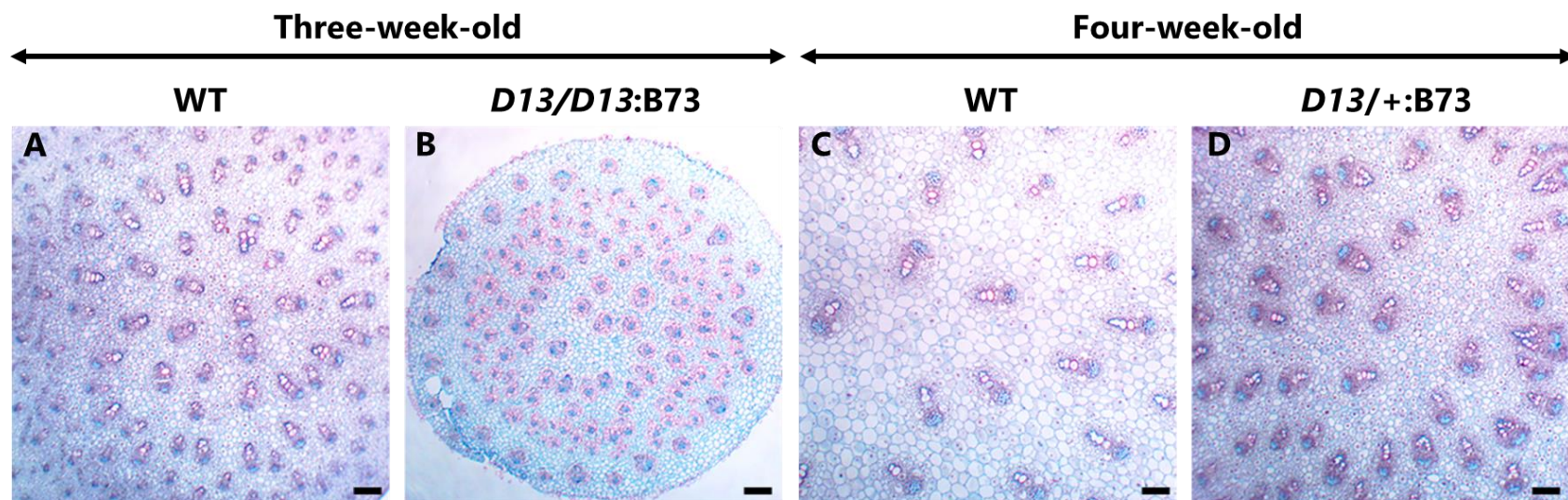
Figure 3.3 Vascular patterns in the stem of wild type (WT) and *D13* mutants in maize. The stem sections were obtained from the second internode of 3-week-old (A-D), or 4-week-old (E-H) plants. (A) Cross-section of WT stem. (B) Stem cross-section of a *D13* homozygote. (C) Structure of vascular bundle in WT. (D) Structure of a vascular bundle in a *D13* homozygote. (E) Cross-section of 4-week-old WT stem. (F) Stem cross-section of a *D13* heterozygote. (G) Structure of a vascular bundle in 4-week-old WT. (H) Structure of a vascular bundle in *D13* heterozygote. Scale bar = 50 μm. (Images contributed by Han Han and Yun Zhou).

Figure 3.4. Distribution of vascular bundles in the stem of wild type (WT) and *D13* mutants in maize. The stem sections were obtained from the second internode of 3-week-old (A, B), and 4-week-old (C, D) plants. (A) Stem cross-section of WT. (B) Stem cross-section of a *D13* homozygote. (C) Stem cross-section of 4-week-old WT. (D) Stem cross-section of *D13* heterozygote. Scale bar = 100 µm. (Images contributed by Han Han and Yun Zhou).
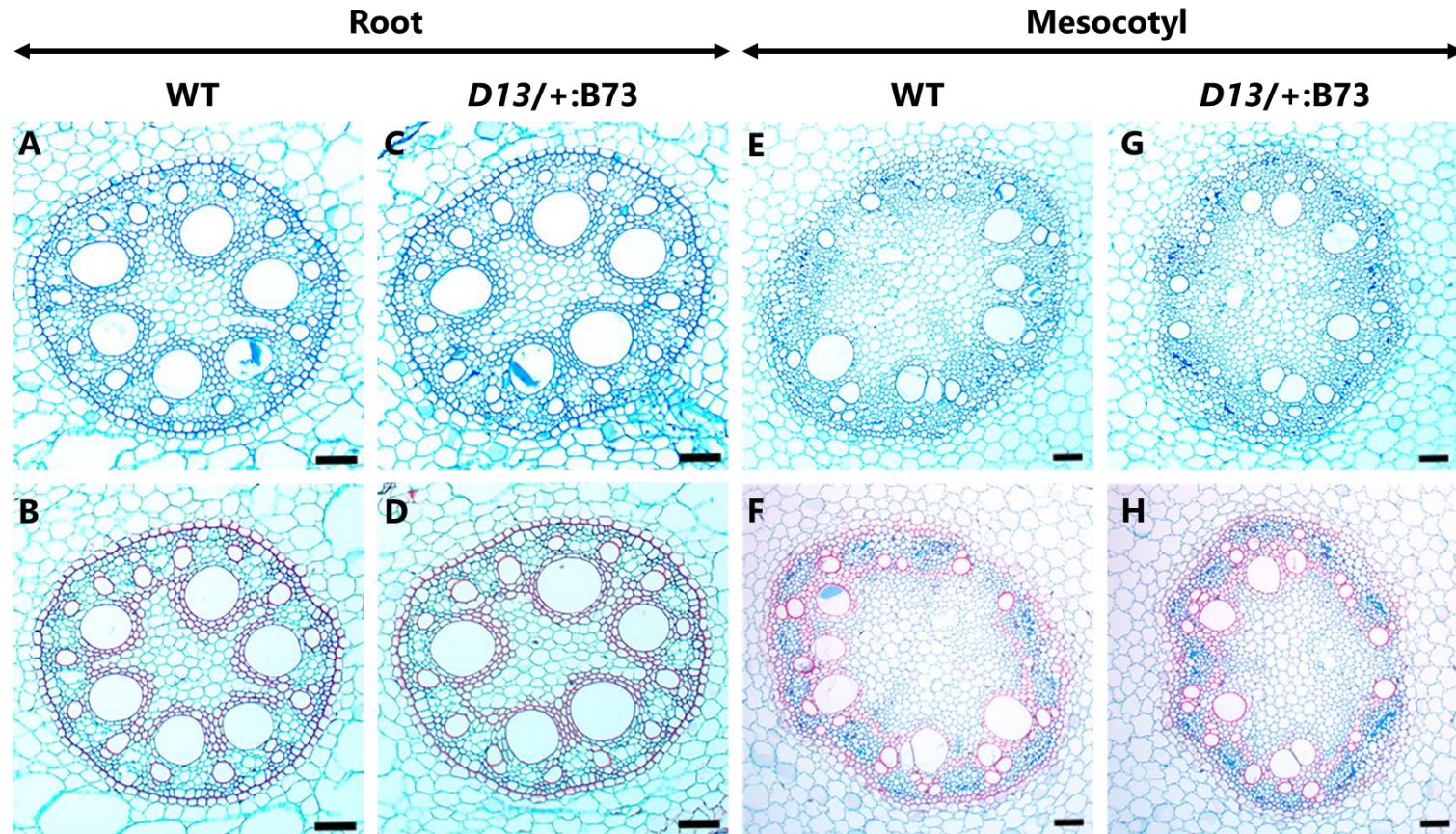
Figure 3.5 Cross-sections of root and mesocotyl from ten-day-old wild type (WT) and *D13* seedlings. (A, B) Cross-section of WT root. (C, D) Root cross-section of *D13* heterozygote. (E, F) Cross-section of WT mesocotyl. (F) Mesocotyl cross-section of *D13* heterozygote. Scale bar = 50 µm. (Images contributed by Han Han and Yun Zhou).

readily visible in CML322/Mo17 background (Figure S3). To determine if inactivating the *D13* allele reverts the mutant phenotype, three M1 families comprising of a total of 16230 plants were screened for tall plants.

A great deal of variability was observed in the heights of M1 plants. Theoretically, all the M1 plants should display a similar reduction in height because they were all *D13* heterozygotes, and only the plants with the knockout of the *D13* allele should appear tall like the wild type plants. However, the number of tall M1 plants observed was much higher than the number expected (approximately 1 per 1000 or 0.1%) based on previous mutagenesis estimates from EMS treatment (Candela and Hake 2008). There were 112 tall plants among 5373 M1 plants obtained from the first pollen parent. Similarly, 2% of the plants (82/4072) were tall in second M1 family. The number of tall plants in third M1 family was much higher than the other two families. It was tough to determine the exact number of tall plants in the third family due to relatively high suppression in all plants in general. We selected 55 of the tallest plants from the third family.

The tallest plants selected from three M1 families were crossed to inbred B73 for progeny testing. Genotyping with an InDel marker linked to the *D13* locus confirmed the presence of *D13* allele in all the selected plants. The seeds from 184 F_1 families obtained from the above crosses (B73 x *D13*/+:Mo17/CML322) were planted in two replications, and F_1 progeny were screened for plant height. If EMS mutagenesis had knocked out the *D13* allele, then all the mutant plants in the F_1 families were expected to be as tall as wild types . The tall parent plants whose mutant progeny were shorter than wild type were false positives. A total of 183 F_1 families showed segregation of mutant and wild type phenotype with few of them showing a partially suppressed *D13* phenotype. Among the 184 F_1 families, only one F_1 family had all the mutant plants of the same height as the wild type siblings. All the plants in this selected F_1 family in both the replications were genotyped with the InDel marker to confirm the 1:1 segregation of mutants and wild type (Figure S4). Two revertant plants were selected from this family for sequencing.

Wide-seq was performed to sequence the full-length glutamate receptor gene (Zm00001d015007) in the revertant plants. We also sequenced two partially suppressed mutants from other F_1 families to serve as controls. The detailed sequencing results are provided in Table S1. A new G to A change (*D13**) upstream of the original *D13* allele was identified in the exon 2 of the gene (Figure 3.6A). This allele was present in the revertant plants and was absent in the suppressed mutants or in B73. The *D13** allele replaced the amino acid glycine with the negatively
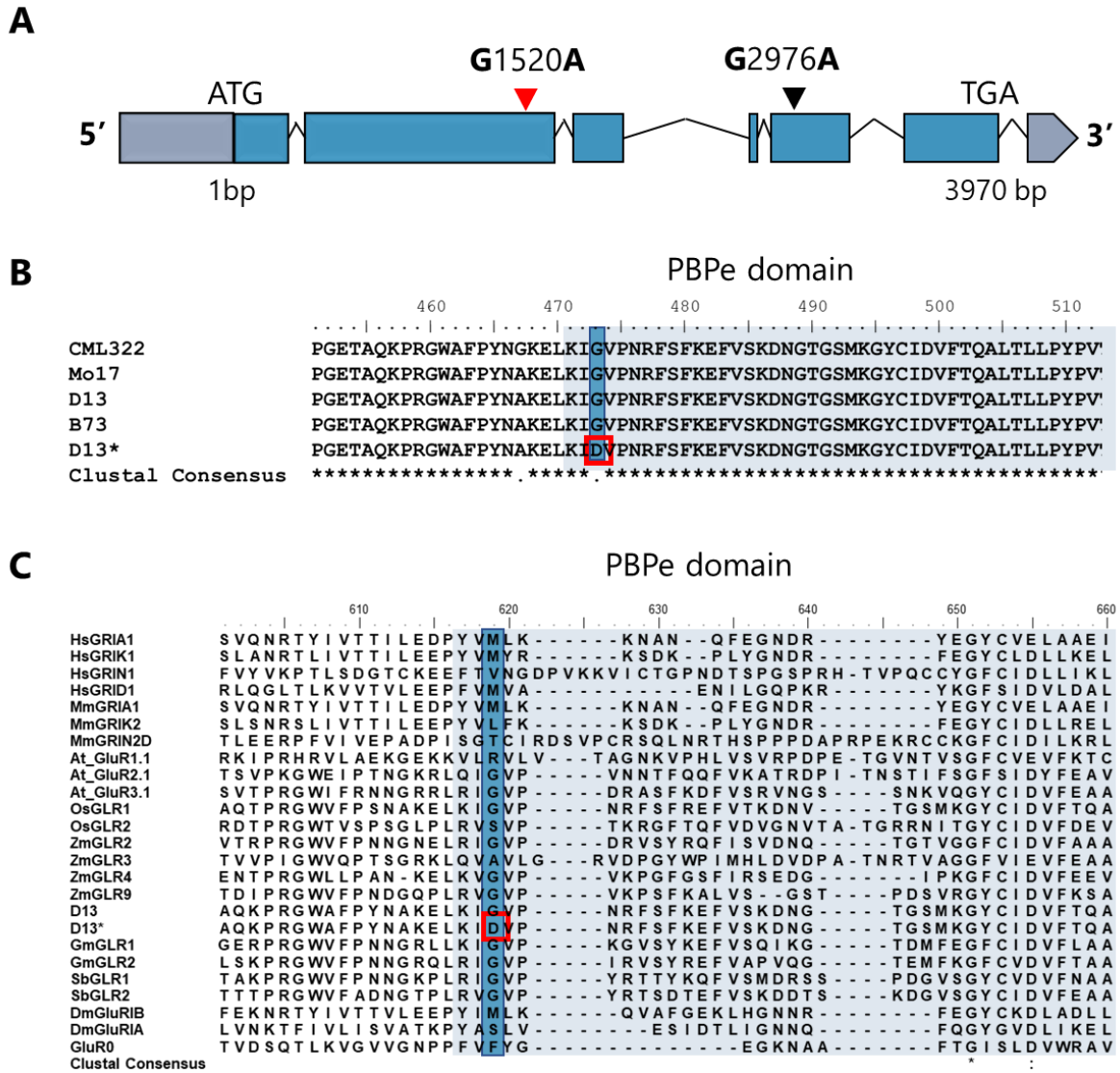
Figure 3.6 Second-site mutation in the candidate glutamate receptor gene. (A) Structure of glutamate receptor gene (Zm00001d015007) indicating the position of *D13** allele (red arrow) and original *D13* allele (black arrow). (B) Amino acid sequence comparison of revertant mutant (*D13**) with original *D13* mutant and inbred lines B73, Mo17 and CML322. The light blue rectangle highlights the PBPe (eukaryotic Periplasmic binding protein) domain, dark blue box highlights the Glycine (G) residue that is changed to Aspartic acid (D) in *D13** mutants. (C) Amino acid sequence comparison of PBPe domain in *D13** with glutamate receptors in other species (Hs: *Homo sapiens*, Mm: *Mus musculus*, At: *Arabidopsis thaliana*, Zm: *Zea mays*, Os: *Oryza sativa*, Gm: *Glycine max*, Sb: *Sorghum bicolor*, Dm: *Drosophila melanogaster*). GluR0 is the glutamate receptor in cyanobacteria.

70

charged aspartic acid (G473D) in the ligand binding domain that is homologous to eukaryotic periplasmic binding protein domain (PBPe) (Figure 3.6B).Comparison with the protein sequence in other organisms showed that the G473 is not conserved in animal glutamate receptors but is conserved in the majority of plant GLRs (Figure 3.6C). The other amino acids frequently occurring at this location in plant GLRs include alanine and serine. None of the GLRs had an aspartic acid or any other negatively charged amino acid at this location. The restoration of the wild type phenotype in plants carrying the *D13* allele due to a second-site mutation (*D13**) in the glutamate receptor gene (Zm00001d015007) validated the relationship between this gene and *D13* phenotype.

3.3.4 *D13* mutants exhibit an upregulation of stress response gene expression

We used transcriptomics to explore the molecular pathways affected in the mutant. As mentioned above, the phenotype of *D13* mutants is very different in B73 and Mo17. So, we selected these two genetic backgrounds to explore this variation in mutant phenotype at the molecular level. One-inch sections from the base of four-week-old mutants (*D13*/+:B73 and *D13*/+:Mo17) and their respective wild type siblings were used for RNA-sequencing. Principle component analysis (PCA) showed a clear separation between the mutant and wild type groups in B73 background, with PC1 explaining 72% of variance, whereas the separation of groups was less distinct in Mo17 with PC1 explaining only 42% of variance (Figure 3.7A-B). These results are consistent with the phenotype of *D13* in both these backgrounds where the mutant phenotype is clearly distinguishable from wild type in B73 and not in Mo17.

We identified 882 genes differentially expressed in the B73 mutant as compared to wild type siblings (Supplemental file 3). Among these 882 genes, 765 were upregulated in the mutant and 117 were downregulated (Figure 3.7C). In contrast, *D13* mutants in Mo17 only had 43 DEGs as compared to their wild type siblings. Among these 43 DEGs, 32 genes were upregulated and 11 were downregulated in the mutant (Figure 3.7D). There was no significant overlap between the DEGs in the two genetic backgrounds, as we identified only 5 genes common in the two gene sets (Figure S5 , Table 3.1). Four of these genes are upregulated in both B73 and Mo17 mutants. However, unlike what is observed in B73, a gene that encodes salicylate/benzoate carboxyl methyltransferase is downregulated in Mo17. This gene plays a role in stress response in plants (Chen et al. 2003).

71
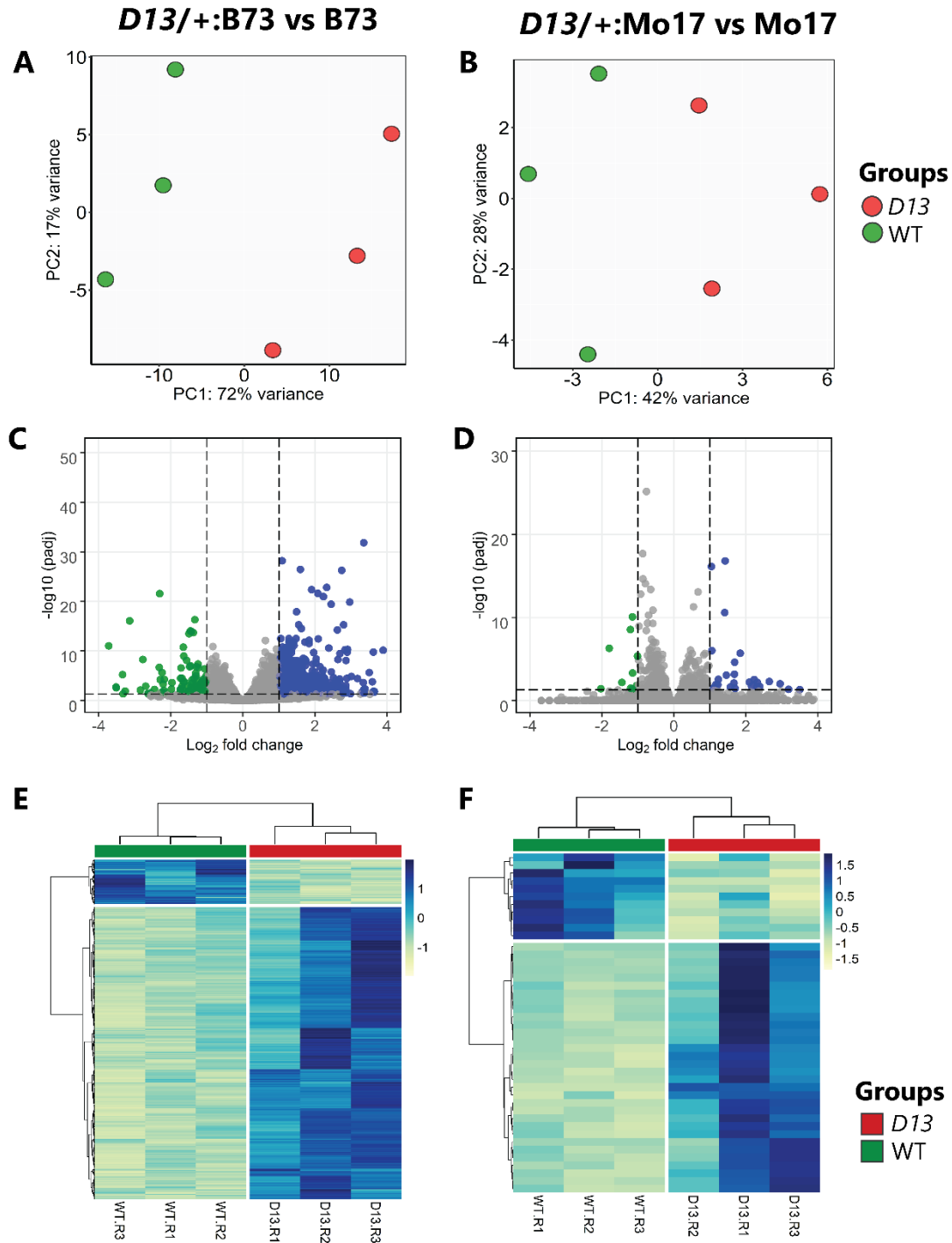
Figure 3.7 Transcriptomic analysis of *D13* mutants in B73 and Mo17 genetic backgrounds. The panel on left (A, C, E) illustrates data for *D13* mutant in B73 background and the panel on right (B, D, F) shows data for *D13* mutant in Mo17. (A and B) Principle component analysis (PCA) plots based on the transcript counts. (C and D) Volcano plots of differentially expressed genes (DEGs). Blue dots display significantly upregulated genes in mutant as compared to wild type (WT) (log2 fold change > 1, p-value ≤ 0.05) . Green dots display downregulated DEGs (log2 fold change < -1, p-value ≤ 0.05). (E and F) Heatmaps of DEGs showing the log2 fold change between the mutant and WT samples.

The functional annotation of the DEGs in B73 background was performed using GO term singular enrichment analysis in AgriGO v2. We identified 328 and 59 significant GO terms (FDR ≤ 0.05) associated with the upregulated and downregulated genes (Supplemental files 4 and 5), respectively. The upregulated *D13* genes were enriched in various metabolic and cellular processes, signaling, and response to stimulus (Figure 3.8A, Table 3.2). Among the GO terms for cellular component, sixty-eight percent of the upregulated genes in *D13* were associated with the GO term 'membrane,' and 29 percent were assigned to the term 'plastid'. Further, these genes were related to various components of plastids, including envelope, thylakoid membrane, and stroma.

Table 3.1 Common DEGs in B73 and Mo17 RNA-seq data

S.No.	Gene ID	B73		Mo17		Description
		log2 FC	padj	log2 FC	padj	
1	Zm00001d048660	3.6495	0.0205	2.9485	0.0096	Bowman-Birk type trypsin inhibitor
2	Zm00001d025490	2.4158	0.0272	2.3823	0.0203	Zea mays ARGOS1
3	Zm00001d003422	2.8424	0.0000	1.6869	0.0000	Amino acid/polyamine transporter II
4	Zm00001d041173	1.6737	0.0022	1.1345	0.0291	Beta-glucosidase 17
5	Zm00001d052827	1.4643	0.0000	-1.1542	0.0416	Salicylate/benzoate carboxyl methyltransferase

Table 3.2 Significant GO terms for biological processes over-represented in upregulated DEGs in *D13* (B73) mutants

GO term	Associated processes
Metabolic processes	Glyceraldehyde-3-phosphate metabolism, Lipid metabolism, Secondary metabolism, and Phenylpropanoid metabolic process
Cellular processes	Photosynthesis, Pigment biosynthesis
Signaling	Ion transport
Response to stimuli	Response to biotic and abiotic stresses Biotic stresses: response to external biotic stimuli (bacteria, fungi), innate immune response, defense response Abiotic stresses: cold, osmotic stress, light radiation

The GO term "response to stimulus" was over-represented in the upregulated gene set and was associated with both biotic and abiotic stresses (Figure 3.8B, C). The genes related with biotic stimuli included those involved in response to bacteria and fungi. The genes for response to reac-
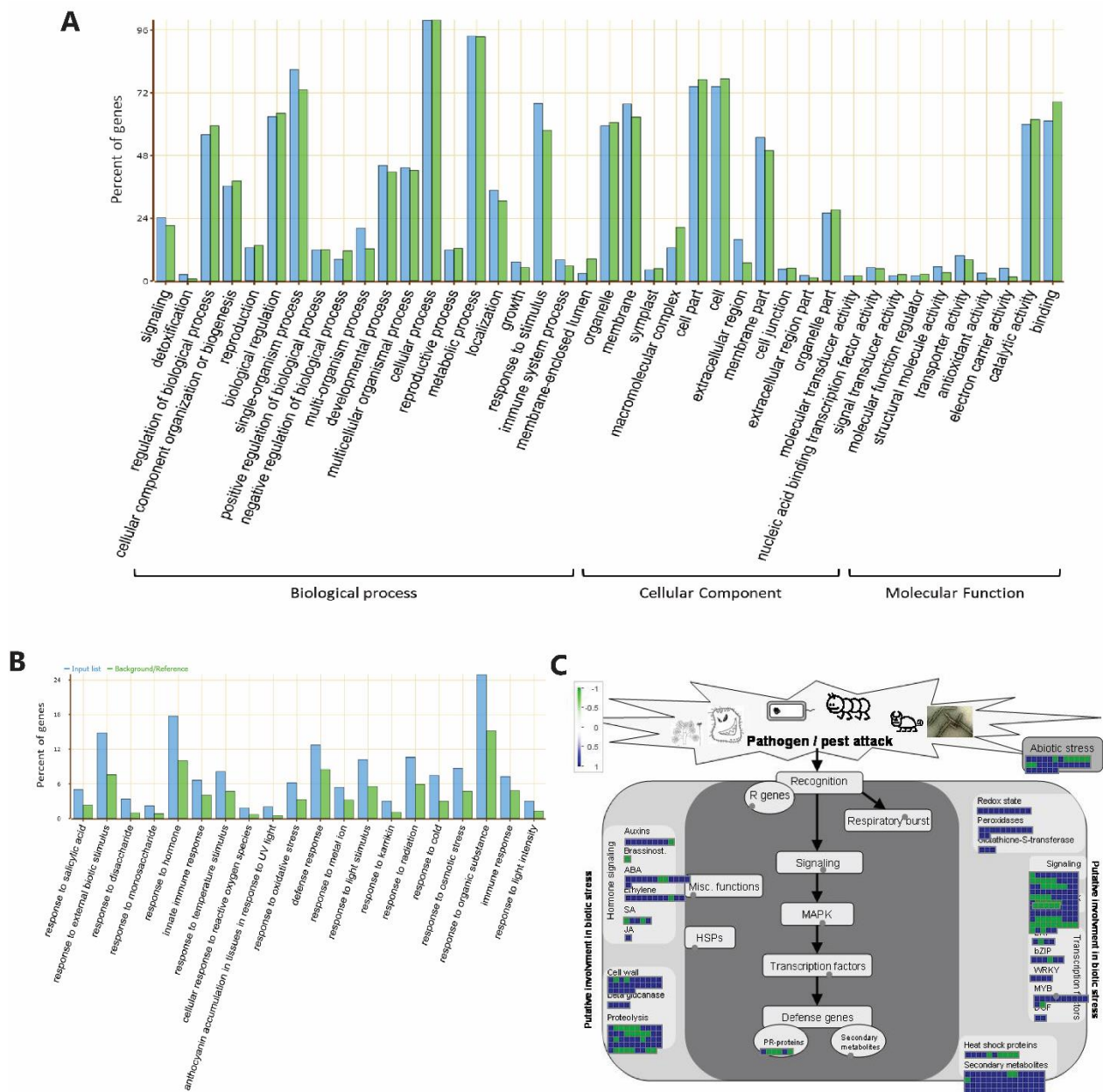
Figure 3.8 Functional annotation of upregulated DEGs in *D13* (B73) vs wild type (WT). (A) Singular enrichment analysis (SEA) for upregulated DEGs in *D13* vs WT in B73 using AgriGO v2. DEGs were annotated based on three categories: biological process, cellular component, and molecular function. Blue bars represent the input gene list and the green bars represent the background reference genome (*Zea mays*). (B) Significant GO terms associated with response to external/internal stimuli. (C) Overview of biotic/abiotic stress response in *D13* mutant vs WT in B73 background.

-tive oxygen species (peroxidases, WRKY transcription factors) were also upregulated in *D13* plants. In addition, mutants showed an upregulation of genes involved in cutin and wax biosynthesis. The abiotic stress in *D13* is evident from the upregulation of genes for cold, light, and radiation response. Other indicators for stress are an enrichment of genes for auxin, ABA, and ethylene response. Taken together, RNA seq data indicates that *D13* mutants are highly stressed and that could be the primary reason for stunted growth, or vice versa. Our hypothesis of increased stress in plants was supported by anthocyanin pigmentation in the *D13* leaves. Moreover, we identified fifteen genes associated with anthocyanin accumulation upregulated in *D13* mutants (Table S2).

The mutants also display a reduction in size of the meristem and length of the internodes. The 117 downregulated genes were associated with shoot system development and its regulation, primarily comprising genes involved in leaf and flower development (Supplemental file 5). Also, genes controlling vegetative to reproductive phase transition were downregulated in *D13*. We also performed functional annotation of down regulated genes using ShinyGO v0.61. and identified genes related to regulation of hormone levels. A gene Zm00001d029648 associated with GA metabolic processes was downregulated in *D13*. Zm00001d029648 encodes a copalyl diphosphate synthase2, that is involved in early stages of GA biosynthesis pathway. Mutations in this gene can lead to lower GA level, that results in a typical dwarf phenotype (Yamaguchi 2008; Bensen et al. 1995). A recent study in maize has demonstrated that mutation of copalyl diphosphate synthase also enhances salt-tolerance in plants (Zhang et al. 2020). The downregulation of copalyl diphosphate synthase in *D13* might be another stress response.

KEGG pathway enrichment analysis displayed seventeen pathways enriched (FDR < 0.2) in *D13* mutants (Figure 3.9). Photosynthesis was the most enriched with an enrichment factor of 0.17. In addition, many of the enriched pathways were associated with secondary metabolism in plants including butanoate metabolism, phenylpropanoid biosynthesis, flavonoid biosynthesis, and biosynthesis of secondary metabolites.

3.3.5   Metabolomic profiling of *D13* mutants

Untargeted metabolite analysis was performed using HPLC/MS platform to investigate the metabolic response of *D13* plants. We utilized the same set of wild type and *D13* samples which

were used for RNA-sequencing. A total of 12131 mass features were detected in our workflow, which were reduced to 5000 after filtering based on RSD (relative standard deviation). Principal component analysis performed to visualize the relationship among the samples showed clear separation of wild type and mutant groups with PC1 explaining 52.9% of the total variance and PC2 explaining 18.4% variance (Figure 3.10A). Among 5000 mass features, 1114 were identified as significantly different (log2 FC > 1 and padj (FDR) < 0.05) between *D13* and wild type (Figure 3.10B, Supplemental file 6).

PLS-DA analysis was performed to identify important mass-features variable between *D13* and wild type with variable importance in projection (VIP) score > 1. The results of PLS-DA were consistent with PCA. The top mass features for which corresponding tentative metabolites were identified are displayed in Figure 3.11A. Due to the complex nature of metabolites, it is difficult to determine the compounds accurately based on their m/z values. Moreover, the publicly available databases are enriched in metabolites from humans and mammals, whereas plant metabolites have not been extensively identified, which often leads to misidentification of compounds unlikely to be plant metabolites. To reduce this problem, we performed MS peak to pathway analysis that examines metabolites based on their enrichment in a pathway rather than as random hits. Using this approach, 557 tentative metabolites were identified and compared with KEGG pathway library of *Arabidopsis thaliana* that revealed 18 significantly enriched pathways (GSEA p-value < 0.05, Figure 3.11B).

The most enriched pathway that was identified was biosynthesis of secondary metabolites followed by anthocyanin biosynthesis. In addition, phenylpropanoid biosynthesis, flavonoid biosynthesis, inositol phosphate metabolism, pentose phosphate pathway, were significantly enriched. All the above-mentioned pathways are associated with secondary metabolism in plants. The RNA-seq data also showed an enrichment of these secondary metabolic pathways. Other pathways that were significantly enriched included glycolysis/gluconeogenesis, fatty acid biosynthesis and terpenoid biosynthesis, which were also enriched in RNA-seq analysis.

3.3.6 Glutamate receptor gene family in maize

The gene Zm00001d015007 is a part of a gene family in maize comprising 17 genes. The homologs of glutamate receptors in maize were identified by using the protein sequences of 20 AtGLRs as queries in a BLAST search against the maize genome. All the members of the GLR
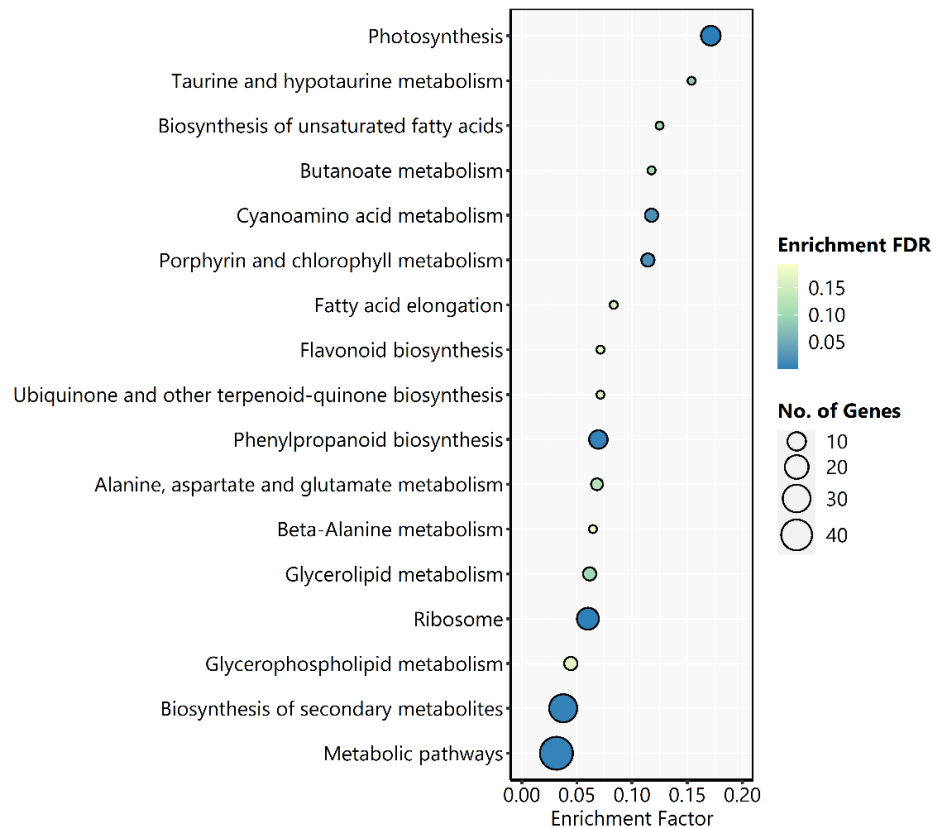
Figure 3.9 KEGG pathway enrichment analysis (FDR < 0.2) of upregulated DEGs in *D13* vs wild type in B73 background.
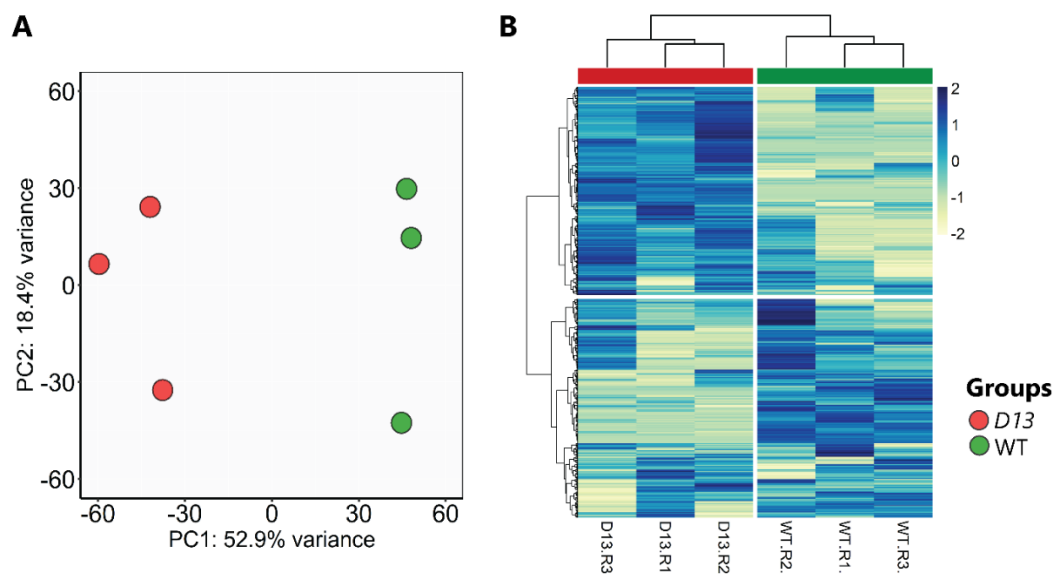
Figure 3.10 Differential metabolite accumulation in *D13* mutants vs wild type (WT) B73. (A) Principle component analysis (PCA) plots based on LC/MS data. (B) Heatmap of differentially accumulated metabolites in *D13* vs WT samples.
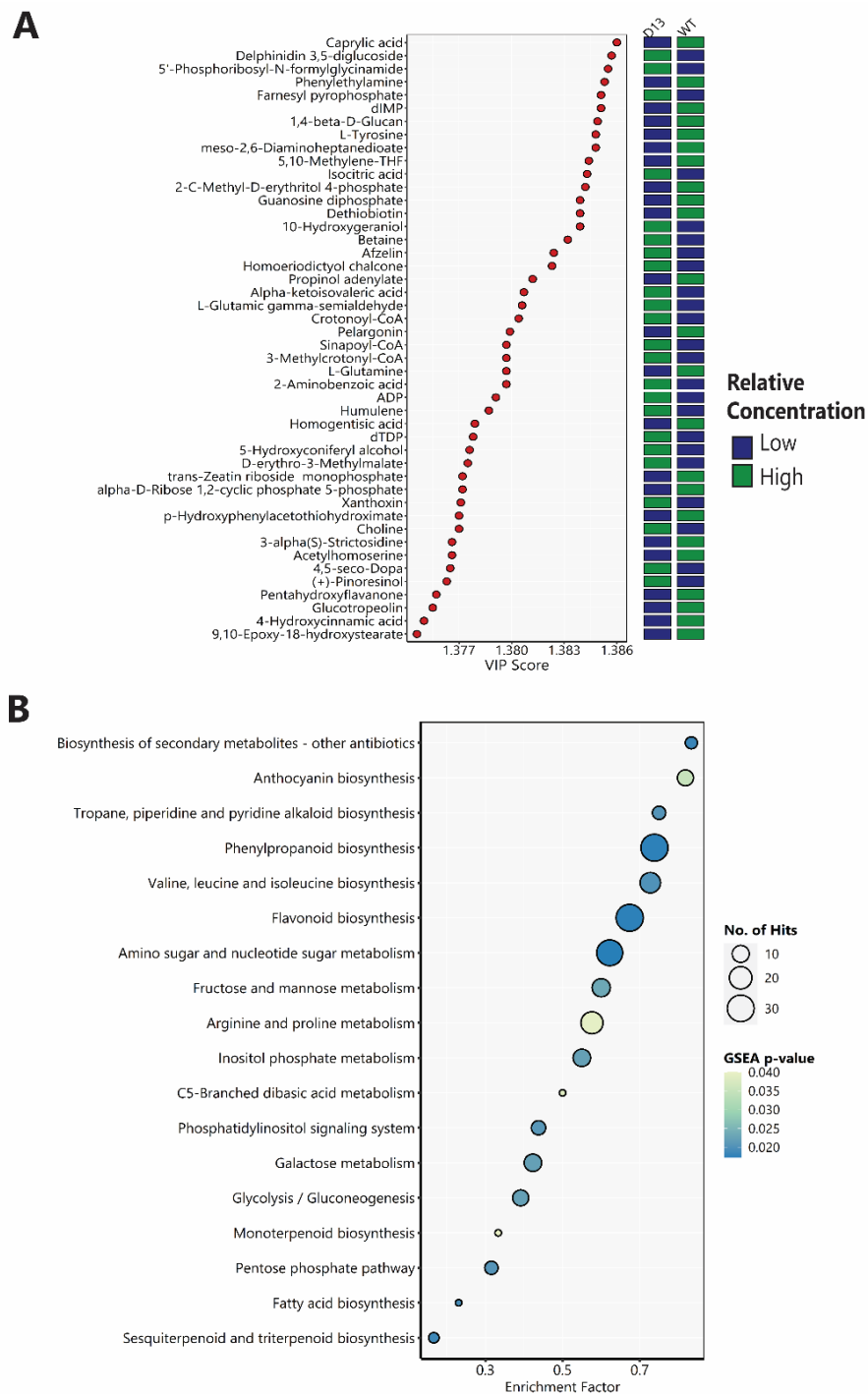
Figure 3.11 Metabolic changes in *D13* mutants in B73 background. (A)Tentative metabolites differentially accumulated in *D13* and wild type (WT) based on variable importance in projection (VIP) in PLS-DA analysis. Colored boxes indicate the relative concentrations of the corresponding metabolite in each group. (B) Pathway enrichment analysis based on altered metabolites in *D13* vs WT using Metaboanalyst 4.0. Size of the circles represents number of metabolites altered in *D13* for the respective pathway and color represents the GSEA (Gene set enrichment analysis) p-value. The FDR cutoff was <0.05.

family in maize are distributed on five chromosomes: 1, 2, 4, 5 and 7 (Figure S6). Some of them are also located in proximity on the same chromosome. For instance, ZmGLR8, 9 and 10 on chromosome 5, and ZmGLR3 and 4 on chromosome 2. However, we do not know if the close location of these ZmGLRs plays a role in their interaction or functioning. This gene family has not been previously characterized in maize, so the ZmGLRs were named from 1 through 17 in ascending order of their chromosomal location (Table 3.3). The genomic length of all the ZmGLRs is variable and ranges from ~2.4kb to 9.3kb. None of the seventeen ZmGLRs were differentially expressed in the *D13* mutants as compared to the wild type.

To confirm the GLR identity of these predicted ZmGLRs, the protein domains for each of the ZmGLRs were predicted using InterPro and HMMER. The protein domains that were common in all proteins include: Ionotropic glutamate receptor domain (IPR001320), Periplasmic binding protein (IPR028082), and ANF-ligand binding receptor (IPR001828). Another domain that was present in 15 GLRs was Bacterial extracellular solute- binding protein, family 3 (IPR001638). The two GLRs, ZmGLR1 and ZmGLR14 did not possess this domain, instead they contained a L-glutamate and glycine-binding domain (IPR019594). All the domains mentioned above are characteristic of glutamate receptors and have also been identified in *Arabidopsis* and tomato (Aouini et al. 2012).

The subcellular localization was predicted using aramemnon (Schwacke and Flügge 2018, http://aramemnon.uni-koeln.de/). The aramemnon database contains information for only 12 ZmGLRs Among those 12, ten ZmGLRs were predicted to be involved in the secretory pathway, indicating their localization in the plasma membrane. Two GLRs, ZmGLR13 and ZmGLR14, were predicted to be localized in the chloroplast. In addition to the plasma membrane, ZmGLR3 is predicted to be in mitochondria. For the remaining five ZmGLRs including ZmGLR1, 4, 6, 10, and 17, the predictions were made using TargetP and all of them were predicted to be localized to plasma membrane due to presence of signal peptide sequence. All the ZmGLRs except ZmGLR1, ZmGLR5, and ZmGLR14 showed the three-plus one transmembrane domain structure characteristic of glutamate receptor gene family (Lam et al. 1998). ZmGLR1, ZmGLR14 and ZmGLR5 had one, two and three transmembrane domains, respectively.

Phylogenetic analysis distributed ZmGLRs into three clades, corresponding to clades I, II and III in *Arabidopsis* (Figure 3.12). The glutamate receptor ZmGLR11 that contains the *D13* mutation is grouped into clade III and is closest to AtGLR3.3 and AtGLR3.6. The maize homologs

Table 3.3 Seventeen glutamate receptor genes in maize

S.No		Gene ID	v3 Gene ID	NCBI ID	Chr	Start	End	Length (bp)	Accession No.	Strand
1	ZmGLR1	Zm00001d033769		LOC103645580	1	273099857	273102264	2408	ONM08572.1	-1
2	ZmGLR2	Zm00001d002532	GRMZM2G066489	LOC100279951	2	14856275	14861080	4806	ONM14608.1	1
3	ZmGLR3	Zm00001d005782	GRMZM2G341499	LOC103647444	2	188139025	188146351	7327	ONM22083.1	1
4	ZmGLR4	Zm00001d005783		LOC103647445	2	188163535	188169807	6273	ONM22087.1	1
5	ZmGLR5	Zm00001d006508	GRMZM2G125495	LOC103647716	2	210172903	210177759	4857	ONM24112.1	1
6	ZmGLR6	Zm00001d052064			4	178258597	178262686	4090	AQK55950.1	-1
7	ZmGLR7	Zm00001d054016	GRMZM2G150337	LOC100275125	4	245187634	245193207	5574	AQK61072.1	-1
8	ZmGLR8	Zm00001d014451	GRMZM2G057459	LOC103626309	5	47928633	47933975	5343	AQK66311.1	1
9	ZmGLR9	Zm00001d014456	GRMZM2G148807	LOC103626311	5	48034203	48043502	9300	AQK66314.1	1
10	ZmGLR10	Zm00001d014458		LOC103626312	5	48260780	48266573	5794	AQK66317.1	1
11	ZmGLR11	Zm00001d015007	GRMZM2G098301	LOC103626528	5	72029738	72034813	5076	AQK67881.1	1
12	ZmGLR12	Zm00001d018329	GRMZM2G391487	LOC103627839	5	218519848	218523059	3212	AQK75625.1	-1
13	ZmGLR13	Zm00001d018332	GRMZM2G428379	LOC103627840	5	218588559	218592271	3713	AQK75634.1	1
14	ZmGLR14	Zm00001d018614	GRMZM2G020104	LOC103631863	7	908414	912556	4143	ONM50886.1	1
15	ZmGLR15	Zm00001d018615	GRMZM2G165828	LOC100383810	7	1022757	1026799	4043	ONM50889.1	1
16	ZmGLR16	Zm00001d020563	GRMZM2G302673	LOC103632790	7	122392697	122398042	5346	ONM55135.1	-1
17	ZmGLR17	Zm00001d020568	GRMZM2G416943	LOC103634135	7	122586114	122609281	23168	ONM55137.1	1
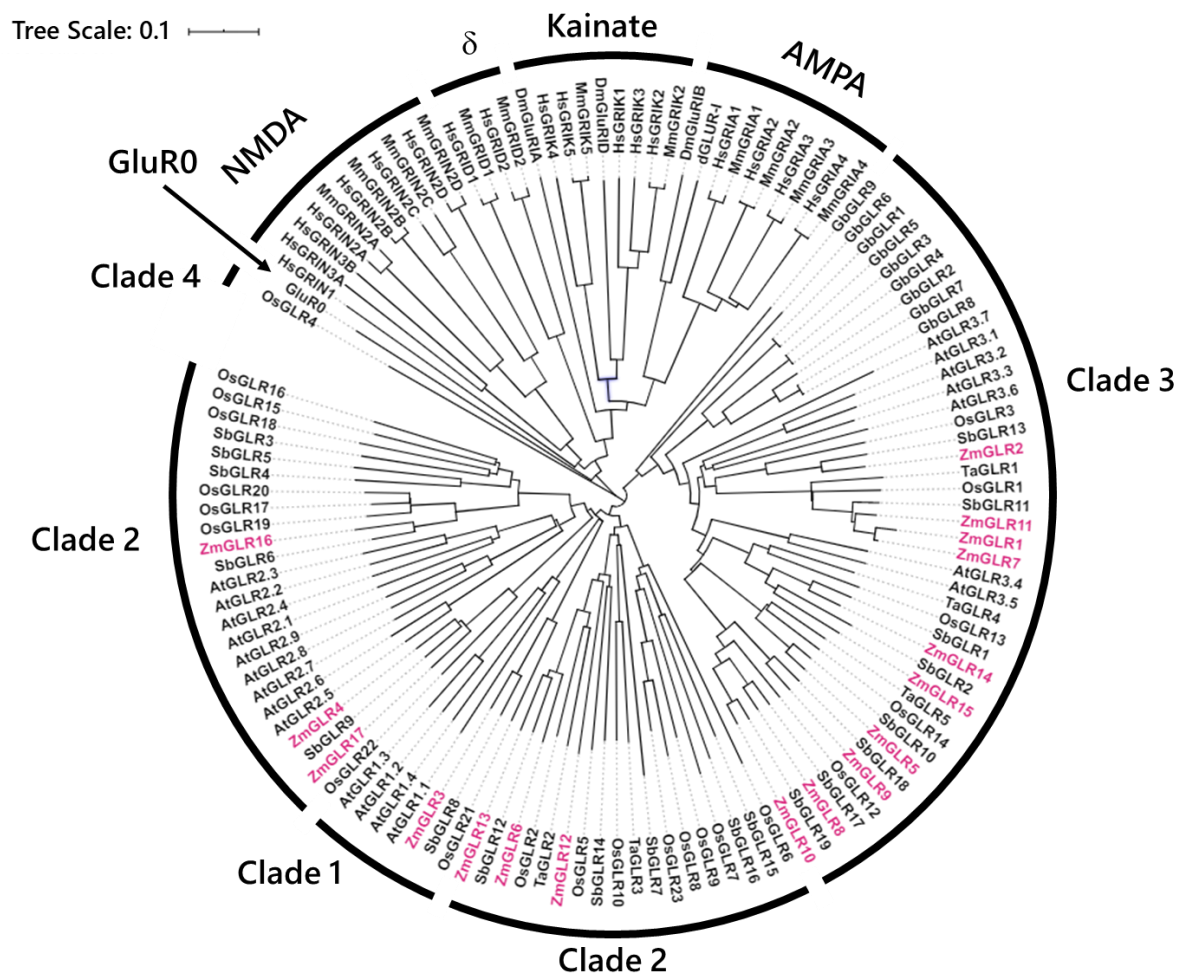
Figure 3.12 Phylogenetic relationship of ZmGLRs with glutamate receptors in other species: cyanobacteria *Synechocystis* (GluR0), *Mus musculus* (Mm), *Drosophila melanogaster* (Dm), *Homo sapiens* (Hm), *Arabidopsis* (At), *Sorghum bicolor* (Sb), *Oryza sativa* (Os), *Triticum aestivum* (Ta), and *Ginkgo biloba* (Gb). The phylogenetic tree was constructed using MEGA X by neighbor-joining method. Bootstrap values from 1000 replicates are indicated at each node.

closest to ZmGLR11 were ZmGLR1 and ZmGLR7. Synteny analysis showed ZmGLR11 and ZmGLR7 are syntelogs that resulted from a maize-specific whole genome duplication. ZmGLR1 is likely a transduplicated sequence, as it showed high identity (91%) with the ZmGLR11 and was not syntenic with homologous sequences in sorghum or rice. The comparison of ZmGLR11 with the next closest homolog, ZmGLR2, showed only the conservation of domains in the two sequences. This along with the separation of these two sequences in the phylogenetic tree indicated a duplication event that predates ancient grass whole genome duplication. The glutamate receptors ZmGLR3 was ZmGLR16 were also identified as syntelogs derived from a pre-grass whole genome duplication event. The glutamate receptors ZmGLR8 and ZmGLR 10 were also identified to be syntenic homologs.

3.4 Discussion

A key goal for the research presented in this chapter was to clone and confirm the gene underlying *D13* and determine the nature of the mutation that led to its partially dominant dwarfing phenotype. As described in detail in chapter 1, the *D13* mutation was generated by EMS mutagenesis, and was mapped to a region of chromosome 5 that contained 15 genes. To pinpoint which of these 15 genes represented *D13*, we conducted exome sequencing of these genes in collaboration with colleagues at Pioneer/Dupont (now Corteva Agriscience). A single G to A change (G2976A), typical of mutations induced by EMS, was found in only one of the 15 genes. This gene Zm00001d015007 was annotated to encode a glutamate receptor-like protein (GLR) with homology to the mammalian ionotropic glutamate receptors (iGluRs). Using the 20 *Arabidopsis* GLRs as reference, we identified 17 GLRs in maize. The GLR that has undergone the G to A mutation in *D13* was designated as ZmGLR11.

The G2976A change is a missense mutation that replaces an alanine at position 670 with threonine (A670T) in ZmGLR11. This finding was significant because this alanine residue (A670) is completely conserved in glutamate receptors across all domains of life, suggesting important functional relevance of this amino acid as well as *D13* mutation. Consistent with this hypothesis, the G2976A SNP was found to be completely linked with the *D13* phenotype as evidenced by genotyping with a dCAPs marker. To validate that the alanine to threonine substitution is in fact responsible for *D13*, an intragenic, second-site suppressor approach was used to identify EMS-induced mutants in which the effect of the *D13* mutant allele was nullified. One mutant (*D13**)

was identified that underwent a second G to A mutation within the *D13* allele, which reverted its phenotype to normal tall height. Together, these data convincingly show that *D13* resulted from a mutation in a GLR, ZmGLR11. This is the first GLR mutant to be discovered in maize.

We also used an alternative approach to validate the gene for *D13* by transgenically expressing the maize *D13* allele in *Arabidopsis* (data not shown). The transgenic *Arabidopsis* plants containing the mutant allele showed an impaired growth as compared to non-transgenic *Arabidopsis* controls. The work was delayed due to arrival of COVID-19 pandemic and is still in progress. In addition, transgenics expressing the wild type allele of *D13* need to be developed to serve as additional controls. Future studies using gene editing can be done to introduce the *D13* mutation (alanine to threonine substitution) in the closest *Arabidopsis* homolog to see if it impacts plant architecture in a similar manner as that observed in maize. Moreover, introduction of this amino acid change in each of the 20 GLR genes of *Arabidopsis* can help us to determine if the impact on plant architecture is general or gene specific.

Isolation of only a single mutant from about 16,000 M1 plants is a rather low efficiency of mutagenesis compared to the expected frequency of 1 in 1000, which could be a concern. Based on our current understanding, we think the main reason for the low efficiency was due to the presence of a very large number of false positives, which masked the identification of genuine mutants. However, other unknown factors may cause low efficiency as well. Furthermore, it is not clear why this experiment had so many false positives. We believe it was likely due to the unstable nature of the *D13* phenotype, which may have been exaggerated in the Mo17/CML322 hybrid background. Another possibility is contamination due to self-pollination of the female parent or pollination by stray pollen, but this was ruled out as genotyping of the tall plants confirmed the presence of *D13* allele in all of them. It is also possible that some tall mutants resulted from compensating mutations in one of the other 16 GLRs or in other modifiers.

The A670T amino acid substitution in ZmGLR11 occurs in the M3 transmembrane domain in a highly conserved eight amino acid motif that has been termed SYT<u>A</u>NLAA in the animal literature. The M3 domain plays a key role in gating the glutamate receptor ion channels (Traynelis et al. 2010). The complete conservation of the A4 amino acid in SYT<u>A</u>NLAA suggests that it is critical for the functioning of glutamate receptors and any mutations in it are likely to disrupt the channel activity. Studies in mammals have shown that closed confirmation of the GluR channel involves cross over of the M3 helices of four channel subunits at the "SYTANLAA" motif

(Wollmuth 2004). This motif lines the entrance to the pore on the extracellular side (Wollmuth 2004) and is also known as the "gate motif". The "SYTANLAA" motif is slightly modified in plants with differences at positions 5, 7 and 8 and most of the known plant GLRs contain "SYTASLTS" motif (Aouini et al. 2012; Price et al. 2012; Wudick et al. 2018a). Mutations in the gating motif are known to alter the channel activity significantly. This is evident in Lurcher mice (*Lc*), where a spontaneous mutation of alanine at position 8 in the motif to threonine (A8T) in the δ2 glutamate receptor constitutively activates the channel. Another mutation in this motif (T3A) in NMDA GluRs resulted in a large holding current, suggesting the channel to be constitutively open (Kashiwagi et al. 2002). Likewise, a substitution of the A4 (SYTANLAA) with cysteine in the NR1 subunit of NMDA receptors leads to significant changes in channel function similar to those observed in Lurcher mice (Sobolevsky et al. 2007). Like this mutation, our *D13* has a mutation in the same amino acid, and like the A4C change in NMDA receptor, A4T is also a non-polar to polar amino acid substitution. This A4 alanine is known to function as a "hinge" that is supposed to pull the M3 helices away from each other for opening the channel gate on the extracellular side (Twomey and Sobolevsky 2018). Based on this information from the mammalian GluRs, we presume that the A to T substitution in *D13* mutants disrupts the hinge-like activity and interferes with the opening/closing of the channel gate, thereby impacting the flow of cations across the membrane. This being the first such mutation in plants, *D13* can serve as an excellent resource to fill in the gaps in our limited understanding of the gating mechanism of glutamate receptors in plants.

There are many similarities in the structure and functioning of the glutamate receptor channels in plants and animals, but their physiological roles are quite diverse. In mammals they are primarily involved in fast excitatory neurotransmission whereas in plants they influence numerous processes related to plant growth and development as well as stress response. Several members of GLR family have been characterized in *Arabidopsis*, but limited information is available in maize. There is only one report that shows possible role of glutamate receptors in heat tolerance in maize (Li et al. 2019). It was based on a pharmaceutical approach in which it was demonstrated that glutamate-induced heat tolerance is weakened by treatment with DNQX, an antagonist of GluRs. There are no other reports on glutamate receptor genes in maize. In our study, a mutation in glutamate receptor gene (Zm00001d015007) led to defects in maize shoot architecture suggesting a role for GLRs in shoot development. *D13* plants were characterized by a

reduction in meristem size and internodes length. In addition, we observed significant aberrations in vascular bundles. The size of the vascular bundles was reduced in both *D13* homozygotes and heterozygotes as compared to the wild type, with the effect being more pronounced in the homozygous condition. The *D13* phenotype is unlike any phenotype observed thus far in GLR mutants in plants. A second-site mutation in the *D13* allele completely recovers the wild type phenotype, further supporting the role of GLRs in influencing plant architecture. Our transcriptomic analysis also shows that the genes related to shoot system development and meristem development are downregulated in *D13* mutants. Although mutations in this glutamate receptor gene influences plant height in maize, it remains unclear whether the effect is direct or occurs indirectly due to some other downstream changes.

Transcriptomic and metabolomic analysis revealed an upregulation of the stress response in *D13*. The genes related to response to abiotic stresses including drought, cold, salt, and light were upregulated in mutant plants as compared to the wild type. This observation is consistent with the previously reported roles of glutamate receptor genes in other plant species (Zheng et al. 2018; Li et al. 2019; Meyerhoff et al. 2005; Lu et al. 2014; Wang et al. 2019; Cheng et al. 2016). The structural aberrations in the xylem cells in the mutants can explain their enhanced response to drought stress. Furthermore, our data also suggests an upregulation of MAMP triggered immune response in mutants. In general, a MAMP recognition triggers several processes in plants including calcium influx, production of reactive oxygen species (ROS), changes in plant cell walls, and nitric oxide burst (Newman et al. 2013). Our data shows that many of the DEGs in *D13* mutants are associated with some of the above processes including response to bacteria and fungi, response to ROS (reactive oxygen species), and cell wall biosynthesis. Moreover, KEGG pathway enrichment analysis showed secondary metabolic pathways overrepresented in the mutant, which is another indicator of stress response in plants. The results of RNA-seq were consistent with those of untargeted metabolite analysis showing modification in same pathways such as photosynthesis, fatty acid biosynthesis and biosynthesis of secondary metabolites. Several studies in *Arabidopsis* have also shown the involvement of glutamate receptor genes in defense against pathogens (Kang and Turano 2003; Kwaaitaal et al. 2011; Li et al. 2013; Manzoor et al. 2013). The RNA-seq data also showed that the *D13* glutamate receptor gene and the other sixteen genes of this family are not differentially expressed in the mutant and wild type plants. This suggests that the changes in

D13 mutants are not due to variations in the expression of the glutamate receptor gene but, rather due to an impact of the mutation on downstream processes.

Based on our knowledge of gating of glutamate receptors in mammals and evidence of disrupted channel activity by mutations in SYTANLAA motif, it is evident that this gating motif plays a critical role in opening and closing of the channel. Thus, we propose that the gain of function mutation in *D13* plants that replaces the A4 residue in "SYTASLTS" motif with a threonine, disrupts the flow of Ca^{2+} into the cytosol. It could either completely close the channel or lead to constant leakage of Ca^{2+} as observed in Lurcher mice. In both cases, the mutation will disrupt the cytosolic calcium signatures that are required to regulate numerous downstream processes in plants. As calcium is crucial in numerous aspects of plant growth and development, this would explain the plethora of processes impacted by the *D13* mutation. Further studies are needed to test the ion channel activity of the glutamate receptor channel and intracellular calcium levels in *D13* plants.

CHAPTER 4.   PHENOTYPIC INSTABILITY IMPACTING PLANT HEIGHT IN *D13* MUTANTS

4.1   Introduction

Phenotypic variation in a trait can arise due to three major factors: genetic variation, environmental changes, or internal stochastic changes. The term phenotypic plasticity is used to describe the capacity of an organism to alter its behavior (morphological, physiological, or gene expression) in response to the environment (West-Eberhard 2008). On the other hand, the variation arising from intrinsic stochastic processes is a consequence of developmental noise and is often termed as developmental instability (Klingenberg 2019). In other words, developmental instability leads to deviation from the target phenotype expected for a given genotype and environment. In this chapter, we will use the terms 'developmental instability' and 'phenotypic instability' interchangeably. For a long time, phenotypic instability has remained ignored due to challenges associated with its measurement. Because of this, the extent to which the phenotypic instability impacts phenotype is not well understood.

There are few studies in plants that highlight phenotypic instability and have shed light on its possible causes (Sakai and Shimamoto 1965; Chopra et al. 2003; Yi and Richards 2008; Forde 2009; Šiukšta et al. 2015). EMS-induced phenotypic instability was observed in two (*cpr1, bal*) of the three (*cpr1*, *snc1*, and *bal*) dwarf *Arabidopsis* mutants that mapped to the *RPP5* locus comprising seven disease resistance genes (Yi and Richards 2008). Instability of *bal* and *cpr1* alleles was evident from an unusually high phenotypic suppression in *bal* and *cpr* M1 populations. Yi and Richards (2008) reported that hybrid formation also induces phenotypic instability. Despite the similarities in the dwarf phenotype of both *bal* × *snc1* F_1 hybrids and *bal* × *cpr1* F_1 hybrids, phenotypic variations were observed in the F_2 populations. While all plants in *bal* × *snc1* F_2 progeny were dwarf as expected, *cpr1* × *snc1* F_2 progeny had 10% plants with wild-type morphology. Šiukšta et al. (2015) reported phenotypic instability in inflorescence and floral organ development in *Hv-Hd/tw₂* double mutants in barley. The inflorescence of the double mutants was highly variable and drastically different from the original single mutants. Some of the double mutants displayed long gaps on rachis, while others had short gaps. The mutants also displayed striking variations in the spike structure, with some plants showing shoot-like and others bearing leaf-like structures in the inflorescence. The variations in inflorescence were even observed within

the same plant. This phenotypic instability was observed in all tested generations from F_1-F_{10}. The effect of 2,4-D and auxin inhibitors on the phenotype of double mutants suggested that phenotypic instability might be caused due to imbalance in auxin distribution in various regions of the inflorescence. Chopra et al. (2003) reported instability in kernel pericarp pigmentation in *Ufo1P1-wr* plants that ranged from deep red to various degrees of variegated red to colorless. Variegated pigmentation was also observed in husks, leaf sheath and tassel branches. *Unstable factor for orange1* (*Ufo1*) is a dominant modifier of maize *pericarp color1* (*p1*) gene. *Ufo1* does not induce pigmentation by itself but increases the expression of *P1-wr* allele, the pigmentation patterns strongly correlated with *P1-wr* expression and *P1-wr* methylation levels, indicating a role of epigenetic regulation in causing instability in phenotype.

Plant height is a complex agronomic trait that plays an important role in determining the yield potential of a crop. The genetic and environmental factors regulating plant height have been extensively studied in maize, which has led to identification of a large number of plant height related QTLs (https://maizegdb.org/data_center/qtl-loci-summary). However, not much information is available regarding developmental instability and the factors associated with this instability that impact plant height.

In this chapter, we will discuss dramatic phenotypic instability in the semi-dominant dwarf mutant (*D13*). The heterozygous *D13* plants display drastic variation in their heights despite their identical genotype. The variability was observed in both the greenhouse and field conditions and had no apparent environmental cause. The *D13/+:B73* mutants showing variable heights were back crossed to inbred B73 to explore the heritability of this variation. The F_1 progenies of these crosses show unstable phenotype irrespective of the phenotype of mutant parent. Moreover, this instability was also dependent on the genetic background. While *D13* phenotype is highly unstable in B73 background, the mutants in CML322 genetic background have a uniform height. The F_1 hybrids generated by crossing severe *D13* heterozygotes to three mapping populations also exhibited significant amounts of instability in mutant height.

4.2 Material and Methods

4.2.1 Plant material

The *D13* mutant was identified previously in our lab by EMS mutagenesis in inbred line B73. The mutant plant was used as a pollen parent and crossed to B73 to generate progeny segregating 1:1 for wild-type (WT) and *D13*/+:B73 heterozygotes. The mutant has been maintained in a heterozygous condition by repeated backcrossing to wild-type (WT) siblings.

The progeny of B73 x *D13*/+:B73, segregating 1:1 for mutant and WT sibling, was used to study the phenotypic variations in *D13* heterozygotes. To test the heritability of phenotypic instability, two mutants from each of the different height groups (very severe, severe, intermediate, intermediate++) were crossed as pollen parents to B73. To explore phenotypic variation in other backgrounds, the mutant plants from the progeny of B73 x *D13*/+:B73, were crossed to inbreds A632, Mo20W, and W22 and to 25 NAM lines in summer of 2017. As the *D13* heterozygotes in B73 show variable severity in the plant height, only severe *D13* plants were used for crossing to ensure uniformity. To generate the CML322/Mo17 M1 population, pollen from three randomly selected *D13* homozygotes (*D13*/*D13*:Mo17) was treated with EMS and individually crossed to CML322 during the summer of 2017, and the M1 plants were screened in summer 2018 for loss of *D13* phenotype. Tall M1 plants were identified and crossed to B73, and the resulting F_1 families were screened in the summer of 2019. *D13* heterozygotes (the pollen parents) were crossed with 81 intermated B73xMo17 (IBM) recombinant inbred lines (RILs) (Lee et al. 2002), 100 B73-Mo17 near-isogenic lines (BM-NILs) (Eichten et al. 2011) and 70 DRIL41 lines obtained from Peter Balint-Kurti (Lopez Zuniga et al. 2016) for mapping the modifiers. The full list of IBM-RILs, BM-NILs, and DRIL41 used to develop F_1 hybrid populations are presented in Supplementary Tables S3-S5.

4.2.2 Experimental design

The field experiments were conducted at Purdue agronomy center for research and education (ACRE) in West Lafayette, Indiana. Each plot was 3.84 m in length and contained 15-16 kernels. The row-to-row spacing for all experiments was 0.79 meters. The 81 F_1 derived IBM-RILs with *D13* heterozygotes were evaluated in summer of 2017 with two replications planted in a completely randomized design (CRD). The F_1 plants derived from crossing NAMs and inbreds

89

with *D13* heterozygotes were evaluated in single replications in 2018 and two replications during 2019.

For the M1 population, 16230 M1 seeds derived from three individual M1 families were planted in the summer of 2018. Highly suppressed revertant M1 plants were selected and crossed to inbred B73 for progeny testing. The resulting 184 F_1 families were planted in two replications in CRD in the summer of 2019. The inbred lines B73, Mo17, CML322, and B73 x *D13*/+:B73, CML322 x *D13*/+:Mo17 were included as controls. The F_1 families derived by crossing *D13*/+:B73 with the B73-Mo17 NILs and the DRIL41 population were evaluated in 2019 in two replications in CRD. The inbred lines B73 and Mo17, B73 x *D13*/+:B73, and Mo17 x *D13*:B73 were included as controls.

4.2.3 EMS mutagenesis

Targeted EMS mutagenesis was performed as described by Neuffer (Neuffer 1994). EMS stock solution was prepared by dissolving 1 mL of EMS (Sigma-Aldrich) in 99 mL of paraffin oil overnight. A fresh working solution was then made by mixing 1ml of stock solution with 14ml paraffin oil. Pollen was collected from three *D13* homozygotes (*D13*/*D13*:Mo17) and placed in individual small Nalgene bottles and freshly prepared EMS working solution was added to the bottles in a ratio of 10 parts solution to 1-part pollen. The bottles were placed on ice for 45 minutes and gently inverted every 5 minutes. The treated pollen was then spread onto the silks of plants of the inbred line CML322. The ears from crosses with the three pollen parents were harvested separately.

4.2.4 Phenotyping

Adult plant height was measured in centimeters from the base of the plant to the topmost leaf collar at maturity. Five mutants and five wild type plants were randomly selected from each F_1 family derived from inbreds and NAMs crossed to *D13/+:B73* during 2018. In 2019, the measurements were taken for three mutant and three wild type plants from the same F_1 families. For IBM F_1s and BM-NIL F_1s, plant height was measured for five enhanced mutants and three wild type plants, respectively. For the DRIL41 derived F_1s, plant height was measured for three

mutants and three wild type plants. The phenotypic data for F_1 hybrids in all three populations is presented in supplementary tables S3-S5.

4.2.5 Genotyping

A dCAPS marker designed using the G to A change in glutamate receptor (Zm00001d015007) gene was used for distinguishing the mutant and wild type plants in the progeny of crosses: B73 x *D13*/+:B73. DNA was extracted using the standard CTAB method (Doyle 1991). PCR amplification was performed in a 12 µl reaction (Saiki 1990) using the forward primer 5'- GCCTTTCCTGTTCAGTCCTTC -3' and reverse primer 5'- TGCACGGTTAGGATGGAAGTAAGACCTG -3'. The PCR products were digested with the *PstI* enzyme (New England Biolabs, MA, USA) for 3 hours at 37°C. An InDel marker flanking the *D13* region was designed to genotype the progeny of CML322 x *D13*/*D13*:Mo17 and B73x*D13*/+:CML322/Mo17 crosses. PCR to detect the InDel marker was performed using forward primer 5'- ATATATCGCATGCAGCGGGG -3' and reverse primer 5'- GCTAGCTGCTTCTTCCGGTT -3'. PCR products were resolved on 3% agarose gel.

4.2.6 Public/open-access data

The genotypic data for IBM-RILs was obtained from Lee et al. (2002). Data comprised a total of 2178 markers. The genotypic data for the B73-Mo17 NIL population obtained from (Eichten et al. 2011) contained a total of 7335 markers. The number of markers was reduced to 1978 after duplicate assessment. Marker data for the DRIL41 population was obtained from Peter Balint-Kurti at NC State University (Lopez Zuniga et al. 2016). Data comprised a total of 337 markers. The genotypic data for BM-NILs and DRIL41 were converted into A, B, and H format using "A" for B73, "B" for Mo17, "H" for the heterozygous individuals and "-" for the missing data.

4.2.7 Statistical analysis

Paired t-test was performed using GraphPad Prism version 8.3.0 (GraphPad Software, San Diego, California USA, www.graphpad.com).

4.3 Results

4.3.1 Phenotypic instability in *D13* heterozygotes

The *D13* mutants used for crossing have been maintained in a heterozygous condition by repeated backcrossing to B73 for several generations. The mutant and wild type progeny obtained from B73 x *D13*/+:B73 crosses segregated approximately 1:1 for mutant and wild type plants. The *D13* heterozygotes were significantly shorter than the wild types (t-test, p-value < 0.0001), however, their heights were highly variable at maturity and ranged from 10 cm to 158 cm. These mutants were grouped based on their height into five categories: very severe, severe, intermediate, intermediate+ (int+), and intermediate ++ (int++) (Figure 4.1). The phenotype of very severe plants was highly enhanced, and the plants were stunted in their growth, whereas int++ were much closer in height to the wild type plants. The first three categories were identified during early growth stages, but the less severe intermediates (int+ and int++) were clearly distinguished from wild type at maturity. The phenotypic variation was not just restricted to plant height but could also be observed in other architectural components, such as the number of tillers and development of inflorescence. The highly enhanced mutants, i.e., the very severe and severe groups, tended to tiller profusely, whereas the relatively suppressed mutants (int, int+, and int++) did not produce any tillers (Figure 2.4A). Like wild type plants, the suppressed mutants formed functional ears, whereas the enhanced ones either did not bear an ear or had sterile ears. This phenotypic instability was observed in all the backcross generations. The number of plants belonging to each height group in a given cross was random and varied among individual B73 x *D13*/+:B73 crosses (Figure 4.1B-E). In some cases, all five height categories of *D13* heterozygotes were observed in mutant siblings from a single cross.

To further study this variation and its inheritance, two plants from each of the mutant height groups were crossed to inbred line B73 and plant height was measured for 28-30 plants in each backcross family. Phenotypic instability was observed in mutant height in all the families we examined. In addition, the phenotype of the mutant parent was not associated with the phenotype of the next generation. The backcross progenies of both the very severe *D13* heterozygotes did not show a very severe or even severe phenotype. In fact, all the plants were suppressed as compared to the parent phenotype. The crosses of B73 with severe or int mutants yielded mutant progeny with variable heights, irrespective of the parent phenotype. While the phenotypes of parents were
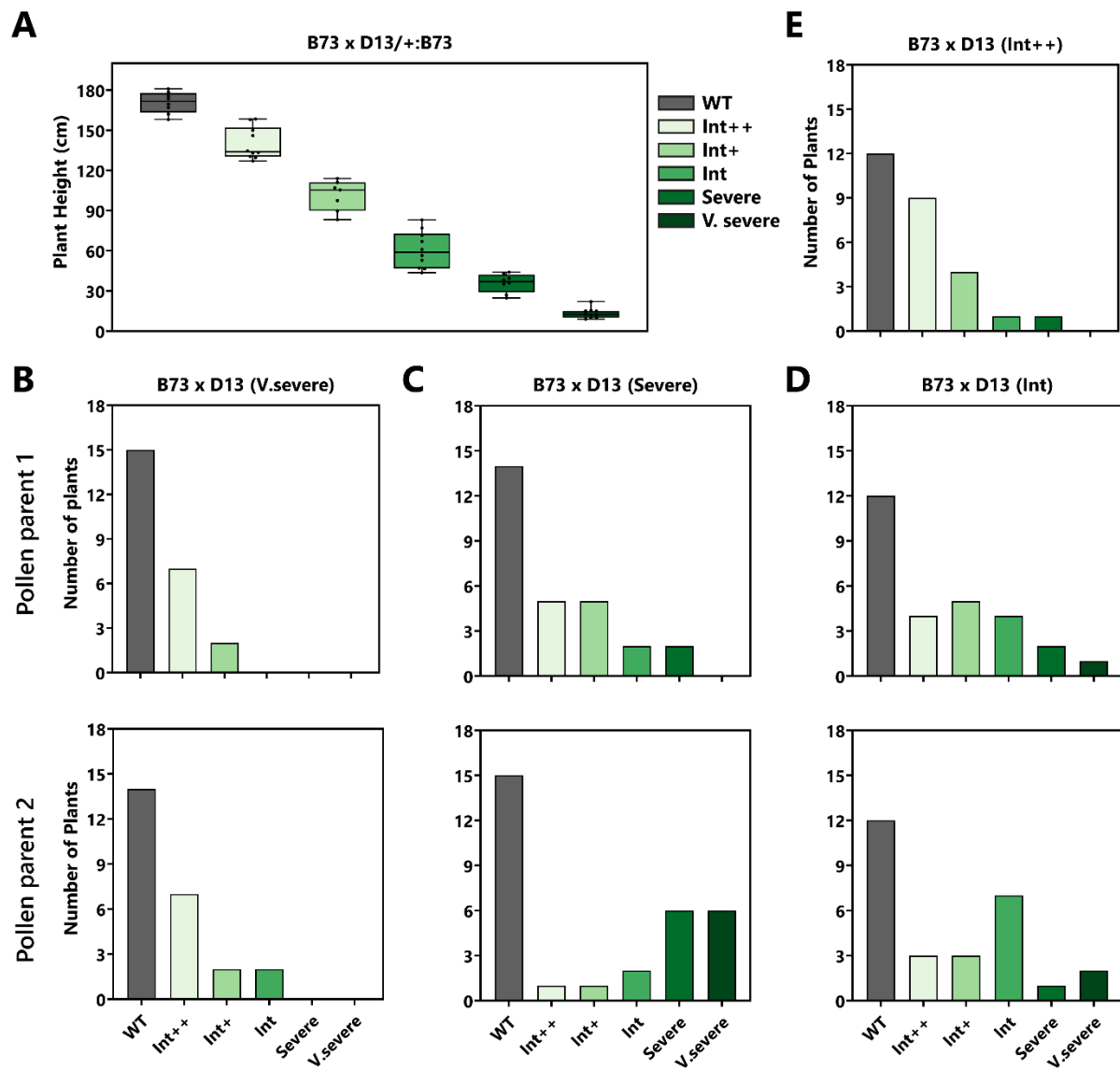
Figure 4.1 Phenotypic instability in *D13* mutants. (A) Variability in plant height in five height categories of *D13* heterozygotes as compared to wild-type siblings in B73xD13/+:B73 crosses. (B) Distribution of progeny of two individual B73 x *D13* (v.severe) crosses based on their plant height. (C) Distribution of progeny of two individual B73 x *D13* (Severe) crosses. (D) Distribution of progeny of two individual B73 x *D13* (Int) crosses. (E) Distribution of progeny of B73 x *D13* (Int++).

identical, no typical pattern was observed in the phenotypes of their progenies. This suggests that the instability in the *D13* phenotype is inherited from one generation to another irrespective of the original phenotype of the mutant parent.

4.3.2 Genetic background impacts phenotypic instability

Previously, the crosses of *D13* heterozygotes with maize inbred lines, including Mo17, A632, W22, Mo20W, and 25 NAM lines, revealed very high sensitivity of the *D13* phenotype to the genetic background (Figure 2.5). The *D13* mutants were severe and stunted in appearance in B73, P39, A632, and CML322 backgrounds, whereas they appeared completely normal in other backgrounds, including Mo17, Oh7B, NC350, and Tx303. In this study, we tested phenotypic variation between mutant plants within the F_1 families generated from the above crosses. Huge differences in the degree of variation were observed in mutant heights within each F_1 family (Figure 4.2, Table 4.1). While there was a great deal of variation in mutant height in B73, the mutants in Mo17 were reasonably uniform. The introgression of the *D13* allele in the Mo17 background led to a high level of suppression of the mutant phenotype, which remained stable despite repeated backcrossing with Mo17 for six generations. The mutants were almost as tall as their wild-type siblings, with a mutant/WT plant height ratio of 0.9. The suppressed phenotype was also observed in homozygous plants. Like Mo17, F_1s generated by crossing *D13* to other suppressing backgrounds like Oh7B produced similar results, with much less variability in the height of mutants. In contrast, the F_1s obtained by crossing CML322 (data not shown) and P39 to *D13*/+:B73 showed a very severe phenotype and did not appear to have any variability. Furthermore, the backgrounds with intermediate *D13* phenotype like W22, Mo18W, and CML247 also showed variation in the height of mutants at maturity.

4.3.3 High suppression of phenotype in M1 population

As discussed in chapter 3, Mo17 when combined with a *D13* enhancing background, CML322, does not suppress the phenotype completely and the mutants display reduced height as compared to wild type siblings (Table 4.2). This information was exploited to generate three M1 families, comprising 5373, 4072, and 6785 plants, respectively.
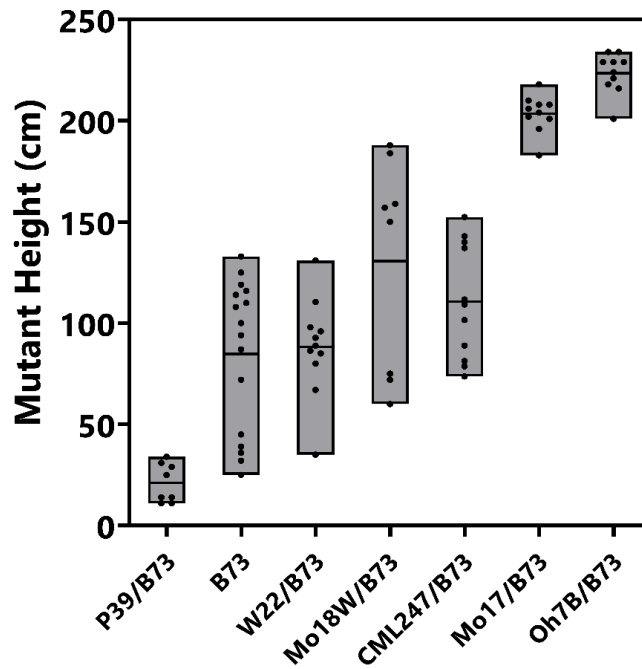
Figure 4.2 Phenotypic variation among *D13* mutants depends on the genetic background. The individual grey boxes depict the range of mutant plant height (cm) in F_1 hybrids obtained by crossing respective genetic backgrounds to *D13*/+:B73. The horizontal black lines represent the average height of mutants.

Table 4.1 Plant height of mutant progeny in F_1 hybrids obtained by crossing
respective lines with *D13*/+:B73

Genetic Background	Mutant plant height (cm)			
	Min. Height	Max. Height	Mean	SD[a]
P39/B73	11	34	21.13	9.61
B73	25	133	84.69	37.43
W22/B73	35	131	88.23	24.22
Mo18W/B73	60	188	130.63	52.83
CML247/B73	74	152	110.7	28.57
Mo17/B73	183	218	203.6	9.34
Oh7B/B73	201	234	223.5	10.06

[a]Standard Deviation

Table 4.2 Average plant height of wild-type (WT) and mutant (Mt) siblings from F_1 hybrids obtained from respective crosses

Cross	WT plant height (cm)			Mutant (Mt) plant height (cm)			Ratio Mt/WT
	Mean	SD[a]	N[b]	Mean	SD[a]	N[b]	
Mo17 x *D13*/+:B73	218.33	8.12	6	203.6	9.34	10	0.9
CML322 x *D13*/+:Mo17	204.47	25.36	5	105.66	11.99	5	0.52

[a]Standard Deviation
[b]Sample Size
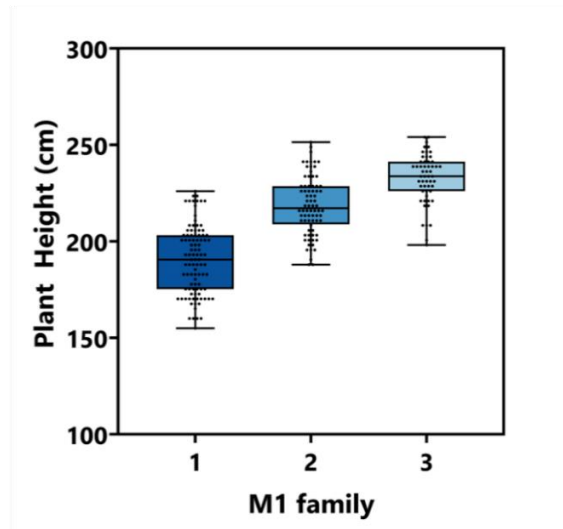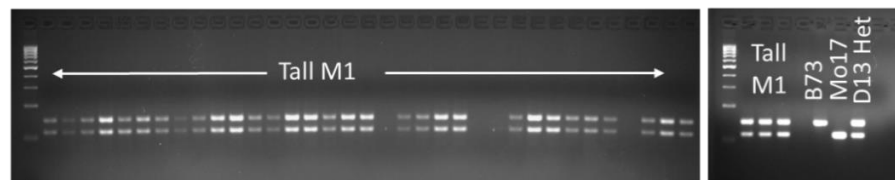
Figure 4.3 Phenotypic instability in M1 population. (A) Variation in plant height of suppressed plants in three M1 families. (B) Genotype of tall plants selected from the M1 population. Marker in lane1 is 100 bp ladder.

Variation in plant height was observed within each M1 family as well as between the three M1 families. We identified two percent suppressed (tall) M1 plants in both families 1 and 2 (112/5373, 82/4072), which was much higher than the expected frequency of 10^{-3} (Candela and Hake 2008). Not only was the number of suppressed plants much higher in these three M1 families, they also exhibited variation in the height of tall mutants (Figure 4.3A). This was particularly evident in family 3, where, unlike the 2% tall observed in family 1 and 2, all the plants were in the taller height categories, which posed difficulty in calculating the exact number of plants showing a revertant phenotype. Thus, we randomly selected 55 of the tallest M1s from group 3. All the selected M1s were found to contain the *D13* allele, thus ruling out the possibility of contamination (Figure 4.3B). It was interesting to note that while the three pollen parents used in this experiment did not exhibit any phenotypic variation among themselves, the progenies showed drastic deviations from the expected phenotype. Among the 184 F_1 families (obtained from B73 x tall M1s), 183 segregated for the dwarf phenotype indicating that tall revertant phenotype in those families was not due to knockdown of the *D13* allele. Only one F_1 family was completely suppressed and was later found to have a second mutation in the glutamate receptor gene (Figure 3.6).

In conclusion, the high frequency of the suppressed plants in three independent M1 families suggests that the phenotype of *D13* mutants is highly unstable despite the stable phenotype in the two parents CML322 and Mo17.

4.3.4 Phenotypic instability in RIL, NIL and DRIL populations derived from B73 and Mo17

It is evident that B73 and Mo17 have contrasting effects on the phenotype of *D13* mutants. The phenotype in B73 is highly enhanced but it is also unstable at the same time. In contrast, in the Mo17 background, it is both suppressed and stable. To map the possible modifying loci in Mo17, we crossed *D13*/+:B73 mutant to three mapping populations derived from B73 and Mo17. These include 81 lines of the intermated B73 x Mo17 (IBM) recombinant inbred line (RIL) population (Lee et al. 2002), 100 B73-Mo17 near-isogenic lines (BM-NILs) (Eichten et al. 2011) and 70 lines of a disease resistance introgression line (DRIL41) population (Lopez Zuniga et al. 2016). The first two populations, i.e., IBM-RILs and BM-NILs, are publicly available and have been utilized extensively for mapping several traits in maize. DRIL41 is a set of chromosome

segment substitution lines ($BC_3F_{4:5}$) generated by crossing Mo17 as the donor to recurrent parent B73. The DRIL41 population has been previously used to map disease resistance loci in maize (Cooper et al. 2018).

Each F_1 family obtained by crossing *D13* (pollen-parent) with the IBM-RILs, BM-NILs and DRIL41 lines, segregated approximately 1:1 for mutant (*D13* heterozygote) and wild type phenotype. Plant height was measured for heterozygous mutants in each F_1 progeny along with their wild type siblings. Phenotypic distribution was based on the average plant height of mutants calculated for data from two replications. The measurements were taken for five extreme mutants for the IBM F_1s and BM-NILs and three extreme mutants for DRIL41. In all three populations, wild type plants displayed a normal frequency distribution for the height (Figure 4.4A, B, C). However, the frequency distribution of plant height in mutant siblings depicted a multimodal pattern (Figure 4.4D, E, F).

The mutants in the B73 background usually display considerable phenotypic instability in the height of individuals. Similar observations were recorded for mutants in a majority of the F_1s in each of the three populations. Figure 4.5 clearly illustrates the amount of variability in mutant height within each F_1 population. Despite only selecting the extreme mutants from each F_1, we could still observe a high degree of variability in mutant height in the progeny of each cross as indicated by the length of the error bars. The highest amount of instability in mutant height was observed in the BM-NIL derived F_1s. The DRIL41 derived F_1 population displayed an interesting pattern with the F_1s at the two extreme ends of the graph (Figure 4.5C) displaying the least amount of variability. The BM-NILs and DRIL41 are both BC_3F_4 populations derived from B73 and Mo17 and are expected to behave in a similar fashion but still show considerable differences in mutant plant height. In contrast, the height of the wild type plants in each F_1 progeny was uniform and did not show much variation.

Although a lot of variation in plant height was present among the F_1s generated from IBM-RILs and BM-NILs, it was challenging to map the modifiers that cause suppression, probably due to high phenotypic instability within individual F_1 families. We were unable to identify any QTLs from these two populations. In case of DRIL41, F_1s on two extreme ends of the graph (Figure 4.5C), i.e. with highly suppressed or highly enhanced phenotypes, showed less phenotypic instability than all other F_1s in this population. Using this population, we were able to identify two QTLs on chromosomes 2 and 6 (Figure 2.6).
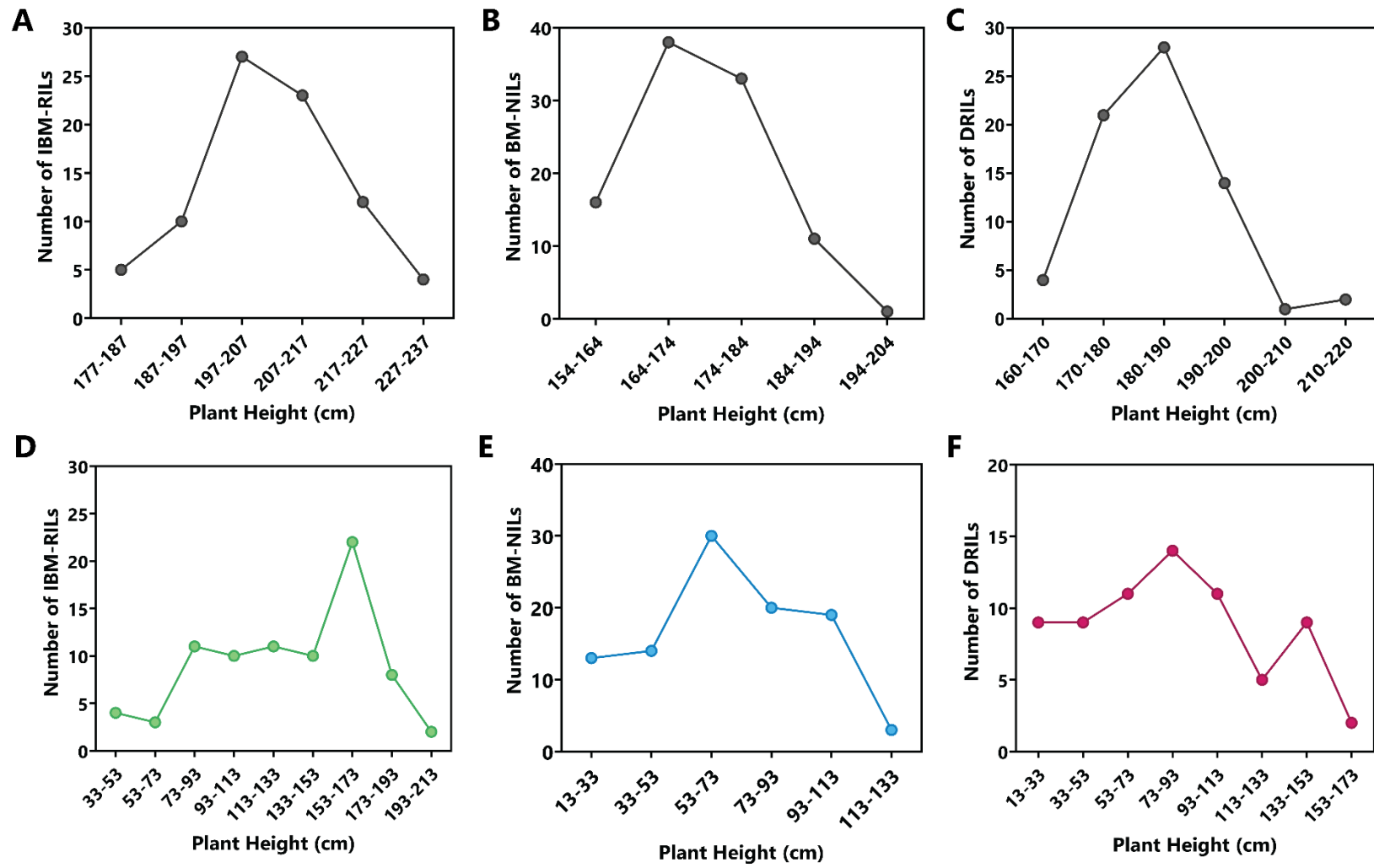
Figure 4.4 Phenotypic distribution of plant height in F$_1$s generated by crossing $D13$/+:B73 to IBM-RIL, BM-NIL, and DRIL populations. Plant height was measured at maturity from the base of the plant to the base of flag leaf. Distribution of wild type (WT) plant height in (A) IBM-RIL x $D13$/+:B73 F$_1$ population, (B) BM-NIL x $D13$/+:B73 F$_1$ population, and (C) DRIL41 x $D13$/+:B73 F$_1$ population. Distribution of mutant plant height in (D) IBM-RIL x $D13$/+:B73 F$_1$ population, (E) BM-NIL x $D13$/+:B73 F$_1$ population, and (F) DRIL41 x $D13$/+:B73 F$_1$ population. The data presented for all the populations is average from two replications planted in CRD.
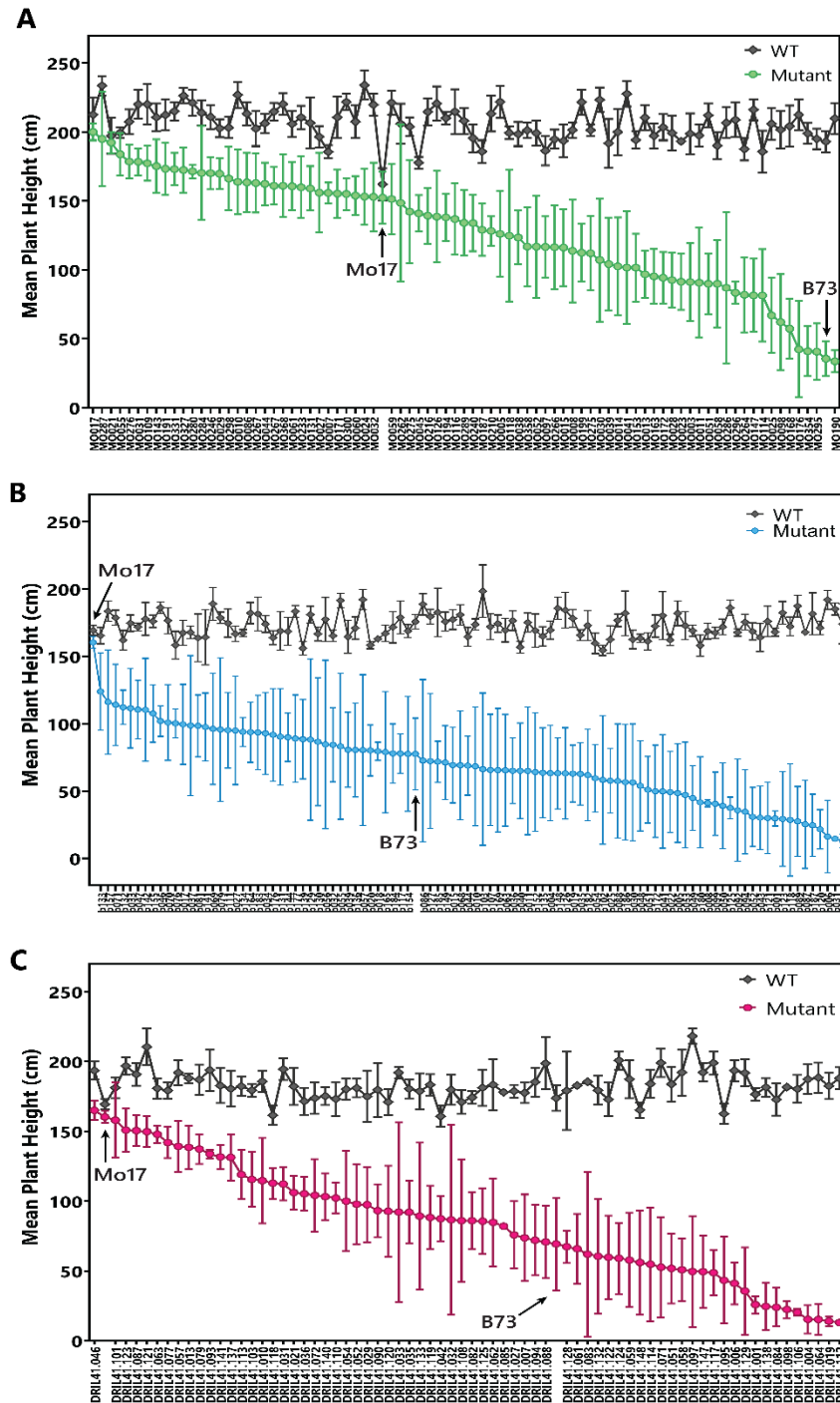
Figure 4.5 Average plant height of mutant and wild type (WT) F_1 hybrids generated by crossing *D13*/+:B73 to (A) IBM-RIL (B) BM-NIL (C) DRIL41 populations. The error bars represent standard deviation from the mean height. The black arrows indicate the progeny of B73 x *D13*/:B73 and Mo17 x *D13*/+: Mo17 crosses used as controls.

4.4 Discussion

In this study, we report unusual instability in the phenotype of heterozygous *D13* mutants. *D13* heterozygotes display up to a 15-fold variation in their plant height. This phenotypic instability in *D13* heterozygotes is observed across generations upon repeated backcrossing to B73. The dramatic variation in the mutant phenotype seems to be random and there is no apparent genetic or environmental cause. In addition, the phenotype of *D13* heterozygotes is independent of the phenotype of their mutant parents.

We identified a gain of function mutation in a glutamate receptor gene (Zm00001d015007) that is responsible for *D13* phenotype (chapter 3). Glutamate receptors are ligand-gated ion channels that transport Ca^{2+} across cell membrane. The formation of a functional channel requires assembly of four subunits to form a tetrameric complex (Madden 2002; Sobolevsky 2015). The *D13* heterozygotes contain both the wildtype and mutant alleles of the glutamate receptor gene (Zm00001d015007), so they will form a mixture of wild type and mutant protein subunits that will copolymerize to form the tetrameric channel. Studies in mammals have shown that incorporation of mutant subunits into the channel can alter the channel activity (Robert et al. 2002; Zuo et al. 1997) and one mutant subunit is sufficient to disrupt the function of the channel (Robert et al. 2002). We propose that severity of *D13* phenotype depends on the proportion of mutant subunits incorporated in the tetrameric complex. According to this hypothesis, if only one of the four subunits is mutated then phenotype should be less severe as compared to when all four subunits are mutated. This would explain the variability in the phenotype of *D13* heterozygotes. The incorporation of the mutant or wildtype subunits into the tetrameric complex depends on their relative expression. Further studies are required to determine the level of expression of wild type and mutant subunits in variable *D13* heterozygotes and its impact on channel formation.

Variation in the phenotypes of genetically identical individuals can be an outcome of response to the external environment (phenotypic plasticity) or due to internal changes in the organism (phenotypic instability). Our data for *D13* mutant suggests that the variation in plant height is not due to the environment because all the plants were grown in the same field at the same time. We also observed the variation in plants grown in more controlled greenhouse conditions. The variability in *D13* phenotype was observed across generations and over multiple years suggesting the involvement of internal factors. Phenotypic instability in plants is poorly understood and very little is known about the extent of its impact on the phenotype but studies

have suggested that instability can serve as an indicator of stress (Freeman et al. 1999; Pertoldi et al. 2006). This is consistent with our observations in *D13* mutants. Our transcriptomic and metabolomic data indicates an increase in stress in *D13* plants.

Taken together, we propose that instability in *D13* phenotype is likely caused by changes in the relative expression of wildtype and mutant subunits caused by intrinsic stochastic factors. Intrinsic factors that can lead to phenotypic instability include epigenetic modifications like changes in DNA methylation (Sekhon and Chopra 2009; Chopra et al. 2003). Chopra et al. (2003) characterized a dominant modifier of maize pericarp color (*p1*) gene, called *Ufo1* (*Unstable factor for orange1*) that induces a pigmentation in the kernel pericarp and other parts of the plant including silk, tassel glumes, husk and leaf sheath, in presence of *P1-wr* allele. The phenotype of the *Ufo1P1-wr* plants is unstable, and plants exhibit somatic mosaicism with variations in pigmentation. This study showed that variation in phenotype is correlated with *P1-wr* overexpression and the levels of *P1-wr* demethylation. It is possible that the differences in *D13* heterozygotes are a result of epigenetic changes.

Our data shows that the degree of instability in *D13* phenotype varies with the genetic background. Like B73, some backgrounds including W22, Mo18W and CML247 show large deviations in the mutant height. The phenotype in highly suppressing backgrounds, Mo17 and Oh7B, is more uniform and stable. The *D13* enhancing backgrounds, CML322 and P39 also show more stability. Studies in *Arabidopsis* have shown high polymorphism in gene methylation patterns among different accessions (Vaughn et al. 2007). This suggests that natural epigenetic variation in different genetic backgrounds can determine the variability in phenotype in these backgrounds. However, the amount of phenotypic variability might depend on additional factors like stress. We observed that B73 background, which shows a great deal of variation in *D13* phenotype, exhibits upregulation of stress response genes. In contrast, no signs of stress response are observed in Mo17 background, which does not show variation in *D13*. This might explain the stable *D13* phenotype in Mo17 background.

Phenotypic instability was also observed in three M1 families obtained by crossing inbred CML322 with EMS treated pollen of three *D13* homozygotes (*D13*/*D13*:Mo17). While CML322 genetic background enhances the *D13* phenotype, Mo17 completely suppresses *D13*. The plants in Mo17/CML322 hybrid background show an intermediate plant height. We observed deviations from the expected intermediate height in all three M1 families. Moreover, the number of tall plants

were much higher than the expected frequency of 10^{-3}. Yi and Richards (2008) also reported instability and high incidence of phenotypic suppression in M1 populations generated from EMS treated *bal* and *cpr* mutants. They suggested that the revertant phenotype in M1 was due to intragenic suppression of *bal* allele. On the contrary, our sequencing of *D13* region in the tall M1 plants showed no new mutations in the glutamate receptor gene (Zm00001d015007), indicating that revertant phenotype was not due to intragenic changes and likely results from EMS induced changes in other regions of the genome. The mutations in the enhancer loci (present in CML322) can also lead to suppressed phenotype. Earlier, we identified three putative QTLs associated with suppression of *D13* (Table 2.2). Mutations in these loci may also contribute to the instability in phenotype in M1 families. The *D13* mutants in untreated CML322/Mo17 background do not show phenotypic instability, which further suggests that instability and high suppression in M1 generation is induced by EMS.

The instability of phenotype was not just restricted to within M1 families. There were large differences between these families as well. The plant height in second and third M1 families was in general taller than the first M1 family. The average height of tall plants selected from each of the three M1 families was also variable. Three *D13* homozygotes used as pollen parents to generate these M1 families were identical in their phenotype. These results were consistent with our observation in B73 background where progenies obtained from phenotypically identical mutant parents showed deviations from the parental phenotype (Figure 4.1). One possibility is that EMS mutagenesis can reset the epigenetic alterations or generate novel epigenetic variation that leads to instability of phenotype in M1 families.

The phenotype of the mutant progeny in the F_1s generated by crossing three B73-Mo17 derived populations IBM-RIL, BM-NIL and DRIL41 with *D13*/+:B73, showed variations just like B73 parent. As these three populations are initially derived from Mo17 (which highly suppresses the *D13* phenotype), we expected the mutant progeny to be highly suppressed and uniform. The BM-NIL F_1 families showed suppression of *D13* phenotype but the frequency of suppressed plants in each F_1 family was variable. The IBM-RIL and DRIL41 populations showed relatively stable suppression of *D13* phenotype. Because the *D13* phenotype is highly unstable in B73 background, one of the challenges in identifying suppressors in these populations was our inability to distinguish the suppression caused by Mo17 from the inherent suppression in B73 background. Moreover, we used multiple pollen parents for generating the F_1 families because a single *D13*

plant does not produce enough pollen. Each pollen parent, although sharing an identical phenotype, does not give rise to same phenotype in progeny resulting in large variations in phenotypes of progenies from one pollen parent and those from another second pollen parent. To eliminate this variation, a new population can be generated using a single pollen parent for crossing.

APPENDIX A

Supplementary Figures and Tables
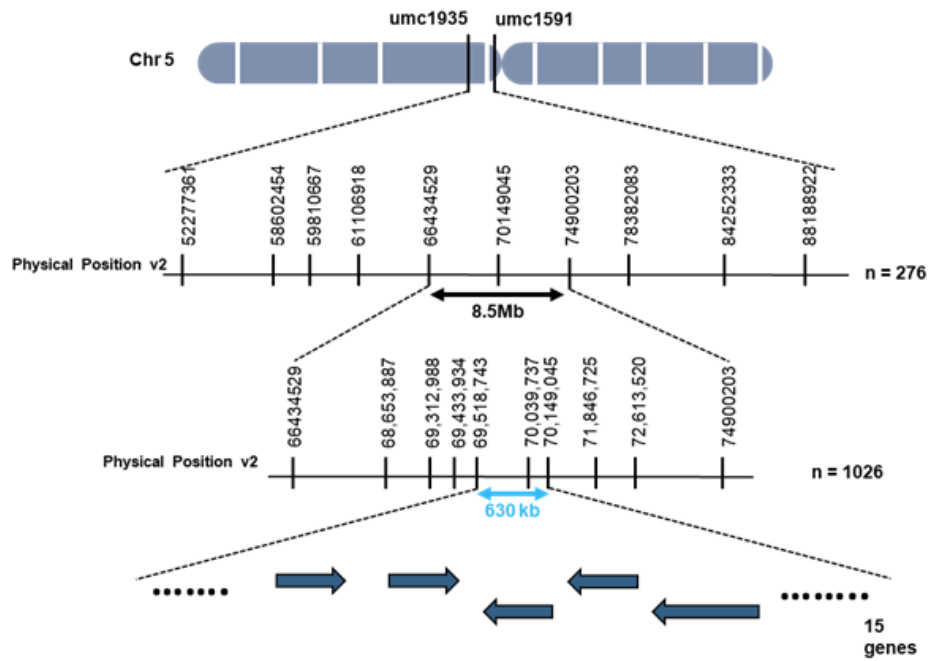
Figure S1 Mapping of *D13* locus.
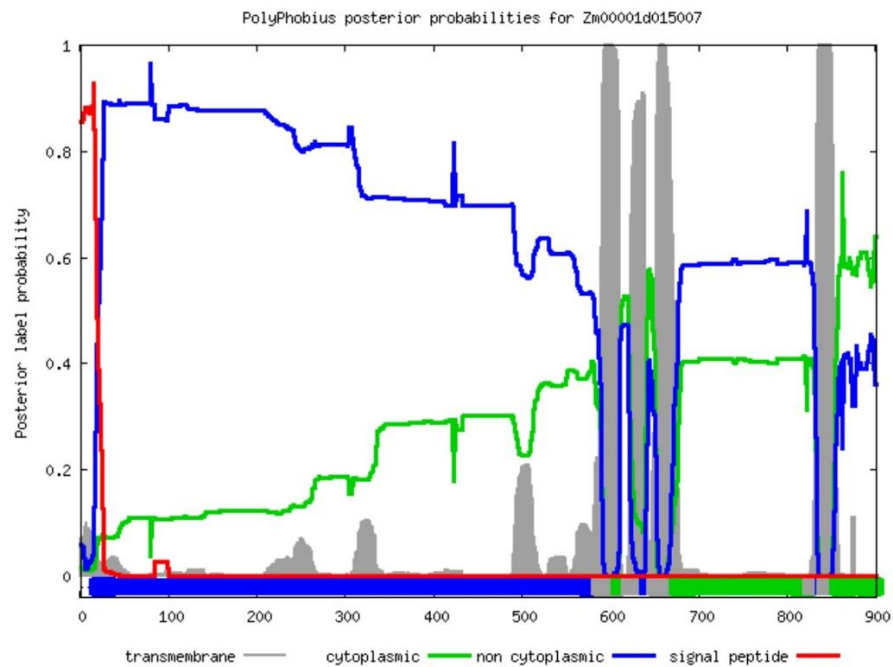
Figure S2. Predicted transmembrane domains for Zm00001d015007 (ZmGLR11) protein. The transmembrane domains and signal peptide were estimated using Polyphobius (http://phobius.sbc.su.se/poly.html). The grey bars indicate transmembrane domains, green line indicates cytoplasmic loop, blue line indicates non-cytoplasmic loop, and red line depicts the signal peptide.
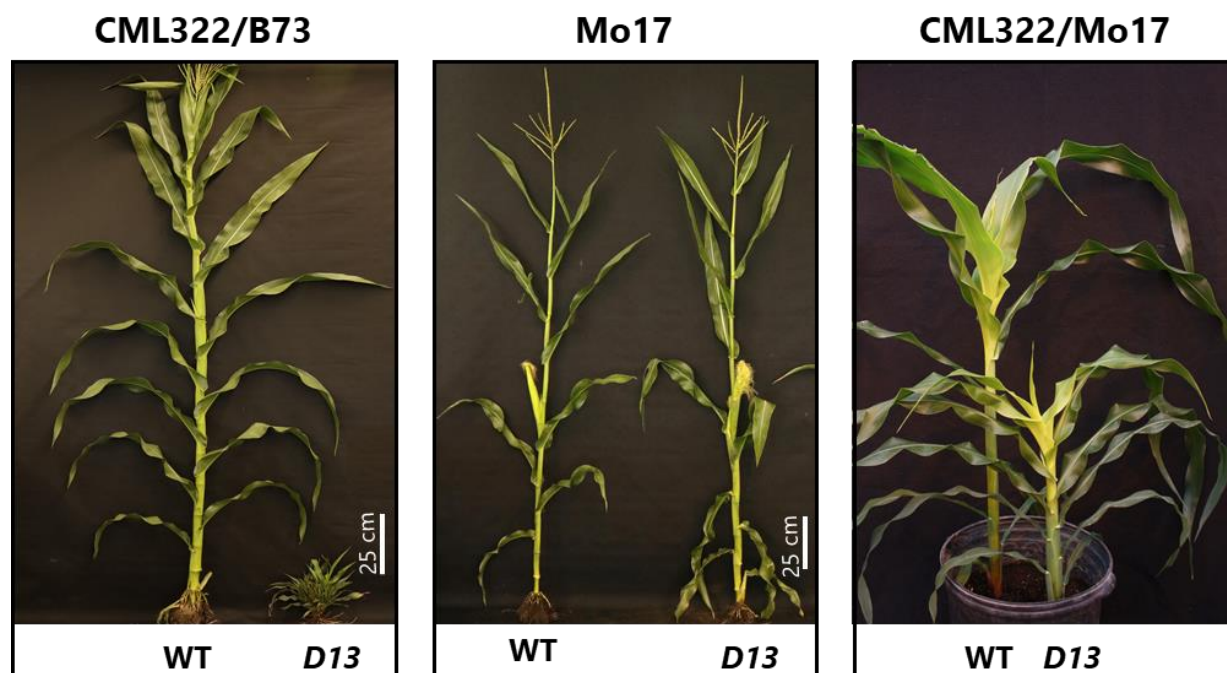
Figure S3 Variable severity of *D13* phenotype in CML322/B73 and CML322/Mo17 hybrids. CML322/Mo17 background does not suppress the phenotype completely as Mo17.
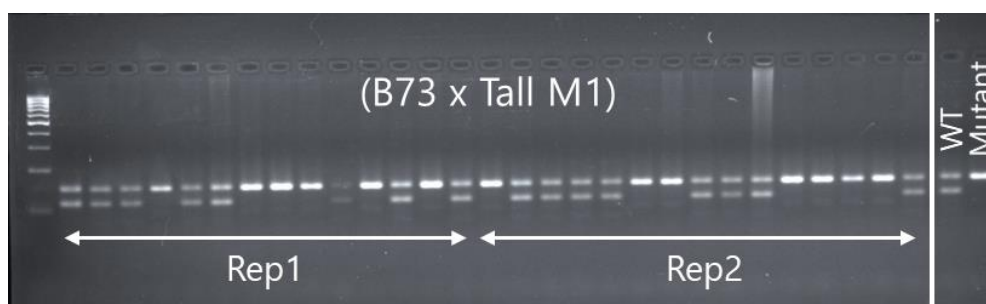
Figure S4 Genotypic segregation of positive (B73 x Tall M1) progeny with InDel marker. The progeny of this cross depicted tall plant height in both the replications and segregated 1:1 (WT:Mutant). Marker in lane1 is 100 bp ladder.
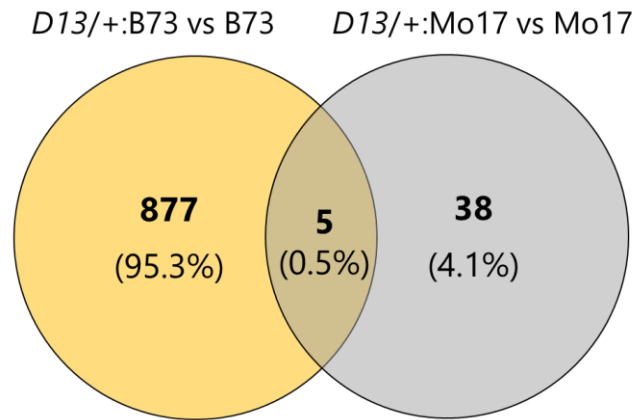
Figure S5 Venn diagram showing the number and percentage of DEGs in B73 and Mo17 backgrounds; percentage values are relative to the total number of DEGs from both groups.
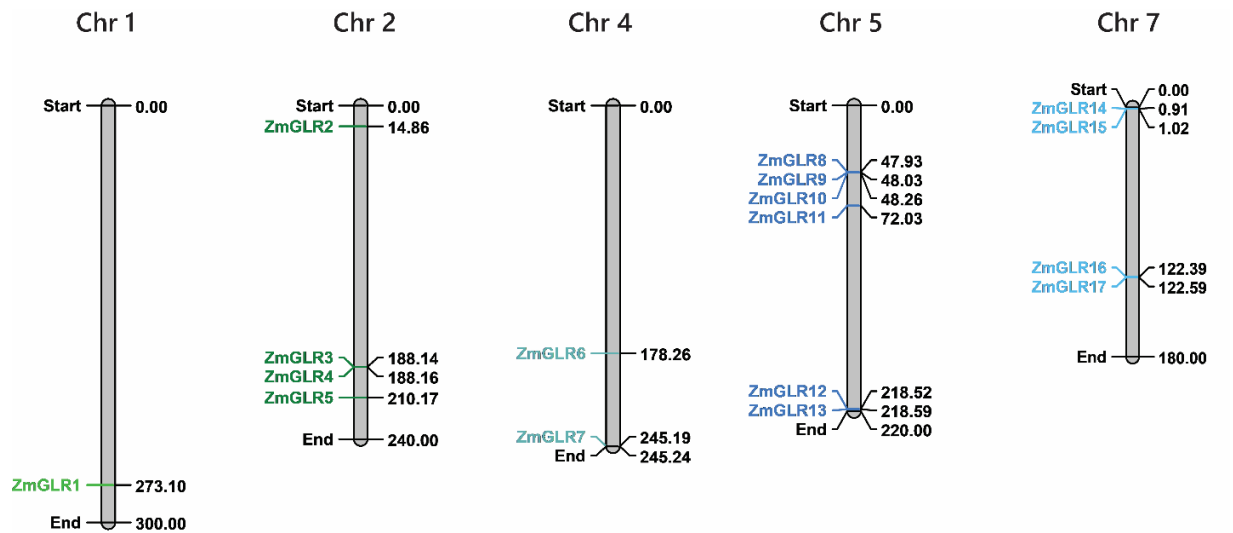
Figure S6 Map positions of ZmGLRs on maize chromosomes. The numbers corresponding to each gene represent its position in Mbp. The end positions represent the total length of each chromosome in Mbp.

Table S1 SNPs identified in revertant plants obtained from single completely suppressed (B73 x Tall M1) F_1 family and Controls.

Sample	Description	Reference Sequence	Position	REF	ALT	QUAL	Genotype	Allele Depth	Read Depth	Genotype Quality	Phred Scale Likelihoods
23-7	Revertant plant #1	B73	2448	G	A	62844.77	0/1	1983, 2275	4258	99	62873,0,51778
			3904	G	A	38759.77	0/1	1576, 1581	3157	99	38788,0,38426
R2-25-1	Revertant plant #2	B73	2448	G	A	41387.77	0/1	1523, 1701	3224	99	41416,0,35852
			3904	G	A	11006.77	0/1	497, 498	975	99	11035,0,11864
B73	Inbred Control	B73	-	-	-	-	-	-	-	-	-
83-4	Partially suppressed mutant	B73	3904	G	A	1943.77	0/1	111, 91	202	99	1972,0,2546
144-6	Partially suppressed mutant	B73	3904	G	A	7798.73	0/1	314, 330	644	99	7836,0,7459

Table S2 Genes associated with anthocyanin accumulation upregulated in *D13*.

S.No.	Gene ID	log2 FC	padj	Description
1	Zm00001d052746	2.8101	0.0029	Transmembrane ascorbate ferrireductase 1
2	Zm00001d043512	1.6187	0.0106	Protein kinase family protein with leucine-rich repeat domain
3	Zm00001d037328	1.6072	0.0000	3-ketoacyl-CoA synthase
4	Zm00001d044579	1.5611	0.0000	3-ketoacyl-CoA synthase
5	Zm00001d018455	1.3755	0.0032	3-ketoacyl-CoA synthase
6	Zm00001d028241	1.2057	0.0000	3-ketoacyl-CoA synthase
7	Zm00001d033234	1.5147	0.0000	Protein Kinase PINOID
8	Zm00001d044083	1.4455	0.0000	PIN4
9	Zm00001d011661	1.4150	0.0000	GDSL esterase/lipase APG
10	Zm00001d045620	1.3551	0.0142	Plastocyanin major isoform chloroplastic
11	Zm00001d035859	1.0599	0.0000	Plastocyanin homolog1
12	Zm00001d020555	1.3119	0.0112	WAT1-related protein
13	Zm00001d040089	1.2671	0.0327	WAT1
14	Zm00001d047208	1.1844	0.0022	WAT1-related protein
15	Zm00001d020556	1.0559	0.0001	WAT1-related protein

Table S3 Average Plant Height (PH) of wild-type (WT) and mutant (Mt) siblings from F_1s
generated by crossing *D13*/+:B73 with respective IBM-RILs.

S.No.	IBM_ID	WT			Mt			Mt/WT
		Mean PH (cm)	SD[a]	N[b]	Mean PH (cm)	SD[a]	N[b]	
1	MO003	198.80	14.76	10	91.10	28.19	10	0.458
2	MO005	221.90	11.78	10	126.10	31.24	10	0.568
3	MO007	185.60	4.88	5	155.80	7.46	5	0.839
4	MO008	201.43	5.71	7	113.80	37.36	10	0.565
5	MO010	227.00	9.42	9	163.89	23.66	9	0.722
6	MO011	197.50	7.91	10	90.67	39.93	9	0.459
7	MO013	210.40	8.93	10	96.80	17.25	10	0.460
8	MO014	200.00	16.84	10	102.60	35.49	10	0.513
9	MO015	193.57	11.73	7	116.14	27.90	7	0.600
10	MO017	212.60	12.30	5	200.00	6.08	3	0.941
11	MO021	197.20	13.06	10	192.30	7.65	10	0.975
12	MO023	193.25	2.75	4	91.33	20.48	6	0.473
13	MO024	234.00	10.56	10	153.13	20.39	8	0.654
14	MO025	206.00	11.43	9	67.00	27.36	9	0.325
15	MO027	196.50	7.92	10	156.00	28.91	9	0.794
16	MO028	199.30	12.68	10	92.60	19.84	10	0.465
17	MO029	202.70	6.60	10	169.73	11.16	11	0.837
18	MO030	223.40	8.98	10	107.13	44.72	8	0.480
19	MO031	220.10	10.34	10	178.38	9.84	8	0.810
20	MO032	219.78	7.87	9	153.00	24.91	8	0.696
21	MO038	198.50	8.78	10	123.50	19.57	10	0.622
22	MO039	191.80	17.57	5	104.18	33.81	11	0.543
23	MO041	227.67	9.24	6	101.60	40.87	5	0.446
24	MO044	206.30	6.86	10	162.33	15.54	9	0.787
25	MO045	177.75	4.27	4	141.00	13.21	5	0.793
26	MO051	212.10	8.52	10	89.91	22.11	11	0.424
27	MO052	199.20	9.20	5	116.80	37.13	5	0.586
28	MO055	199.44	3.94	9	183.86	15.48	7	0.922
29	MO058	190.10	9.86	10	89.90	31.67	10	0.473
30	MO059	221.20	8.61	10	151.40	25.50	10	0.684
31	MO060	207.50	11.77	10	153.80	14.25	10	0.741
32	MO061	205.90	9.49	10	160.71	17.37	7	0.781
33	MO086	213.30	8.50	10	163.44	21.47	9	0.766
34	MO097	186.40	10.67	5	116.60	22.22	5	0.626
35	MO098	201.67	13.41	9	62.10	34.77	10	0.308
36	MO109	220.20	14.53	10	177.30	12.68	10	0.805
37	MO114	185.80	15.17	10	81.40	33.57	10	0.438
38	MO116	214.80	16.19	10	136.86	25.96	7	0.637
39	MO118	199.40	4.60	10	124.75	47.63	8	0.626

Table S3 continued.

S.No.	IBM_ID	WT			Mt			Mt/WT
		Mean PH (cm)	SD[a]	N[b]	Mean PH (cm)	SD[a]	N[b]	
40	MO126	220.70	12.43	10	138.57	33.23	7	0.628
41	MO131	206.60	18.32	10	159.11	16.10	9	0.770
42	MO143	210.70	9.99	10	175.33	19.42	9	0.832
43	MO147	216.20	7.64	10	81.50	26.55	8	0.377
44	MO153	194.20	6.21	10	101.60	24.56	10	0.523
45	MO163	197.20	8.99	10	95.25	19.81	12	0.483
46	MO168	204.20	14.99	10	57.38	21.88	8	0.281
47	MO171	210.70	15.20	10	155.25	17.66	8	0.737
48	MO172	203.40	9.47	10	94.27	18.67	11	0.463
49	MO176	212.50	11.19	10	42.44	34.92	9	0.200
50	MO187	185.90	8.12	10	129.00	18.97	10	0.694
51	MO190	209.90	11.30	10	33.70	8.01	10	0.161
52	MO191	212.30	11.22	10	173.30	19.05	10	0.816
53	MO194	210.10	4.68	10	138.09	17.03	11	0.657
54	MO199	221.70	9.13	10	112.40	21.04	10	0.507
55	MO210	213.25	13.00	4	128.20	10.69	5	0.601
56	MO216	214.67	9.76	9	139.33	20.30	9	0.649
57	MO233	210.70	8.45	10	159.89	22.32	9	0.759
58	MO240	195.60	10.18	10	134.00	20.47	11	0.685
59	MO246	210.90	8.70	10	170.14	11.81	7	0.807
60	MO262	206.00	14.58	10	148.55	57.08	11	0.721
61	MO264	187.63	8.31	8	81.92	27.21	12	0.437
62	MO266	194.80	6.98	5	116.50	30.56	6	0.598
63	MO267	202.50	12.77	10	163.00	21.44	10	0.805
64	MO267	214.80	6.46	5	161.00	13.51	5	0.750
65	MO275	203.90	6.76	10	142.20	37.39	10	0.697
66	MO275	201.40	4.16	5	112.00	27.09	4	0.556
67	MO276	207.50	8.91	10	178.56	12.06	9	0.861
68	MO280	221.20	9.65	5	171.50	4.95	2	0.775
69	MO284	213.90	9.24	10	170.27	34.18	11	0.796
70	MO286	206.67	11.19	9	87.00	54.95	12	0.421
71	MO287	233.60	7.03	10	195.00	34.11	10	0.835
72	MO289	208.10	9.41	10	134.10	23.60	10	0.644
73	MO295	195.00	7.38	10	40.63	20.52	8	0.208
74	MO296	208.80	12.52	5	83.33	8.14	12	0.399
75	MO298	203.20	7.70	10	166.25	23.02	12	0.818
76	MO300	221.80	6.06	5	155.00	11.62	5	0.699
77	MO327	226.30	5.66	10	172.44	16.34	9	0.762
78	MO331	215.00	6.73	10	173.11	11.87	9	0.805

S.No.	IBM_ID	WT			Mt			Mt/WT
		Mean PH (cm)	SD[a]	N[b]	Mean PH (cm)	SD[a]	N[b]	
79	MO354	199.00	7.68	5	41.00	18.14	5	0.206
80	MO358	201.30	5.40	10	116.91	28.71	11	0.581
81	MO368	220.30	7.96	10	161.00	22.79	9	0.731

The data are presented as mean and standard deviation derived from two replications planted in CRD. For each replication, data were collected for five independent mutants and WT siblings.
[a]Standard Deviation
[b]Sample Size

Table S4 Average Plant Height (PH) of wild-type (WT) and mutant (Mt) siblings from F$_1$s generated by crossing *D13*/+:B73 with respective BM-NILs.

S.No.	BM-NIL_ID	WT			Mt			Mt/WT
		Mean PH (cm)	SD[a]	N[b]	Mean PH (cm)	SD[a]	N[b]	
1	b001	168.17	3.06	6	29.70	5.68	10	0.177
2	b004	169.50	6.75	6	63.28	35.51	10	0.373
3	b005	182.00	9.21	6	48.43	36.55	7	0.266
4	b006	192.00	7.07	6	16.21	26.90	9	0.084
5	b008	168.67	5.85	6	41.05	2.78	10	0.243
6	b010	173.67	4.23	6	68.35	44.19	10	0.394
7	b011	175.17	7.11	6	64.95	47.41	10	0.371
8	b015	177.33	7.31	6	69.30	28.10	10	0.391
9	b017	167.50	9.46	6	99.50	29.73	10	0.594
10	b018	163.00	2.45	6	79.50	6.79	10	0.488
11	b019	178.17	6.62	6	62.90	21.14	10	0.353
12	b020	158.33	2.66	6	80.15	18.99	10	0.506
13	b022	162.17	4.22	6	49.20	30.07	10	0.303
14	b025	162.50	10.25	6	57.65	23.90	10	0.355
15	b027	166.67	5.85	6	94.94	40.24	10	0.570
16	b030	162.50	6.95	6	56.41	43.35	8	0.347
17	b031	185.17	4.45	6	14.53	1.54	9	0.078
18	b032	165.33	4.32	6	84.38	27.56	10	0.510
19	b033	174.67	6.12	6	111.50	29.54	6	0.638
20	b034	174.00	6.23	6	92.83	30.38	8	0.534
21	b035	165.75	4.11	4	62.65	23.14	10	0.378
22	b036	176.50	7.23	6	65.06	24.38	7	0.369
23	b037	167.83	4.79	6	98.58	51.98	10	0.587
24	b039	164.50	12.28	6	80.63	27.92	9	0.490
25	b040	156.83	4.36	6	65.00	35.51	10	0.414
26	b041	180.33	17.72	6	49.70	42.18	10	0.276
27	b043	164.00	10.43	6	30.16	23.50	10	0.184

Table S4 continued.

S.No.	BM-NIL_ID	WT			Mt			Mt/WT
		Mean PH (cm)	SD[a]	N[b]	Mean PH (cm)	SD[a]	N[b]	
28	b044	164.50	7.06	6	68.79	21.93	9	0.418
29	b046	186.17	4.22	6	101.89	11.36	10	0.547
30	b047	171.83	2.99	6	110.45	21.73	8	0.643
31	b048	163.50	3.11	4	53.85	33.55	3	0.329
32	b049	169.00	4.10	6	44.80	24.09	10	0.265
33	b050	171.83	5.88	6	39.00	31.94	10	0.227
34	b051	161.17	6.49	6	50.95	24.77	10	0.316
35	b052	168.50	6.38	6	30.80	21.92	10	0.183
36	b053	172.83	10.36	6	47.05	39.36	10	0.272
37	b054	159.67	7.55	6	59.50	25.00	10	0.373
38	b055	191.50	5.36	6	83.18	54.16	8	0.434
39	b056	177.40	16.32	5	84.58	62.65	9	0.477
40	b057	192.17	7.52	6	80.45	55.95	10	0.419
41	b063	169.50	8.76	6	65.45	41.54	10	0.386
42	b068	180.83	7.52	6	69.15	40.55	10	0.382
43	b069	189.00	12.15	6	96.15	41.24	10	0.509
44	b070	176.50	9.69	6	100.89	28.13	10	0.572
45	b071	178.67	5.57	6	114.00	30.10	8	0.638
46	b076	158.33	10.33	6	100.20	10.63	10	0.633
47	b079	178.67	4.32	6	95.65	53.28	10	0.535
48	b081	163.67	17.80	6	98.35	22.99	10	0.601
49	b086	188.67	7.92	6	72.61	60.30	10	0.385
50	b087	168.00	1.00	3	25.33	32.69	6	0.151
51	b088	176.75	4.57	4	57.39	42.42	10	0.325
52	b089	187.33	8.12	6	27.50	25.94	6	0.147
53	b092	167.83	2.79	6	35.74	37.95	9	0.213
54	b094	175.50	5.86	6	34.55	31.24	10	0.197
55	b099	167.50	4.09	6	40.56	23.54	10	0.242
56	b102	154.50	3.79	4	58.28	47.68	8	0.377
57	b103	198.40	19.50	5	66.27	56.61	10	0.334
58	b107	172.00	9.57	6	65.64	41.47	5	0.382
59	b111	174.67	10.50	6	95.16	28.13	9	0.545
60	b117	178.83	12.22	6	77.85	14.65	10	0.435
61	b118	172.17	7.00	6	28.53	41.63	10	0.166
62	b120	171.17	5.04	6	21.63	14.59	9	0.126
63	b121	176.00	11.35	6	29.95	26.52	10	0.170
64	b123	182.33	8.43	6	29.25	35.13	8	0.160
65	b125	186.00	5.69	6	37.40	8.05	10	0.201
66	b126	184.33	13.29	6	63.10	33.96	10	0.342
67	b127	179.50	5.39	6	72.20	50.13	10	0.402

Table S4 continued.

S.No.	BM-NIL_ID	WT			Mt			Mt/WT
		Mean PH (cm)	SD[a]	N[b]	Mean PH (cm)	SD[a]	N[b]	
68	b129	181.00	6.20	6	88.15	59.84	10	0.487
69	b130	166.67	5.16	6	86.65	47.52	10	0.520
70	b131	168.83	14.37	6	90.35	35.89	10	0.535
71	b132	162.00	7.24	6	112.20	12.76	10	0.693
72	b133	165.40	6.15	5	123.90	28.68	10	0.749
73	b134	167.33	2.58	6	93.90	10.86	10	0.561
74	b135	164.83	7.19	6	63.56	33.39	10	0.386
75	b136	171.00	8.34	6	80.50	34.92	6	0.471
76	b139	156.00	5.06	6	88.50	29.51	10	0.567
77	b141	164.17	20.55	6	97.45	25.32	10	0.594
78	b142	177.83	12.16	6	110.28	38.19	10	0.620
79	b144	168.50	10.33	6	89.89	17.97	8	0.533
80	b148	185.67	8.36	6	63.20	26.48	10	0.340
81	b149	175.83	7.14	6	71.15	27.37	10	0.405
82	b152	169.17	12.35	6	64.05	43.98	10	0.379
83	b154	168.83	4.88	6	77.55	42.68	10	0.459
84	b155	176.00	4.60	6	107.60	21.39	10	0.611
85	b157	183.50	7.56	6	116.10	38.63	10	0.633
86	b164	182.17	7.83	6	93.70	22.37	10	0.514
87	b165	167.00	6.13	6	78.90	45.06	10	0.472
88	b169	174.33	6.44	6	65.50	45.90	10	0.376
89	b172	172.50	8.31	6	49.80	34.25	10	0.289
90	b176	163.83	5.27	6	91.68	34.42	10	0.560
91	b177	183.33	4.41	6	88.95	32.41	9	0.485
92	b180	158.00	7.94	3	41.58	33.87	10	0.263
93	b182	173.00	11.12	6	61.83	34.01	9	0.357
94	b183	181.50	12.52	6	93.53	27.62	9	0.515
95	b184	171.67	11.67	6	77.90	21.89	10	0.454
96	b185	182.67	18.00	6	71.70	15.30	10	0.393
97	b186	182.00	16.53	6	56.60	42.95	10	0.311
98	b187	181.60	15.63	5	24.55	23.10	10	0.135
99	b189	174.00	14.78	6	13.00	5.10	10	0.075

The data are presented as mean and standard deviation derived from two replications planted in CRD. For each replication, data were collected for five independent mutants and three WT siblings.
[a]Standard Deviation
[b]Sample Size

Table S5 Average Plant Height (PH) of wild-type (WT) and mutant (Mt) siblings from F$_1$s generated by crossing *D13*/+:B73 with respective DRIL41 lines.

S.No.	BM-NIL_ID	WT			Mt			Mt/WT
		Mean PH (cm)	SD[a]	N[b]	Mean PH (cm)	SD[a]	N[b]	
1	DRIL41.001	176.5	4.4	6	25.8	6.2	6	0.146
2	DRIL41.004	187.3	10.7	6	15.3	10.1	6	0.082
3	DRIL41.006	193.5	7.6	6	41.0	15.0	6	0.212
4	DRIL41.007	177.5	7.3	6	73.7	31.0	6	0.415
5	DRIL41.010	185.7	7.7	6	114.7	30.7	6	0.618
6	DRIL41.013	188.0	3.3	6	138.5	15.6	6	0.737
7	DRIL41.019	182.5	9.5	6	14.0	3.5	6	0.077
8	DRIL41.021	182.2	13.4	6	106.2	12.0	6	0.583
9	DRIL41.027	178.7	4.6	6	75.8	24.1	4	0.424
10	DRIL41.029	175.0	18.5	6	97.4	27.1	5	0.557
11	DRIL41.031	194.5	7.7	6	112.3	11.8	6	0.578
12	DRIL41.032	179.7	10.8	6	86.5	68.0	6	0.481
13	DRIL41.033	192.0	4.0	6	92.2	64.3	6	0.480
14	DRIL41.035	180.4	6.8	5	92.0	22.5	6	0.510
15	DRIL41.036	171.5	9.7	6	105.2	12.1	6	0.613
16	DRIL41.042	160.7	7.6	6	87.4	16.0	5	0.544
17	DRIL41.046	193.5	6.5	6	165.0	6.9	6	0.853
18	DRIL41.051	183.8	12.6	6	51.8	25.1	6	0.282
19	DRIL41.052	181.0	6.6	6	97.8	28.7	6	0.541
20	DRIL41.054	180.2	7.6	6	100.0	36.0	5	0.555
21	DRIL41.057	192.0	9.2	6	139.2	18.5	6	0.725
22	DRIL41.058	192.2	16.6	6	50.8	22.3	6	0.265
23	DRIL41.059	187.3	13.6	6	57.8	33.8	6	0.309
24	DRIL41.061	182.8	2.1	6	65.8	25.0	5	0.360
25	DRIL41.062	183.3	18.2	6	84.8	31.5	4	0.462
26	DRIL41.063	180.8	7.3	6	147.8	6.4	6	0.818
27	DRIL41.064	188.4	10.8	5	15.2	11.0	5	0.081
28	DRIL41.071	199.0	10.1	6	52.6	35.8	5	0.264
29	DRIL41.072	173.8	11.2	6	104.2	26.0	6	0.599
30	DRIL41.077	179.2	5.7	6	142.0	11.1	6	0.793
31	DRIL41.079	187.0	10.8	6	137.3	10.7	4	0.734
32	DRIL41.082	174.2	4.7	6	86.0	20.4	6	0.494
33	DRIL41.083	185.5	2.7	6	62.0	59.0	6	0.334
34	DRIL41.084	172.7	11.6	6	24.0	13.8	6	0.139
35	DRIL41.085	178.0		1	82.0		1	0.461
36	DRIL41.087	190.8	8.2	6	150.5	11.3	6	0.789

Table S5 continued.

S.No.	BM-NIL_ID	WT			Mt			Mt/WT
		Mean PH (cm)	SD[a]	N[b]	Mean PH (cm)	SD[a]	N[b]	
37	DRIL41.088	198.7	18.7	6	70.8	26.1	4	0.356
38	DRIL41.090	179.7	19.3	6	93.2	19.0	6	0.519
39	DRIL41.093	193.8	14.9	6	133.8	3.1	6	0.690
40	DRIL41.094	185.3	10.4	6	72.0	25.3	6	0.388
41	DRIL41.095	162.5	7.4	6	43.3	31.1	6	0.267
42	DRIL41.097	218.2	5.3	6	49.6	39.8	5	0.227
43	DRIL41.098	181.7	2.4	6	22.3	6.1	3	0.123
44	DRIL41.101	181.2	7.5	6	158.0	27.0	6	0.872
45	DRIL41.103	179.3	4.7	6	115.5	19.6	6	0.644
46	DRIL41.106	180.3	10.0	6	20.3	2.5	3	0.113
47	DRIL41.108	171.0	8.4	6	86.0	43.9	6	0.503
48	DRIL41.110	173.2	12.2	6	102.2	10.8	6	0.590
49	DRIL41.112	188.0	7.9	6	13.0	1.0	3	0.069
50	DRIL41.113	182.3	6.9	6	119.0	17.7	5	0.653
51	DRIL41.114	184.0	9.9	6	54.7	40.8	6	0.297
52	DRIL41.117	199.0	8.2	6	48.7	16.0	6	0.245
53	DRIL41.118	161.5	7.1	6	112.8	11.0	6	0.699
54	DRIL41.119	183.3	7.7	6	88.3	22.6	6	0.482
55	DRIL41.120	171.0	9.4	6	92.8	32.6	5	0.543
56	DRIL41.121	210.5	13.2	6	149.8	11.0	6	0.712
57	DRIL41.122	172.8	12.0	6	59.7	29.8	6	0.345
58	DRIL41.123	196.8	6.4	6	150.8	15.7	6	0.766
59	DRIL41.124	200.8	6.6	6	59.0	25.5	2	0.294
60	DRIL41.125	181.2	13.1	6	85.6	23.7	5	0.472
61	DRIL41.128	179.0	28.2	6	67.3	11.7	6	0.376
62	DRIL41.129	191.8	9.6	6	35.5	31.2	6	0.185
63	DRIL41.132	179.3	10.4	6	60.5	40.9	6	0.337
64	DRIL41.133	178.7	12.9	6	89.2	52.7	6	0.499
65	DRIL41.137	180.5	12.8	6	131.3	16.6	6	0.728
66	DRIL41.138	181.5	6.6	6	24.6	17.1	5	0.136
67	DRIL41.140	175.2	6.4	6	103.2	16.7	5	0.589
68	DRIL41.141	182.7	12.5	6	131.7	8.8	6	0.721
69	DRIL41.147	192.2	6.6	6	49.5	26.0	6	0.258
70	DRIL41.148	165.2	5.5	6	56.0	37.1	5	0.339

The data are presented as mean and standard deviation derived from two replications planted in CRD. For each replication, data were collected for three independent mutants and WT siblings.
[a]Standard Deviation, [b]Sample Size

APPENDIX B

List of supplemental files

Supplemental File 1: Glutamate receptors in plants used for phylogenetic analysis.

Supplemental File 2: Sequences used to generate phylogenetic tree.

Supplemental File 3: Differentially Expressed Genes (DEGs) in *D13* mutant w.r.t. WT in B73

Supplemental File 4: GO annotation from AgriGO v2 for upregulated genes in *D13* (FDR ≤ 0.05). Term types are abbreviated as Biological process (P), Molecular function (F), Cellular component (C).

Supplemental File 5: GO annotation from AgriGO v2 for downregulated genes in *D13* (FDR ≤ 0.05). Term types are abbreviated as Biological process (P), Molecular function (F), Cellular component (C).

Supplemental File 6: Differential mass features in *D13* mutant vs WT in B73 background. The tentative compound names were identified using MetaboAnalyst 4.0.

REFERENCES

Achard, P., and P. Genschik. 2009. "Releasing the Brakes of Plant Growth: How GAs Shutdown DELLA Proteins." *Journal of Experimental Botany* 60 (4): 1085–92. https://doi.org/10.1093/jxb/ern301.

Adusumilli, Ravali, and Parag Mallick. 2017. "Data Conversion with ProteoWizard MsConvert." In *Comai L., Katz J., Mallick P. (Eds) Proteomics. Methods in Molecular Biology*, 339–68. https://doi.org/10.1007/978-1-4939-6747-6_23.

Allen, G. J., S. P. Chu, C. L. Harrington, K. Schumacher, T. Hoffmann, Y. Y. Tang, E. Grill, and J. I. Schroeder. 2001. "A Defined Range of Guard Cell Calcium Oscillation Parameters Encodes Stomatal Movements." *Nature* 411 (6841): 1053–57. https://doi.org/10.1038/35082575.

Altschul, Stephen F., Warren Gish, Webb Miller, Eugene W. Myers, and David J. Lipman. 1990. "Basic Local Alignment Search Tool." *Journal of Molecular Biology* 215 (3): 403–10. https://doi.org/10.1016/S0022-2836(05)80360-2.

Anders, Simon, Paul Theodor Pyl, and Wolfgang Huber. 2015. "HTSeq-a Python Framework to Work with High-Throughput Sequencing Data." *Bioinformatics* 31 (2): 166–69. https://doi.org/10.1093/bioinformatics/btu638.

Anderson, Alyssa, Brian St. Aubin, María Jazmín Abraham-Juárez, Samuel Leiboff, Zhouxin Shen, Steve Briggs, Jacob O. Brunkard, and Sarah Hake. 2019. "The Second Site Modifier, Sympathy for the Ligule, Encodes a Homolog of *Arabidopsis* ENHANCED DISEASE RESISTANCE4 and Rescues the Liguleless Narrow Maize Mutant." *The Plant Cell* 31 (8): 1829–44. https://doi.org/10.1105/tpc.18.00840.

Aouini, Asma, Chiaki Matsukura, Hiroshi Ezura, and Erika Asamizu. 2012. "Characterisation of 13 Glutamate Receptor-like Genes Encoded in the Tomato Genome by Structure, Phylogeny and Expression Profiles." *Gene* 493 (1): 36–43. https://doi.org/10.1016/j.gene.2011.11.037.

Bajguz, Andrzej. 2007. "Metabolism of Brassinosteroids in Plants." *Plant Physiology and Biochemistry* 45 (2): 95–107. https://doi.org/10.1016/j.plaphy.2007.01.002.

Bensen, Robert J., Gurmukh S. Johal, Virginia C. Crane, John T. Tossberg, Patrick S. Schnable, Robert B. Meeley, and Steven P. Briggs. 1995. "Cloning and Characterization of the Maize *An1* Gene." *The Plant Cell* 7 (1): 75. https://doi.org/10.2307/3869839.

Best, Norman B, Thomas Hartwig, Josh Budka, Shozo Fujioka, Gurmukh (Guri) S. Johal, Burkhard Schulz, and Brian P Dilkes. 2016. "nana plant2 Encodes a Maize Ortholog of the *Arabidopsis* Brassinosteroid Biosynthesis Protein Dwarf1, Identifying Developmental Interactions between Brassinosteroids and Gibberellins." *Plant Physiology* 171. https://doi.org/10.1104/pp.16.00399.

Bishop, Gerard J. 2003. "Brassinosteroid Mutants of Crops." *Journal of Plant Growth Regulation* 22 (4): 325–35. https://doi.org/10.1007/s00344-003-0064-1.

Bocianowski, Jan. 2013. "Epistasis Interaction of QTL Effects as a Genetic Parameter Influencing Estimation of the Genetic Additive Effect." *Genetics and Molecular Biology* 36 (1): 93–100. https://doi.org/10.1590/S1415-47572013000100013.

Bortiri, Esteban, and Sarah Hake. 2007. "Flowering and Determinacy in Maize." *Journal of Experimental Botany* 58 (5): 909–16. https://doi.org/10.1093/jxb/erm015.

Bortoli, Sara De, Enrico Teardo, Ildikò Szabò, Tomas Morosinotto, and Alessandro Alboresi. 2016. "Evolutionary Insight into the Ionotropic Glutamate Receptor Superfamily of Photosynthetic Organisms." *Biophysical Chemistry* 218: 14–26. https://doi.org/10.1016/j.bpc.2016.07.004.

Braun, David M., Yi Ma, Noriko Inada, Michael G. Muszynski, and R. Frank Baker. 2006. "Tie - Dyed1 Regulates Carbohydrate Accumulation in Maize Leaves." *Plant Physiology* 142 (4): 1511–22. https://doi.org/10.1104/pp.106.090381.

Brenner, Eric D., Nora Martinez-Barboza, Alexandra P. Clark, Quail S. Liang, Dennis W. Stevenson, and Gloria M. Coruzzi. 2000. "Arabidopsis Mutants Resistant to S(+)-β-Methyl-α, β-Diaminopropionic Acid, a Cycad-Derived Glutamate Receptor Agonist." *Plant Physiology* 124 (4): 1615–24. https://doi.org/10.1104/pp.124.4.1615.

Buckler, Edward S., Brandon S. Gaut, and Michael D. McMullen. 2006. "Molecular and Functional Diversity of Maize." *Current Opinion in Plant Biology* 9 (2): 172–76. https://doi.org/10.1016/j.pbi.2006.01.013.

Candela, Héctor, and Sarah Hake. 2008. "The Art and Design of Genetic Screens: Maize." *Nature Reviews Genetics* 9 (3): 192–203. https://doi.org/10.1038/nrg2291.

Cano-Delgado, A. 2004. "BRL1 and BRL3 Are Novel Brassinosteroid Receptors That Function in Vascular Differentiation in Arabidopsis." *Development* 131 (21): 5341–51. https://doi.org/10.1242/dev.01403.

Cassani, Elena, Edoardo Bertolini, Francesco Cerino Badone, Michela Landoni, Dario Gavina,

Alberto Sirizzotti, and Roberto Pilu. 2009. "Characterization of the First Dominant Dwarf Maize Mutant Carrying a Single Amino Acid Insertion in the VHYNP Domain of the Dwarf8 Gene." *Molecular Breeding* 24 (4): 375–85. https://doi.org/10.1007/s11032-009-9298-3.

Chen, Feng, John C. D'Auria, Dorothea Tholl, Jeannine R. Ross, Jonathan Gershenzon, Joseph P. Noel, and Eran Pichersky. 2003. "An *Arabidopsis thaliana* Gene for Methylsalicylate Biosynthesis, Identified by a Biochemical Genomics Approach, Has a Role in Defense." *The Plant Journal* 36 (5): 577–88. https://doi.org/10.1046/j.1365-313X.2003.01902.x.

Chen, Guo-Qiang, Changhai Cui, Mark L. Mayer, and Eric Gouaux. 1999. "Functional Characterization of a Potassium-Selective Prokaryotic Glutamate Receptor." *Nature* 402 (6763): 817–21. https://doi.org/10.1038/45568.

Chen, Yi, Mingming Hou, Lijuan Liu, Shan Wu, Yun Shen, Kanako Ishiyama, Masatomo Kobayashi, Donald R. McCarty, and Bao-Cai Tan. 2014. "The Maize DWARF1 Encodes a Gibberellin 3-Oxidase and Is Dual Localized to the Nucleus and Cytosol." *Plant Physiology* 166 (4): 2028–39. https://doi.org/10.1104/pp.114.247486.

Cheng, Yao, Qiuying Tian, and Wen-Hao Zhang. 2016. "Glutamate Receptors Are Involved in Mitigating Effects of Amino Acids on Seed Germination of *Arabidopsis thaliana* under Salt Stress." *Environmental and Experimental Botany* 130: 68–78. https://doi.org/10.1016/j.envexpbot.2016.05.004.

Chinnusamy, Viswanathan, and Jian-Kang Zhu. 2009. "Epigenetic Regulation of Stress Responses in Plants." *Current Opinion in Plant Biology* 12 (2): 133–39. https://doi.org/10.1016/j.pbi.2008.12.006.

Chiu, J., R. DeSalle, H. M. Lam, L. Meisel, and G. Coruzzi. 1999. "Molecular Evolution of Glutamate Receptors: A Primitive Signaling Mechanism That Existed before Plants and Animals Diverged." *Molecular Biology and Evolution* 16 (6): 826–38. https://doi.org/10.1093/oxfordjournals.molbev.a026167.

Chiu, Joanna C., Eric D. Brenner, Rob DeSalle, Michael N. Nitabach, Todd C. Holmes, and Gloria M. Coruzzi. 2002. "Phylogenetic and Expression Analysis of the Glutamate-Receptor–Like Gene Family in *Arabidopsis thaliana*." *Molecular Biology and Evolution* 19 (7): 1066–82. https://doi.org/10.1093/oxfordjournals.molbev.a004165.

Cho, Daeshik, Sun A. Kim, Yoshiyuki Murata, Sangmee Lee, Seul-Ki Jae, Hong Gil Nam, and June M. Kwak. 2009. "De-Regulated Expression of the Plant Glutamate Receptor Homolog

AtGLR3.1 Impairs Long-Term Ca 2+ -Programmed Stomatal Closure." *The Plant Journal* 58 (3): 437–49. https://doi.org/10.1111/j.1365-313X.2009.03789.x.

Chong, Jasmine, David S. Wishart, and Jianguo Xia. 2019. "Using MetaboAnalyst 4.0 for Comprehensive and Integrative Metabolomics Data Analysis." *Current Protocols in Bioinformatics* 68 (1). https://doi.org/10.1002/cpbi.86.

Chopra, Surinder, Suzy M. Cocciolone, Shaun Bushman, Vineet Sangar, Michael D. McMullen, and Thomas Peterson. 2003. "The Maize Unstable Factor for Orange1 Is a Dominant Epigenetic Modifier of a Tissue Specifically Silent Allele of Pericarp Color1." *Genetics* 163 (3): 1135–46.

Christie, Peter J., Mark R. Alfenito, and Virginia Walbot. 1994. "Impact of Low-Temperature Stress on General Phenylpropanoid and Anthocyanin Pathways: Enhancement of Transcript Abundance and Anthocyanin Pigmentation in Maize Seedlings." *Planta* 194 (4): 541–49. https://doi.org/10.1007/BF00714468.

Chung, Yuhee, and Sunghwa Choe. 2013. "The Regulation of Brassinosteroid Biosynthesis in Arabidopsis." *Critical Reviews in Plant Sciences* 32 (6): 396-410. https://doi.org/10.1080/07352689.2013.797856.

Churchill, G. A., and R. W. Doerge. 1994. "Empirical Threshold Values for Quantitative Trait Mapping." *Genetics* 138 (3): 963–71. https://doi.org/10.1007/s11703-007-0022-y.

Clouse, Steven D., and Jenneth M. Sasse. 1998. "BRASSINOSTEROIDS: Essential Regulators of Plant Growth and Development." *Annual Review of Plant Physiology and Plant Molecular Biology* 49 (1): 427–51. https://doi.org/10.1146/annurev.arplant.49.1.427.

Cooper, Julian S., Peter J. Balint-Kurti, and Tiffany M. Jamann. 2018. "Identification of Quantitative Trait Loci for Goss's Wilt of Maize." *Crop Science* 58 (3): 1192–1200. https://doi.org/10.2135/cropsci2017.10.0618.

Davenport, Romola. 2002. "Glutamate Receptors in Plants." *Annals of Botany* 90 (5): 549–57. https://doi.org/10.1093/aob/mcf228.

Doyle, Jeffrey. 1991. "DNA Protocols for Plants." In *Molecular Techniques in Taxonomy*, 283–93. Berlin, Heidelberg: Springer. https://doi.org/10.1007/978-3-642-83962-7_18.

Dubos, Christian, David Huggins, Guy H. Grant, Marc R. Knight, and Malcolm M. Campbell. 2003. "A Role for Glycine in the Gating of Plant NMDA-like Receptors." *The Plant Journal* 35 (6): 800–810. https://doi.org/10.1046/j.1365-313X.2003.01849.x.

Efeoğlu, B., Y. Ekmekçi, and N. Çiçek. 2009. "Physiological Responses of Three Maize Cultivars to Drought Stress and Recovery." *South African Journal of Botany* 75 (1): 34–42. https://doi.org/10.1016/j.sajb.2008.06.005.

Eichten, Steven R., Jillian M. Foerster, Natalia de Leon, Ying Kai, Cheng-Ting Yeh, Sanzhen Liu, Jeffrey A. Jeddeloh, Patrick S. Schnable, Shawn M. Kaeppler, and Nathan M. Springer. 2011. "B73-Mo17 Near-Isogenic Lines Demonstrate Dispersed Structural Variation in Maize." *Plant Physiology* 156 (4): 1679–90. https://doi.org/10.1104/pp.111.174748.

Forde, Brian G. 2009. "Is It Good Noise? The Role of Developmental Instability in the Shaping of a Root System." *Journal of Experimental Botany* 60 (14): 3989–4002. https://doi.org/10.1093/jxb/erp265.

Forde, Brian G., and Michael R. Roberts. 2014. "Glutamate Receptor-like Channels in Plants: A Role as Amino Acid Sensors in Plant Defence?" *F1000prime Reports* 6: 37. https://doi.org/10.12703/P6-37.

Freeman, D. Carl, John H. Graham, Mary Tracy, John M. Emlen, and C. L. Alados. 1999. "Developmental Instability as a Means of Assessing Stress in Plants: A Case Study Using Electromagnetic Fields and Soybeans." *International Journal of Plant Sciences* 160 (S6): S157–66. https://doi.org/10.1086/314213.

Fu, Jingye, Fei Ren, Xuan Lu, Hongjie Mao, Meimei Xu, Jörg Degenhardt, Reuben J. Peters, and Qiang Wang. 2016. "A Tandem Array of ent -Kaurene Synthases in Maize with Roles in Gibberellin and More Specialized Metabolism." *Plant Physiology* 170 (2): 742–51. https://doi.org/10.1104/pp.15.01727.

Fujioka, Shozo, Jianming Li, Yong-Hwa Choi, Hideharu Seto, Suguru Takatsuto, Takahiro Noguchi, Tsuyoshi Watanabe, et al. 1997. "The Arabidopsis Deetiolated2 Mutant Is Blocked Early in Brassinosteroid Biosynthesis." *The Plant Cell* 9 (11): 1951. https://doi.org/10.2307/3870556.

Fujioka, S., H. Yamane, C. R .Spray, M. Katsumi, B. O. Phinney, P. Gaskin, J. MacMillan, and N. Takahashi. 1988a. "The Dominant Non-Gibberellin-Responding Dwarf Mutant (D8) of Maize Accumulates Native Gibberellins." *Proceedings of the National Academy of Sciences* 85 (23): 9031–35. https://doi.org/10.1073/pnas.85.23.9031.

Fujioka, Shozo, Hisakazu Yamane, Clive R. Spray, Paul Gaskin, Jake Macmillan, Bernard O. Phinney, and Nobutaka Takahashi. 1988b. "Qualitative and Quantitative Analyses of

Gibberellins in Vegetative Shoots of Normal, Dwarf -1, Dwarf -2, Dwarf -3, and Dwarf -5 Seedlings of *Zea mays* L." *Plant Physiology* 88 (4): 1367–72. https://doi.org/10.1104/pp.88.4.1367.

Galen Wo, Z., and Robert E. Oswald. 1995. "Unraveling the Modular Design of Glutamate-Gated Ion Channels." *Trends in Neurosciences* 18 (4): 161–68. https://doi.org/10.1016/0166-2236(95)93895-5.

Harberd, Nicholas P., and Michael Freeling. 1989. "Genetics of Dominant Gibberellin-Insensitive Dwarfism in Maize." *Genetics* 121: 827–38.

Hartwig, Thomas, George S. Chuck, Shozo Fujioka, Antje Klempien, Renate Weizbauer, Devi Prasad V. Potluri, Sunghwa Choe, Gurmukh S. Johal, and Burkhard Schulz. 2011. "Brassinosteroid Control of Sex Determination in Maize." *Proceedings of the National Academy of Sciences* 108 (49): 19814–19. https://doi.org/10.1073/pnas.1108359108.

Hedden, Peter, and Stephen G. Thomas. 2012. "Gibberellin Biosynthesis and Its Regulation." *Biochemical Journal* 444 (1): 11–25. https://doi.org/10.1042/BJ20120245.

Hedrich, Rainer, Vicenta Salvador-Recatalà, and Ingo Dreyer. 2016. "Electrical Wiring and Long-Distance Plant Communication." *Trends in Plant Science* 21 (5): 376–87. https://doi.org/10.1016/j.tplants.2016.01.016.

Helliwell, Chris A., Peter M. Chandler, Andrew Poole, Elizabeth S. Dennis, and W. James Peacock. 2001. "The CYP88A Cytochrome P450, ent-Kaurenoic Acid Oxidase, Catalyzes Three Steps of the Gibberellin Biosynthesis Pathway." *Proceedings of the National Academy of Sciences* 98 (4): 2065–70. https://doi.org/10.1073/pnas.98.4.2065.

Hirano, Ko, Eriko Kouketu, Hiroe Katoh, Koichiro Aya, Miyako Ueguchi-Tanaka, and Makoto Matsuoka. 2012. "The Suppressive Function of the Rice DELLA Protein SLR1 Is Dependent on Its Transcriptional Activation Activity." *The Plant Journal* 71: 443–53. https://doi.org/10.1111/j.1365-313X.2012.05000.x.

Hoisington, D.A., M. G. Neuffer, and Virginia Walbot. 1982. "Disease Lesion Mimics in Maize." *Developmental Biology* 93 (2): 381–88. https://doi.org/10.1016/0012-1606(82)90125-7.

Hu, Songlin, Cuiling Wang, Darlene L. Sanchez, Alexander E. Lipka, Peng Liu, Yanhai Yin, Michael Blanco, and Thomas Lübberstedt. 2017. "Gibberellins Promote Brassinosteroids Action and Both Increase Heterosis for Plant Height in Maize (Zea Mays L.)." *Frontiers in Plant Science* 8. https://doi.org/10.3389/fpls.2017.01039.

Igielski, Rafał, and Ewa Kępczyńska. 2017. "Gene Expression and Metabolite Profiling of Gibberellin Biosynthesis during Induction of Somatic Embryogenesis in *Medicago truncatula* Gaertn." *PLOS ONE* 12 (7). https://doi.org/10.1371/journal.pone.0182055.

Janda, T., G. Szalai, and E. Paldi. 1996. "Chlorophyll Fluorescence and Anthocyanin Content in Chilled Maize Plants after Return to a Non- Chilling Temperature under Various Irradiances." *Biologia Plantarum* 38 (4): 625–27. https://doi.org/10.1007/BF02890623.

Jiang, Fukun, Mei Guo, Fang Yang, Keith Duncan, David Jackson, Antoni Rafalski, Shoucai Wang, and Bailin Li. 2012. "Mutations in an AP2 Transcription Factor-Like Gene Affect Internode Length and Leaf Shape in Maize." *PLoS ONE* 7 (5). https://doi.org/10.1371/journal.pone.0037040.

Kaeppler, Shawn M., Jennifer L. Parke, Suzanne M. Mueller, Lynn Senior, Charles Stuber, and William F. Tracy. 2000. "Variation among Maize Inbred Lines and Detection of Quantitative Trait Loci for Growth at Low Phosphorus and Responsiveness to Arbuscular Mycorrhizal Fungi." *Crop Science* 40 (2): 358–64. https://doi.org/10.2135/cropsci2000.402358x.

Kang, Jiman, and Frank J. Turano. 2003. "The Putative Glutamate Receptor 1.1 (AtGLR1.1) Functions as a Regulator of Carbon and Nitrogen Metabolism in *Arabidopsis thaliana*." *Proceedings of the National Academy of Sciences* 100 (11): 6872–77. https://doi.org/10.1073/pnas.1030961100.

Kang, Seock, Ho Bang Kim, Hyoungseok Lee, Jin Young Choi, Sunggi Heu, Chang Jae Oh, Soon Il Kwon, and Chung Sun An. 2006. "Overexpression in Arabidopsis of a Plasma Membrane-Targeting Glutamate Receptor from Small Radish Increases Glutamate-Mediated Ca2+ Influx and Delays Fungal Infection." *Molecules and Cells* 21 (3): 418–27. http://www.ncbi.nlm.nih.gov/pubmed/16819306.

Kashiwagi, Keiko, Takashi Masuko, Christopher D Nguyen, Tomoko Kuno, Ikuko Tanaka, Kazuei Igarashi, and Keith Williams. 2002. "Channel Blockers Acting at N -Methyl-d-Aspartate Receptors: Differential Effects of Mutations in the Vestibule and Ion Channel Pore." *Molecular Pharmacology* 61 (3): 533–45. https://doi.org/10.1124/mol.61.3.533.

Katsumi, M., B. O. Phinney, P. R. Jefferies, and C. A. Henrick. 1964. "Growth Response of the d-5 and an-1 Mutants of Maize to some Kaurene Derivatives." *Science* 144 (3620): 849–50. https://doi.org/10.1126/science.144.3620.849.

Khush, Gurdev S. 2001. "Green Revolution: The Way Forward." *Nature Reviews Genetics* 2 (10):

815–22. https://doi.org/10.1038/35093585.

Kir, Gokhan, Huaxun Ye, Hilde Nelissen, Anjanasree K. Neelakandan, Andree S. Kusnandar, Anding Luo, Dirk Inzé, Anne W. Sylvester, Yanhai Yin, and Philip W. Becraft. 2015. "RNA Interference Knockdown of BRASSINOSTEROID INSENSITIVE1 in Maize Reveals Novel Functions for Brassinosteroid Signaling in Controlling Plant Architecture." *Plant Physiology* 169 (1): 826–39. https://doi.org/10.1104/pp.15.00367.

Klingenberg, Christian Peter. 2019. "Phenotypic Plasticity, Developmental Instability, and Robustness: The Concepts and How They Are Connected." *Frontiers in Ecology and Evolution* 7: 56. https://doi.org/10.3389/fevo.2019.00056.

Kong, Dongdong, Heng-Cheng Hu, Eiji Okuma, Yuree Lee, Hui Sun Lee, Shintaro Munemasa, Daeshik Cho, et al. 2016. "L-Met Activates Arabidopsis GLR Ca 2+ Channels Upstream of ROS Production and Regulates Stomatal Movement." *Cell Reports* 17 (10): 2553–61. https://doi.org/10.1016/j.celrep.2016.11.015.

Kong, Dongdong, Chuanli Ju, Aisha Parihar, So Kim, Daeshik Cho, and June M. Kwak. 2015. "Arabidopsis Glutamate Receptor Homolog3.5 Modulates Cytosolic Ca 2+ Level to Counteract Effect of Abscisic Acid in Seed Germination." *Plant Physiology* 167 (4): 1630–42. https://doi.org/10.1104/pp.114.251298.

Kwaaitaal, Mark, Rik Huisman, Jens Maintz, Anja Reinstädler, and Ralph Panstruga. 2011. "Ionotropic Glutamate Receptor (IGluR)-like Channels Mediate MAMP-Induced Calcium Influx in *Arabidopsis thaliana*." *Biochemical Journal* 440 (3): 355–73. https://doi.org/10.1042/BJ20111112.

Lam, Hon-Ming, Joanna Chiu, Ming-Hsiun Hsieh, Lee Meisel, Igor C. Oliveira, Michael Shin, and Gloria Coruzzi. 1998. "Glutamate-Receptor Genes in Plants." *Nature* 396 (6707): 125–26. https://doi.org/10.1038/24066.

Landoni, Michela, Francesca Dalla Vecchia, Giuseppe Gavazzi, Anna Giulini, Nicoletta La Rocca, Nicoletta Rascio, Monica Colombo, Monica Bononi, and Gabriella Consonni. 2007. "The An1-4736 Mutation of *Anther Ear1* in Maize Alters Scotomorphogenesis and the Light Response." *Plant Science* 172 (1): 172–80. https://doi.org/10.1016/j.plantsci.2006.08.004.

Larkin, M.A., G. Blackshields, N.P. Brown, R. Chenna, P.A. McGettigan, H. McWilliam, F. Valentin, et al. 2007. "Clustal W and Clustal X Version 2.0." *Bioinformatics* 23 (21): 2947–48. https://doi.org/10.1093/bioinformatics/btm404.

Lawit, Shai J., Heidi M. Wych, Deping Xu, Suman Kundu, and Dwight T. Tomes. 2010. "Maize DELLA Proteins Dwarf Plant8 and Dwarf Plant9 as Modulators of Plant Development." *Plant and Cell Physiology* 51 (11): 1854–68. https://doi.org/10.1093/pcp/pcq153.

Lee, Michael, Natalya Sharopova, William D. Beavis, David Grant, Maria Katt, Deborah Blair, and Arnel Hallauer. 2002. "Expanding the Genetic Map of Maize with the Intermated B73 x Mo17 (IBM) Population." *Plant Molecular Biology* 48 (5–6): 453–61. https://doi.org/10.1023/a:1014893521186.

Li, Feng, Jing Wang, Chunli Ma, Yongxiu Zhao, Yingchun Wang, Agula Hasi, and Zhi Qi. 2013. "Glutamate Receptor-Like Channel3.3 Is Involved in Mediating Glutathione-Triggered Cytosolic Calcium Transients, Transcriptional Changes, and Innate Immunity Responses in Arabidopsis." *Plant Physiology* 162 (3): 1497–1509. https://doi.org/10.1104/pp.113.217208.

Li, Huizi, Xiaochun Jiang, Xiangzhang Lv, Golam Jalal Ahammed, Zhixin Guo, Zhenyu Qi, Jingquan Yu, and Yanhong Zhou. 2019. "Tomato GLR3.3 and GLR3.5 Mediate Cold Acclimation-induced Chilling Tolerance by Regulating Apoplastic H2O2 Production and Redox Homeostasis." *Plant, Cell & Environment* 42 (12): 3326–39. https://doi.org/10.1111/pce.13623.

Li, Jing, Shihua Zhu, Xinwei Song, Yi Shen, Hanming Chen, Jie Yu, Keke Yi, et al. 2006. "A Rice Glutamate Receptor–Like Gene Is Critical for the Division and Survival of Individual Cells in the Root Apical Meristem." *The Plant Cell* 18 (2): 340–49. https://doi.org/10.1105/tpc.105.037713.

Li, Qian-Feng, and Jun-Xian He. 2013. "Mechanisms of Signaling Crosstalk between Brassinosteroids and Gibberellins." *Plant Signaling & Behavior* 8 (7). https://doi.org/10.4161/psb.24686.

Li, Wei, Fanghui Ge, Zhiquan Qiang, Lei Zhu, Shuaisong Zhang, Limei Chen, Xiqing Wang, Jiansheng Li, and Ying Fu. 2019. "Maize ZmRPH1 Encodes a Microtubule-associated Protein That Controls Plant and Ear Height." *Plant Biotechnology Journal* 18 (6): 1345–47. https://doi.org/10.1111/pbi.13292.

Li, Zhong-Guang, Xin-Yu Ye, and Xue-Mei Qiu. 2019. "Glutamate Signaling Enhances the Heat Tolerance of Maize Seedlings by Plant Glutamate Receptor-like Channels-Mediated Calcium Signaling." *Protoplasma* 256 (4): 1165–69. https://doi.org/10.1007/s00709-019-01351-9.

Lopez Zuniga, Luis Orlando, James B. Holland, Matthew D. Krakowsky, and Marc Cubeta. 2016. "Use of Chromosome Segment Substitution Lines for the Identification of Multiple Disease Resistance Loci in Maize." *Doctoral Thesis*.

Love, Michael I., Wolfgang Huber, and Simon Anders. 2014. "Moderated Estimation of Fold Change and Dispersion for RNA-Seq Data with DESeq2." *Genome Biology* 15 (12): 550. https://doi.org/10.1186/s13059-014-0550-8.

Lu, Guihua, Xiping Wang, Junhua Liu, Kun Yu, Yang Gao, Haiyan Liu, Changgui Wang, et al. 2014. "Application of T-DNA Activation Tagging to Identify Glutamate Receptor-like Genes That Enhance Drought Tolerance in Plants." *Plant Cell Reports* 33 (4): 617–31. https://doi.org/10.1007/s00299-014-1586-7.

Lukens, Lewis N., and John Doebley. 1999. "Epistatic and Environmental Interactions for Quantitative Trait Loci Involved in Maize Evolution." *Genetical Research* 74 (3): 291–302. https://doi.org/10.1017/S0016672399004073.

Madden, Dean R. 2002. "The Structure and Function of Glutamate Receptor Ion Channels." *Nature Reviews Neuroscience* 3 (2): 91–101. https://doi.org/10.1038/nrn725.

Makarevitch, Irina, Addie Thompson, Gary J. Muehlbauer, and Nathan M. Springer. 2012. "Brd1 Gene in Maize Encodes a Brassinosteroid C-6 Oxidase." *PLoS ONE* 7 (1). https://doi.org/10.1371/journal.pone.0030798.

Manzoor, Hamid, Jani Kelloniemi, Annick Chiltz, David Wendehenne, Alain Pugin, Benoit Poinssot, and Angela Garcia-Brugger. 2013. "Involvement of the Glutamate Receptor AtGLR3.3 in Plant Defense Signaling and Resistance to *Hyaloperonospora arabidopsidis*." *The Plant Journal* 76 (3): 466–80. https://doi.org/10.1111/tpj.12311.

Mayer, Mark L., and Neali Armstrong. 2004. "Structure and Function of Glutamate Receptor Ion Channels." *Annual Review of Physiology* 66 (1): 161–81. https://doi.org/10.1146/annurev.physiol.66.050802.084104.

McSteen, Paula. 2009. "Hormonal Regulation of Branching in Grasses." *Plant Physiology* 149 (1): 46–55. https://doi.org/10.1104/pp.108.129056.

Meyerhoff, Oliver, Katharina Müller, M. Rob G. Roelfsema, Andreas Latz, Benoit Lacombe, Rainer Hedrich, Petra Dietrich, and Dirk Becker. 2005. "AtGLR3.4, a Glutamate Receptor Channel-like Gene Is Sensitive to Touch and Cold." *Planta* 222 (3): 418–27. https://doi.org/10.1007/s00425-005-1551-3.

Michard, Erwan, Pedro T. Lima, Filipe Borges, Ana Catarina Silva, Maria Teresa Portes, João E Carvalho, Matthew Gilliham, L.-H. Liu, Gerhard Obermeyer, and J. A. Feijo. 2011. "Glutamate Receptor-Like Genes Form Ca2+ Channels in Pollen Tubes and Are Regulated by Pistil D-Serine." *Science* 332 (6028): 434–37. https://doi.org/10.1126/science.1201101.

Mickelson, S. M., C. S. Stuber, L. Senior, and S. M. Kaeppler. 2002. "Quantitative Trait Loci Controlling Leaf and Tassel Traits in a B73 × Mo17 Population of Maize." *Crop Science* 42 (6): 1902–9. https://doi.org/10.2135/cropsci2002.1902.

Monna, Lisa, Noriyuki Kitazawa, Rika Yoshino, Junko Suzuki, Haruka Masuda, Maehara Yumiko, Tanji Masao, Sato Mizuho, Shinobu Nasu, and Minobe Yuzo. 2002. "Positional Cloning of Rice Semidwarfing Gene, Sd-1: Rice 'Green Revolution Gene' Encodes a Mutant Enzyme Involved in Gibberellin Synthesis." *DNA Research* 9 (1): 11–17. https://doi.org/10.1093/dnares/9.1.11.

Mousavi, Seyed A. R., Adeline Chauvin, François Pascaud, Stephan Kellenberger, and Edward E. Farmer. 2013. "GLUTAMATE RECEPTOR-LIKE Genes Mediate Leaf-to-Leaf Wound Signalling." *Nature* 500 (7463): 422–26. https://doi.org/10.1038/nature12478.

Multani, Dilbag S., Steven P. Briggs, Mark A. Chamberlin, Joshua J. Blakeslee, Angus S. Murphy, and Gurmukh S. Johal. 2003. "Loss of an MDR Transporter in Compact Stalks of Maize *br2* and Sorghum *dw3* Mutants." *Science* 302 (5642): 81–84. https://doi.org/10.1126/science.1086072.

Nakamura, Ayako, Shozo Fujioka, Hidehiko Sunohara, Noriko Kamiya, Zhi Hong, Yoshiaki Inukai, Kotaro Miura, et al. 2006. "The Role of OsBRI1 and Its Homologous Genes, OsBRL1 and OsBRL3 , in Rice." *Plant Physiology* 140 (2): 580–90. https://doi.org/10.1104/pp.105.072330.

Nakanishi, Shigetada. 1992. "Molecular Diversity of Glutamate Receptors and Implications for Brain Function." *Science* 258 (5082): 597–603. https://doi.org/10.1126/science.1329206.

Nath, Amar, George W. Vetrovec, Michael J. Cowley, Mark Newton, Germano Disciascio, Jhulan Mukharji, and Stephen A. Lewis. 1988. "Double-Wire Angioplasty of the Right Coronary Artery Bifurcational Stenosis." *Catheterization and Cardiovascular Diagnosis* 14 (1): 37–40. https://doi.org/10.1002/ccd.1810140108.

Neuffer, M. G. 1994. "Mutagenesis." In *Freeling M., Walbot V. (Eds) The Maize Handbook*, 212–19. New York, NY: Springer. https://doi.org/10.1007/978-1-4612-2694-9_23.

Newman, Mari-Anne, Thomas Sundelin, Jon T. Nielsen, and Gitte Erbs. 2013. "MAMP (Microbe-Associated Molecular Pattern) Triggered Immunity in Plants." *Frontiers in Plant Science* 4: 139. https://doi.org/10.3389/fpls.2013.00139.

Ni, Jun, Zhiming Yu, Guankui Du, Yanyan Zhang, Jemma L. Taylor, Chenjia Shen, Jing Xu, Xunyan Liu, Yifeng Wang, and Yunrong Wu. 2016. "Heterologous Expression and Functional Analysis of Rice GLUTAMATE RECEPTOR-LIKE Family Indicates Its Role in Glutamate Triggered Calcium Flux in Rice Roots." *Rice* 9 (1): 9. https://doi.org/10.1186/s12284-016-0081-x.

Noguchi, Takahiro, Shozo Fujioka, Suguru Takatsuto, Akira Sakurai, Shigeo Yoshida, Jianming Li, and Joanne Chory. 1999. "Arabidopsis Det2 Is Defective in the Conversion of (24 R)-24-Methylcholest-4-En-3-One to (24R)-24-Methyl-5α-Cholestan-3-One in Brassinosteroid Biosynthesis." *Plant Physiology* 120 (3): 833–40. https://doi.org/10.1104/pp.120.3.833.

Ortiz-Ramírez, Carlos, Erwan Michard, Alexander A. Simon, Daniel S. C. Damineli, Marcela Hernández-Coronado, Jörg D. Becker, and José A. Feijó. 2017. "GLUTAMATE RECEPTOR-LIKE Channels Are Essential for Chemotaxis and Reproduction in Mosses." *Nature* 549 (7670): 91–95. https://doi.org/10.1038/nature23478.

Ozawa, Seiji. 1998. "Glutamate Receptors in the Mammalian Central Nervous System." *Progress in Neurobiology* 54 (5): 581–618. https://doi.org/10.1016/S0301-0082(97)00085-3.

Pearce, Stephen, Robert Saville, Simon P. Vaughan, Peter M. Chandler, Edward P. Wilhelm, Caroline A. Sparks, Nadia Al-Kaff, et al. 2011. "Molecular Characterization of Rht-1 Dwarfing Genes in Hexaploid Wheat." *Plant Physiology* 157 (4): 1820–31. https://doi.org/10.1104/pp.111.183657.

Peng, Jinrong, Donald E. Richards, Nigel M. Hartley, George P. Murphy, Katrien M. Devos, John E. Flintham, James Beales, et al. 1999. "'Green Revolution' Genes Encode Mutant Gibberellin Response Modulators." *Nature* 400 (6741): 256–61. https://doi.org/10.1038/22307.

Penning, Bryan W., Gurmukh S. Johal, and Michael D. McMullen. 2004. "A Major Suppressor of Cell Death, *Slm1* , Modifies the Expression of the Maize (Zea Mays L.) Lesion Mimic Mutation Les23." *Genome* 47 (5): 961–69. https://doi.org/10.1139/g04-046.

Pertoldi, C., T. N. Kristensen, D. H. Andersen, and V. Loeschcke. 2006. "Developmental Instability as an Estimator of Genetic Stress." *Heredity* 96 (2): 122–27.

https://doi.org/10.1038/sj.hdy.6800777.

Portwood, John L., Margaret R. Woodhouse, Ethalinda K. Cannon, Jack M. Gardiner, Lisa C. Harper, Mary L. Schaeffer, Jesse R. Walsh, et al. 2019. "MaizeGDB 2018: The Maize Multi-Genome Genetics and Genomics Database." *Nucleic Acids Research* 47 (D1): D1146–54. https://doi.org/10.1093/nar/gky1046.

Price, Michelle B., Dongdong Kong, and Sakiko Okumoto. 2013. "Inter-Subunit Interactions between Glutamate-Like Receptors in Arabidopsis." *Plant Signaling & Behavior* 8 (12). https://doi.org/10.4161/psb.27034.

Price, Michelle Beth, John Jelesko, and Sakiko Okumoto. 2012. "Glutamate Receptor Homologs in Plants: Functions and Evolutionary Origins." *Frontiers in Plant Science* 3: 235. https://doi.org/10.3389/fpls.2012.00235.

Robert, Antoine, Rhonda Hyde, Thomas E. Hughes, and James R. Howe. 2002. "The Expression of Dominant-Negative Subunits Selectively Suppresses Neuronal AMPA and Kainate Receptors." *Neuroscience* 115 (4): 1199–1210. https://doi.org/10.1016/S0306-4522(02)00534-1.

Roy, S. J., M. Gilliham, Berger B., P. A. Essah, C. Cheffing, A. J. Miller, R. J. Davenport, et al. 2008. "Investigating Glutamate Receptor-like Gene Co-Expression in Arabidopsis Thaliana." *Plant, Cell & Environment* 31 (6): 861–71. https://doi.org/10.1111/j.1365-3040.2008.01801.x.

Saiki, Randall K. 1990. "Amplification of Genomic DNA." In *PCR Protocols*, 13–20. Elsevier. https://doi.org/10.1016/B978-0-12-372180-8.50006-8.

Saitou, N., and M. Nei. 1987. "The Neighbor-Joining Method: A New Method for Reconstructing Phylogenetic Trees." *Molecular Biology and Evolution* 4 (4): 406–25. https://doi.org/10.1093/oxfordjournals.molbev.a040454.

Sakai, Kan-Ichi, and Yoshiya Shimamoto. 1965. "Developmental Instability in Leaves and Flowers of Nicotiana Tabacum." *Genetics* 51 (5): 801.

Salvador-Recatalà, Vicenta. 2016. "New Roles for the GLUTAMATE RECEPTOR-LIKE 3.3, 3.5 , and 3.6 Genes as on/off Switches of Wound-Induced Systemic Electrical Signals." *Plant Signaling & Behavior* 11 (4). https://doi.org/10.1080/15592324.2016.1161879.

Schwacke, Rainer, and Ulf-Ingo Flügge. 2018. "Identification and Characterization of Plant Membrane Proteins Using ARAMEMNON." In *Methods in Molecular Biology*, 249–59.

https://doi.org/10.1007/978-1-4939-7411-5_17.

Sekhon, Rajandeep S., and Surinder Chopra. 2009. "Progressive Loss of DNA Methylation Releases Epigenetic Gene Silencing From a Tandemly Repeated Maize Myb Gene." *Genetics* 181 (1): 81–91. https://doi.org/10.1534/genetics.108.097170.

Shapiro, S. S., and M. B. Wilk. 1965. "An Analysis of Variance Test for Normality (Complete Samples)." *Biometrika* 52 (3/4): 591–611. https://doi.org/10.2307/2333709.

Singh, Amarjeet, Poonam Kanwar, Akhilesh K. Yadav, Manali Mishra, Saroj K. Jha, Vinay Baranwal, Amita Pandey, Sanjay Kapoor, Akhilesh K. Tyagi, and Girdhar K. Pandey. 2014. "Genome-Wide Expressional and Functional Analysis of Calcium Transport Elements during Abiotic Stress and Development in Rice." *FEBS Journal* 281 (3): 894–915. https://doi.org/10.1111/febs.12656.

Singh, Shashi Kant, Ching-Te Chien, and Ing-Feng Chang. 2016. "The Arabidopsis Glutamate Receptor-like Gene GLR3.6 Controls Root Development by Repressing the Kip-Related Protein Gene KRP4." *Journal of Experimental Botany* 67 (6): 1853–69.
 https://doi.org/10.1093/jxb/erv576.

Šiukšta, Raimondas, Virginija Vaitkūnienė, Greta Kaselytė, Vaiva Okockytė, Justina Žukauskaitė, Donatas Žvingila, and Vytautas Rančelis. 2015. "Inherited Phenotype Instability of Inflorescence and Floral Organ Development in Homeotic Barley Double Mutants and Its Specific Modification by Auxin Inhibitors and 2,4-D." *Annals of Botany* 115 (4): 651–63. https://doi.org/10.1093/aob/mcu263.

Sivaguru, Mayandi, Sharon Pike, Walter Gassmann, and Tobias I Baskin. 2003. "Aluminum Rapidly Depolymerizes Cortical Microtubules and Depolarizes the Plasma Membrane: Evidence That These Responses Are Mediated by a Glutamate Receptor." *Plant and Cell Physiology* 44 (7): 667–75. https://doi.org/10.1093/pcp/pcg094.

Sobolevsky, Alexander I. 2015. "Structure and Gating of Tetrameric Glutamate Receptors." *The Journal of Physiology* 593 (1): 29–38. https://doi.org/10.1113/jphysiol.2013.264911.

Sobolevsky, Alexander I., Michael L. Prodromou, Maria V. Yelshansky, and Lonnie P. Wollmuth. 2007. "Subunit-Specific Contribution of Pore-Forming Domains to NMDA Receptor Channel Structure and Gating." *Journal of General Physiology* 129 (6): 509–25. https://doi.org/10.1085/jgp.200609718.

Sorgini, Crystal A., Ilse Barrios-Perez, Patrick J. Brown, and Elizabeth A. Ainsworth. 2019.

"Examining Genetic Variation in Maize Inbreds and Mapping Oxidative Stress Response QTL in B73-Mo17 Nearly Isogenic Lines." *Frontiers in Sustainable Food Systems* 3: 51. https://doi.org/10.3389/fsufs.2019.00051.

Spielmeyer, W., M. H. Ellis, and P. M. Chandler. 2002. "Semidwarf (Sd-1), 'Green Revolution' Rice, Contains a Defective Gibberellin 20-Oxidase Gene." *Proceedings of the National Academy of Sciences* 99 (13): 9043–48. https://doi.org/10.1073/pnas.132266399.

Springer, Nathan M., Kai Ying, Yan Fu, Tieming Ji, Cheng-Ting Yeh, Yi Jia, Wei Wu, et al. 2009. "Maize Inbreds Exhibit High Levels of Copy Number Variation (CNV) and Presence/Absence Variation (PAV) in Genome Content." *PLoS Genetics* 5 (11). https://doi.org/10.1371/journal.pgen.1000734.

Sun, Cui, Lifei Jin, Yiting Cai, Yining Huang, Xiaodong Zheng, and Ting Yu. 2019. "L-Glutamate Treatment Enhances Disease Resistance of Tomato Fruit by Inducing the Expression of Glutamate Receptors and the Accumulation of Amino Acids." *Food Chemistry* 293 (September): 263–70. https://doi.org/10.1016/j.foodchem.2019.04.113.

Sündermann, Annika, Lars F. Eggers, and Dominik Schwudke. 2016. "Liquid Extraction: Bligh and Dyer." In *Wenk M. (Eds) Encyclopedia of Lipidomics*, 1–4. Dordrecht: Springer Netherlands. https://doi.org/10.1007/978-94-007-7864-1_88-1.

Szalma, S. J., B. M. Hostert, J. R. LeDeaux, C. W. Stuber, and J. B. Holland. 2007. "QTL Mapping with Near-Isogenic Lines in Maize." *Theoretical and Applied Genetics* 114 (7): 1211–28. https://doi.org/10.1007/s00122-007-0512-6.

Tapken, Daniel, U. Anschutz, L.-H. Liu, Thomas Huelsken, Guiscard Seebohm, Dirk Becker, and Michael Hollmann. 2013. "A Plant Homolog of Animal Glutamate Receptors Is an Ion Channel Gated by Multiple Hydrophobic Amino Acids." *Science Signaling* 6 (279): ra47. https://doi.org/10.1126/scisignal.2003762.

Teardo, Enrico, Luca Carraretto, Sara De Bortoli, Alex Costa, Smrutisanjita Behera, Richard Wagner, Fiorella Lo Schiavo, Elide Formentin, and Ildiko Szabo. 2015. "Alternative Splicing-Mediated Targeting of the Arabidopsis GLUTAMATE RECEPTOR3.5 to Mitochondria Affects Organelle Morphology." *Plant Physiology* 167 (1): 216–27. https://doi.org/10.1104/pp.114.242602.

Teardo, Enrico, Elide Formentin, Anna Segalla, Giorgio Mario Giacometti, Oriano Marin, Manuela Zanetti, Fiorella Lo Schiavo, Mario Zoratti, and Ildikò Szabò. 2011. "Dual

Localization of Plant Glutamate Receptor AtGLR3.4 to Plastids and Plasmamembrane." *Biochimica et Biophysica Acta (BBA) - Bioenergetics* 1807 (3): 359–67. https://doi.org/10.1016/j.bbabio.2010.11.008.

Thiebaut, Flávia, Adriana Silva Hemerly, and Paulo Cavalcanti Gomes Ferreira. 2019. "A Role for Epigenetic Regulation in the Adaptation and Stress Responses of Non-Model Plants." *Frontiers in Plant Science* 10: 246. https://doi.org/10.3389/fpls.2019.00246.

Tian, Tian, Yue Liu, Hengyu Yan, Qi You, Xin Yi, Zhou Du, Wenying Xu, and Zhen Su. 2017. "AgriGO v2.0: A GO Analysis Toolkit for the Agricultural Community, 2017 Update." *Nucleic Acids Research* 45 (W1): W122–29. https://doi.org/10.1093/nar/gkx382.

Toyota, Masatsugu, Dirk Spencer, Satoe Sawai-Toyota, Wang Jiaqi, Tong Zhang, Abraham J. Koo, Gregg A. Howe, and Simon Gilroy. 2018. "Glutamate Triggers Long-Distance, Calcium-Based Plant Defense Signaling." *Science* 361 (6407): 1112–15. https://doi.org/10.1126/science.aat7744.

Trapnell, Cole, Lior Pachter, and Steven L. Salzberg. 2009. "TopHat: Discovering Splice Junctions with RNA-Seq." *Bioinformatics* 25 (9): 1105–11. https://doi.org/10.1093/bioinformatics/btp120.

Trapnell, Cole, Adam Roberts, Loyal Goff, Geo Pertea, Daehwan Kim, David R. Kelley, Harold Pimentel, Steven L. Salzberg, John L. Rinn, and Lior Pachter. 2012. "Differential Gene and Transcript Expression Analysis of RNA-Seq Experiments with TopHat and Cufflinks." *Nature Protocols* 7 (3): 562–78. https://doi.org/10.1038/nprot.2012.016.

Traynelis, Stephen F., Lonnie P. Wollmuth, Chris J. McBain, Frank S. Menniti, Katie M. Vance, Kevin K. Ogden, Kasper B. Hansen, Hongjie Yuan, Scott J. Myers, and Ray Dingledine. 2010. "Glutamate Receptor Ion Channels: Structure, Regulation, and Function." Edited by David Sibley. *Pharmacological Reviews* 62 (3): 405–96. https://doi.org/10.1124/pr.109.002451.

Twomey, Edward C., and Alexander I. Sobolevsky. 2018. "Structural Mechanisms of Gating in Ionotropic Glutamate Receptors." *Biochemistry* 57 (3): 267–76. https://doi.org/10.1021/acs.biochem.7b00891.

Ueguchi-Tanaka, Miyako, Motoyuki Ashikari, Masatoshi Nakajima, Hironori Itoh, Etsuko Katoh, Masatomo Kobayashi, Teh-yuan Chow, et al. 2005. "GIBBERELLIN INSENSITIVE DWARF1 Encodes a Soluble Receptor for Gibberellin." *Nature* 437 (7059): 693–98. https://doi.org/10.1038/nature04028.

Usadel, Björn, Axel Nagel, Oliver Thimm, Henning Redestig, Oliver E Blaesing, Natalia Palacios-Rojas, Joachim Selbig, et al. 2005. "Extension of the Visualization Tool MapMan to Allow Statistical Analysis of Arrays, Display of Coresponding Genes, and Comparison with Known Responses." *Plant Physiology* 138 (3): 1195–1204. https://doi.org/10.1104/pp.105.060459.

Vatsa, Parul, Annick Chiltz, Stéphane Bourque, David Wendehenne, Angela Garcia-Brugger, and Alain Pugin. 2011. "Involvement of Putative Glutamate Receptors in Plant Defence Signaling and NO Production." *Biochimie* 93 (12): 2095–2101. https://doi.org/10.1016/j.biochi.2011.04.006.

Vaughn, Matthew W., Miloš Tanurdžić, Zachary Lippman, Hongmei Jiang, Robert Carrasquillo, Pablo D. Rabinowicz, Neilay Dedhia, et al. 2007. "Epigenetic Natural Variation in *Arabidopsis thaliana*." *PLoS Biology* 5 (7). https://doi.org/10.1371/journal.pbio.0050174.

Vincill, Eric D., Anthony M. Bieck, and Edgar P. Spalding. 2012. "Ca 2+ Conduction by an Amino Acid-Gated Ion Channel Related to Glutamate Receptors." *Plant Physiology* 159 (1): 40–46. https://doi.org/10.1104/pp.112.197509.

Vincill, Eric D., Arielle E. Clarin, Jennifer N. Molenda, and Edgar P. Spalding. 2013. "Interacting Glutamate Receptor-Like Proteins in Phloem Regulate Lateral Root Initiation in Arabidopsis." *The Plant Cell* 25 (4): 1304–13. https://doi.org/10.1105/tpc.113.110668.

Wang, Bing, Steven M. Smith, and Jiayang Li. 2018. "Genetic Regulation of Shoot Architecture." *Annual Review of Plant Biology* 69 (1): 437–68. https://doi.org/10.1146/annurev-arplant-042817-040422.

Wang, Po-Hsun, Cheng-En Lee, Yi-Sin Lin, Man-Hsuan Lee, Pei-Yuan Chen, Hui-Chun Chang, and Ing-Feng Chang. 2019. "The Glutamate Receptor-Like Protein GLR3.7 Interacts With 14-3-3ω and Participates in Salt Stress Response in *Arabidopsis thaliana*." *Frontiers in Plant Science* 10: 1169. https://doi.org/10.3389/fpls.2019.01169.

Wang, Yijun, Dexiang Deng, Haidong Ding, Xiangming Xu, Rong Zhang, Suxin Wang, Yunlong Bian, Zhitong Yin, and Yao Chen. 2013. "Gibberellin Biosynthetic Deficiency Is Responsible for Maize Dominant Dwarf11 (D11) Mutant Phenotype: Physiological and Transcriptomic Evidence." *PLoS ONE* 8 (6). https://doi.org/10.1371/journal.pone.0066466.

War, Abdul Rashid, Michael Gabriel Paulraj, Tariq Ahmad, Abdul Ahad Buhroo, Barkat Hussain, Savarimuthu Ignacimuthu, and Hari Chand Sharma. 2012. "Mechanisms of Plant Defense against Insect Herbivores." *Plant Signaling & Behavior* 7 (10): 1306–20.

https://doi.org/10.4161/psb.21663.

West-Eberhard, M.J. 2008. "Phenotypic Plasticity." In *Encyclopedia of Ecology*, 2701–7. Elsevier. https://doi.org/10.1016/B978-008045405-4.00837-5.

Winkler, R. G., and T. Helentjaris. 1995. "The Maize Dwarf3 Gene Encodes a Cytochrome P450-Mediated Early Step in Gibberellin Biosynthesis." *The Plant Cell* 7 (8): 1307–17. https://doi.org/10.1105/tpc.7.8.1307.

Wollmuth, L. 2004. "Structure and Gating of the Glutamate Receptor Ion Channel." *Trends in Neurosciences* 27 (6): 321–28. https://doi.org/10.1016/j.tins.2004.04.005.

Wudick, Michael M., Erwan Michard, Custódio Oliveira Nunes, and José A. Feijó. 2018a. "Comparing Plant and Animal Glutamate Receptors: Common Traits but Different Fates?" *Journal of Experimental Botany* 69 (17): 4151–63. https://doi.org/10.1093/jxb/ery153.

Wudick, Michael M., Maria Teresa Portes, Erwan Michard, Paul Rosas-Santiago, Michael A. Lizzio, Custódio Oliveira Nunes, Cláudia Campos, et al. 2018b. "CORNICHON Sorting and Regulation of GLR Channels Underlie Pollen Tube Ca 2+ Homeostasis." *Science* 360 (6388): 533–36. https://doi.org/10.1126/science.aar6464.

Yamaguchi, Shinjiro. 2008. "Gibberellin Metabolism and Its Regulation." *Annual Review of Plant Biology* 59 (1): 225–51. https://doi.org/10.1146/annurev.arplant.59.032607.092804.

Yekutieli, Daniel, and Yoav Benjamini. 2001. "Under Dependency." *The Annals of Statistics* 29 (4): 1165–88. https://doi.org/10.1214/aos/1013699998.

Yi, Hankuil, and Eric J. Richards. 2008. "Phenotypic Instability of Arabidopsis Alleles Affecting a Disease Resistance Gene Cluster." *BMC Plant Biology* 8 (1): 36. https://doi.org/10.1186/1471-2229-8-36.

Yoshida, Riichiro, Izumi C. Mori, Nobuto Kamizono, Yudai Shichiri, Tetsuo Shimatani, Fumika Miyata, Kenji Honda, and Sumio Iwai. 2016. "Glutamate Functions in Stomatal Closure in Arabidopsis and Fava Bean." *Journal of Plant Research* 129 (1): 39–49. https://doi.org/10.1007/s10265-015-0757-0.

Zhang, Yushi, Yubin Wang, Jiapeng Xing, Jiachi Wan, Xilei Wang, Juan Zhang, Xiaodong Wang, Zhaohu Li, and Mingcai Zhang. 2020. "Copalyl Diphosphate Synthase Mutation Improved Salt Tolerance in Maize (*Zea mays*. L) via Enhancing Vacuolar Na+ Sequestration and Maintaining ROS Homeostasis." *Frontiers in Plant Science* 11: 457. https://doi.org/10.3389/fpls.2020.00457.

Zhao, Baolin, and Jia Li. 2012. "Regulation of Brassinosteroid Biosynthesis and Inactivation F." *Journal of Integrative Plant Biology* 54 (10): 746–59. https://doi.org/10.1111/j.1744-7909.2012.01168.x.

Zheng, Yan, Landi Luo, Jingjing Wei, Qian Chen, Yongping Yang, Xiangyang Hu, and Xiangxiang Kong. 2018. "The Glutamate Receptors AtGLR1.2 and AtGLR1.3 Increase Cold Tolerance by Regulating Jasmonate Signaling in *Arabidopsis thaliana*." *Biochemical and Biophysical Research Communications* 506 (4): 895–900. https://doi.org/10.1016/j.bbrc.2018.10.153.

Zhou, Yun, Xing Liu, Eric M. Engstrom, Zachary L. Nimchuk, Jose L. Pruneda-Paz, Paul T. Tarr, An Yan, Steve A. Kay, and Elliot M. Meyerowitz. 2015. "Control of Plant Stem Cell Function by Conserved Interacting Transcriptional Regulators." *Nature* 517 (7534): 377–80. https://doi.org/10.1038/nature13853.

Zhou, Yun, An Yan, Han Han, Ting Li, Yuan Geng, Xing Liu, and Elliot M. Meyerowitz. 2018. "HAIRY MERISTEM with WUSCHEL Confines CLAVATA3 Expression to the Outer Apical Meristem Layers." *Science* 361 (6401): 502–6. https://doi.org/10.1126/science.aar8638.

Zuo, Jian, Philip L. De Jager, Kanji A. Takahashi, Weining Jiang, David J. Linden, and Nathaniel Heintz. 1997. "Neurodegeneration in Lurcher Mice Caused by Mutation in Δ2 Glutamate Receptor Gene." *Nature* 388 (6644): 769–73. https://doi.org/10.1038/42009.